

ISTANBUL TECHNICAL UNIVERSITY ★ GRADUATE SCHOOL OF SCIENCE
ENGINEERING AND TECHNOLOGY

**NUMERICAL SIMULATIONS OF WAVES
GENERATED BY
MOVING PRESSURE FIELDS**

Ph.D. THESIS

Deniz BAYRAKTAR ERSAN

**Department of Shipbuilding and Ocean Engineering
Shipbuilding and Ocean Engineering Programme**

SEPTEMBER 2012

**NUMERICAL SIMULATIONS OF WAVES
GENERATED BY
MOVING PRESSURE FIELDS**

Ph.D. THESIS

**Deniz BAYRAKTAR ERSAN
(508072102)**

**Department of Shipbuilding and Ocean Engineering
Shipbuilding and Ocean Engineering Programme**

Thesis Advisor: Prof. Dr. Serdar BEJİ

SEPTEMBER 2012

**HAREKET EDEN BASINÇ ALANLARININ
YARATTIĞI DALGALARIN
SAYISAL MODELLENMESİ**

DOKTORA TEZİ

**Deniz BAYRAKTAR ERSAN
(508072102)**

Gemi ve Deniz Teknolojisi Mühendisliği Anabilim Dalı

Gemi ve Deniz Teknolojisi Mühendisliği Programı

Tez Danışmanı: Prof. Dr. Serdar BEJİ

EYLÜL 2012

To my parents

FOREWORD

I am deeply grateful to my Ph.D. supervisor Prof. Dr. Serdar Beji for his supervision, advice and key scientific insights guiding me to the completion of this thesis. Whenever I lost track on how to proceed he offered helpful advice. On the other hand, he made numerous suggestions on how to improve this thesis and without his input many issues would not have been spotted. I also would like to thank Prof. Dr. Muhittin Söylemez and Prof. Dr. Emel İrtem for their support.

It is only now that I fully realize how much support I have received from my parents, Şule-Kadri Bayraktar, which allowed me to continue with this research career path. All the support they have provided me over the years was the greatest gift anyone has ever given me. I would like to thank all my friends who created such a good atmosphere in the department; Emre Peşman, Bilge Baş, Murat Özbulut, Sevil Deniz Yakan Dündar, Serdar Köroğlu, Burak Karacık and of course Çiğdem Akan. Although she was living in another continent, our phone calls made me feel that I am not alone during this time.

Finally, I want to thank my husband, Murat Ersan for inspiring me with confidence and more important making me smile even in hard times.

September 2012

Deniz BAYRAKTAR ERSAN

TABLE OF CONTENTS

	<u>Page</u>
FOREWORD	ix
TABLE OF CONTENTS	xi
LIST OF TABLES	xiii
LIST OF FIGURES	xv
SUMMARY	xvii
ÖZET	xix
1. INTRODUCTION	1
2. GENERAL MATHEMATICAL DESCRIPTION OF WATER WAVE	
PROBLEM	5
2.1 Linear Wave Theory	9
2.2 Particle Velocities	14
2.3 Dynamic Pressure	19
2.4 Wave Groups	21
2.5 Wave Energy and Energy Flux	23
3. BOUSSINESQ EQUATIONS	27
3.1 Nonlinear Long Waves in Shallow Water: Derivation and Classification of Approximate Equations.....	28
3.1.1 Airy’s theory for very long waves	33
3.1.2 Boussinesq theory.....	33
3.1.3 Variable depth.....	35
3.2 The Mathematical Framework for Nonlinear, Dispersive Shallow Water Waves.....	36
3.2.1 Non-dimensionalization and scaling	37
3.3 The Classical Form of the Boussinesq Equations for Constant Depth.....	40
3.4 The Classical Form of the Boussinesq Equations for Varying Depth	44
3.5 Improved Boussinesq Equations	47
3.5.1 Derivation of Beji and Nadaoka’s improved Boussinesq equations.....	49
3.5.2 Specification of dispersion parameter	49
4. A NEW DISCRETIZATION SCHEME FOR 1-D and 2-D IMPROVED BOUSSINESQ EQUATIONS	53
4.1 A New Discretization Scheme for 1-D Improved Boussinesq Equations	54
4.2 A New Discretization Scheme for 2-D Improved Boussinesq Equations	58
5. SOLITARY WAVES AND CNOIDAL WAVES	71
5.1 Theoretical Description of Solitary Waves.....	71
5.2 Numerical Simulations of Solitary Waves.....	73
5.3 Theoretical Description of Cnoidal Waves.....	76

6. 1-D LINEAR SHALLOW WATER WAVES FORCED BY A MOVING PRESSURE FIELD	79
6.1 Analytical Solution of 1-D Linear Shallow Water Waves Forced By A Moving Pressure Field.....	80
6.2 Numerical Solution of 1-D Linear Shallow Water Waves Forced By A Moving Pressure Field.....	82
7. SHIP GENERATED WAVES	87
7.1 Kelvin Waves for Infinite Depth.....	87
7.2 Havelock’s Analytical Solution for Finite Depth	95
8. 2-D NUMERICAL SIMULATIONS OF SURFACE GENERATED WAVES	101
8.1 Hemispherical Pressure Forcing.....	103
8.2 Slender-Body Type Pressure Forcing	107
9. RESULTS AND CONCLUSION.....	115
REFERENCES.....	119
CURRICULUM VITAE	127

LIST OF TABLES

	<u>Page</u>
Table 2.1 : Classifications of water waves according to the relative depth h/L	12
Table 7.1 : Havelock's analytical results for subcritical Froude numbers ($Fr < 1$) computed from the iterative solution of $m(3 - n) = 2/p$	97
Table 7.2 : Havelock's analytical results for supercritical Froude numbers ($Fr > 1$) computed from the relationship $\cos^2 \theta = 1 - p$	98
Table 8.1 : Comparisons of numerically obtained wedge angles (a hemispherical moving pressure field) from with Havelock's analytical results for a range of depth-based Froude numbers.	104
Table 8.2 : Comparisons of numerically obtained wedge angles (a slender-body type moving pressure field) from with Havelock's analytical results for a range of depth-based Froude numbers.	110

LIST OF FIGURES

	<u>Page</u>
Figure 2.1 : Schematic view of a simple progressive wave moving in the $+x$ direction, adapted from Coastal Engineering Manual [1]......	9
Figure 2.2 : Local fluid velocities and accelerations under a sinusoidal progressive wave, adapted from Coastal Engineering Manual [1].	15
Figure 2.3 : Profiles of particle velocity and acceleration by Airy theory in relation to the surface elevation, adapted from Coastal Engineering Manual [1]......	15
Figure 2.4 : Water particle displacements from mean position for shallow-water and deep water waves, adapted from Coastal Engineering Manual [1]......	16
Figure 2.5 : Variation of wave parameters with h/L_0 , adapted from Dean and Dalrymple [2]......	20
Figure 2.6 : Wave group formed by the addition of two sinusoidal waves with slightly different periods, adapted from Coastal Engineering Manual [1]......	22
Figure 2.7 : Variation of the ratios of group and phase velocities to deepwater phase speed using linear theory, adapted from Sarpkaya and Isaacson [3].	24
Figure 3.1 : Validity zone of different type of Boussinesq equations.	48
Figure 3.2 : Dispersion curves for various values of dispersion parameter β compared with linear theory.....	52
Figure 4.1 : The Arakawa-C grid.	54
Figure 4.2 : Numerical tests for 1-D Boussinesq equations for varying bathymetries.....	59
Figure 4.3 : Ring test for 2-D Boussinesq equations with $\beta = 1/5$ at $t = 0.2$, $t = 0.4$ and $t = 0.5$ seconds. Left column: perspective views, right column: contour graphics.....	68
Figure 4.4 : Ring test for 2-D Boussinesq equations with $\beta = 1/5$ at $t = 0.6$, $t = 0.8$ and $t = 1.0$ seconds. Left column: perspective views, right column: contour graphics.....	69
Figure 5.1 : Solitary waves for different wave heights $\varepsilon = H/h = 0.1, 0.2, 0.3$ when $\beta = 0$	74
Figure 5.2 : Solitary waves for different wave heights $\varepsilon = H/h = 0.1, 0.2, 0.3$ when $\beta = 1/5$	75
Figure 5.3 : Relative error of the calculated wave height versus nonlinearity parameter.....	76
Figure 5.4 : Wave profiles of different progressive waves, adapted from Coastal Engineering Manual [1].	77

Figure 6.1 : Comparison of numerical and analytical solutions of linear shallow water wave equations for a moving pressure with $v = 0$ m/s, $v = 10$ m/s and $v = 18$ m/s at $t = 50$ s (left column) and $t = 100$ s (right column).	83
Figure 6.2 : Comparison of analytical solution with 1-D Boussinesq solution generated by a moving pressure with $v = 0$ m/s, $v = 10$ m/s and $v = 18$ m/s for $\beta = 1/5$ at $t = 50$ s (left column) and $t = 100$ s (right column).	84
Figure 6.3 : Average relative error of the calculated and analytical surface elevation versus Froude number.....	85
Figure 7.1 : Kelvin wave pattern and Kelvin wedge.....	87
Figure 7.2 : View from above of a plane progressive wave system, moving parallel to the x' -axis at an angle θ relative to x . The wave crests are shown by dashed lines, adapted from Newman [4].	89
Figure 7.3 : Waves situated along the radial line moving in the direction θ , adapted from Lighthill [5].....	92
Figure 7.4 : Positions C_1, C_2, C_3 of any waves generated t_g seconds ago (when the ship was at A) if their energy had travelled a distance ct_g , adapted from Lighthill [5].....	92
Figure 7.5 : Waves generated in deep water by a ship B, adapted from Lighthill [5].....	93
Figure 7.6 : Detailed view of Kelvin Wedge, adapted from Lighthill [5].....	93
Figure 7.7 : Kelvin ship-wave pattern.	95
Figure 7.8 : Havelock's analytical results for a range of Froude numbers.....	99
Figure 8.1 : Definition of the pressure distribution $p(x, y) = p_0 \sqrt{R^2 - x^2 - y^2}$. ..	103
Figure 8.2 : Wave contours of a moving hemisphere at different time steps using Boussinesq model with $\beta = 1/5$ for $Fr = 0.99$	105
Figure 8.3 : Wave contours of a moving hemisphere at different time steps using Boussinesq model with $\beta = 1/5$ for $Fr = 1.3$	106
Figure 8.4 : Perspective view of the slender-body type pressure distribution.....	107
Figure 8.5 : Wave contours generated by a slender-body type moving pressure field using Boussinesq model with $\beta = 1/5$ for $Fr = 0.98$	108
Figure 8.6 : Wave contours generated by a slender-body type moving pressure field using Boussinesq model with $\beta = 1/5$ for $Fr = 1.3$	109
Figure 8.7 : Comparison of numerically obtained wedge angles with Havelock's theoretical formulas.....	111
Figure 8.8 : Perspective views of nonlinear waves generated by slender-body type moving pressure for $Fr = 0.9$ at $t = 9$ s, $t = 18$ s and $t = 24$ s. .	113
Figure 8.9 : Perspective views of nonlinear waves generated by two slender-body type moving pressures for $Fr = 0.9$ at $t = 9$ s, $t = 18$ s and $t = 24$ s.	114

NUMERICAL SIMULATIONS OF WAVES GENERATED BY MOVING PRESSURE FIELDS

SUMMARY

The objective of this study is to simulate the generation and propagation of waves due to a moving pressure field by employing Boussinesq equations with improved dispersion characteristics. In Boussinesq models, the horizontal velocities are allowed to vary parabolically over the water depth while the vertical velocity increases linearly from zero at the bottom. Boussinesq equations are normally valid from intermediate to shallow waters before the waves break. However, in engineering applications, the equations are often used beyond the breaking point, up to wave run-up in the swash zone. The original equations were derived for constant depth only. Later, they are derived for variable depth. The standard Boussinesq equations are valid only for relatively small kh and H/h values where kh and H/h represents the parameters indicating the relative depth (dispersion) and the wave steepness (nonlinearity), respectively. To extend the validity range of the equations, researchers have suggested various ways to improve the linear dispersion characteristics in relatively deeper water as well as including higher order wave nonlinearity.

The Boussinesq equations are also extended to describe wave generation and propagation by moving surface disturbance. The surface disturbance may come from a free surface, bottom, or a moving object in between. The first scenario is associated with either the large-scale wave generation by wind or the local-scale ship wave generation by a moving hull. In this case, the equations need to be revised to include the surface pressure gradient. There has been several studies to represent moving surface disturbance by using different numerical methods. The second scenario corresponds to tsunami generation by underwater landslides or earthquakes.

In this study, the improved Boussinesq equations with appropriate surface pressure gradient terms in the momentum equations are used so that better dispersion characteristics could be achieved for relatively shorter waves generated on the surface. Then, the equations are manipulated in the discretization procedure such that the numerical scheme could be run either in the long wave mode or the Boussinesq mode. By specifying a single parameter the proposed discretization enables the user to run the program either in the long wave mode without dispersion terms or in the Boussinesq mode. Furthermore, the Boussinesq mode may be run either in the classical Boussinesq mode or in the improved Boussinesq mode by setting the dispersion parameter appropriately. In any one of these modes it is possible to specify a fixed or a moving surface pressure for simulating a moving object on the surface. Thus, the new discretization procedure makes it possible to use a single computer code for solving three different set of equations in turn. Such a versatility allows performance comparisons of all these different sets of wave equations.

The discretization of 1-D Boussinesq model has been tested and numerically simulated solitary waves are compared with their analytical counterparts. Moreover, the

numerically 2-D but actually 3-D model is tested for the performance of the non-reflective boundaries. These boundaries are checked by a ring test which reveals the symmetrical accuracy of the model. For all the modes (long wave, classical Boussinesq and improved Boussinesq) of the numerical scheme the ring tests are performed. The other tests compare the numerical solutions of moving surface pressures with the analytical solutions of the long wave equations for all possible modes (long wave, classical, and improved Boussinesq). For a Gaussian shaped moving pressure field, the analytical solution obtained from the linearized 1-D long wave equations is used for comparisons with the numerical solutions obtained from three different modes of the scheme. All these test cases provide support about the reliability of the numerical program and they are important for the verification of the numerical scheme. The surface pressure field is not specified in the usually employed simple cosine form but in a much more shiplike form, which is constructed newly in this work. Besides a hemispherical moving object, slender body type moving pressure has been used for simulating the waves generated. For the verification, the wedge angles are compared with theoretical results of Havelock.

Furthermore, more than a single pressure field is specified in sample simulations to investigate the combined wave patterns in catamaran-like surface vessels. In the future, studies of wave patterns related to catamaran-like surface vessels can be done and more realistic ship-like objects can be used to investigate the wave generation.

HAREKET EDEN BASINÇ ALANLARININ YARATTIĞI DALGALARIN SAYISAL MODELLENMESİ

ÖZET

Su dalgalarının teorik ve fiziksel modellenmesi, üzerinde onaltıncı yüzyıldan bu yana çalışılan bir konudur. Genel olarak rüzgar etkisi ile oluşan açık deniz ve kıyı bölgesi dalgalarının yanı sıra su içindeki bir cismin (gemi v.b.) hareketinden ötürü oluşan dalgaların incelenmesi de önem taşımaktadır. Gemi hareketlerinden kaynaklanan dalgaların modellenmesi özellikle son yılların güncel konularındandır. Su yüzeyinde hareket eden bir cismin (gemi v.b.) farklı hızlarda oluşturduğu lineer olmayan dalgaların, dispersiyon karakteristikleri yönünden gelişmiş Boussinesq denklemleri ile simülasyonu bu çalışmanın temel konusudur. En önemli avantajı derinlik integre edilmiş bir dalga modeli olması olan Boussinesq denklemleri, üç boyutlu bir problemi iki boyutlu bir probleme indirgemektedir.

Boyuttaki bu azalma ve bilgisayar teknolojisinin ilerlemesine paralel olarak, Boussinesq denklemleri farklı tipte dip batimetrisi ve kıyı şekilleri ile geniş yüzeyleri kaplayan bölgeler için yaygın olarak kullanılabilir. Boussinesq modellerinde, yatay hızlar su derinliğine göre parabolik olarak değişirken, dikey hızlar sıfır tabanından itibaren lineer olarak artar. Boussinesq denklemleri genellikle orta derinlikten sığ sulara kadar olan bölgede, dalgaların kırılmasından öncesine kadar geçerlidir. Fakat, mühendislik uygulamalarında, bu denklemler genellikle kırılma noktasının ötesinde, dalganın yükselerek çarpma bölgesinden dalgaların tırmanmasına kadar olan yerde kullanılabilir.

Orijinal Boussinesq denklemleri, sadece sabit su derinliği için türetilmiştir. Daha sonra, değişken su derinlikleri için de türetilmişlerdir. Standart Boussinesq denklemleri, görece küçük kh ve H/h değerleri için geçerli olup, kh ve H/h sırasıyla bağıl derinliği (dispersiyon) ve dalga dikliğini (nonlineerite) ifade eder. Bu denklemlerin geçerli olduğu aralığı artırmak için, araştırmacılar görece derin sulara lineer dispersiyon karakteristiğini iyileştirmenin yanı sıra, yüksek mertebeden dalga dikliğini göz önüne almak için bir çok çalışma yapmışlardır.

Tüm bunların yanı sıra, Boussinesq denklemleri, deniz dibindeki hareketlere bağlı dalga oluşumu ve su yüzeyinde ilerleyen cisimlerin yarattığı dalgaları ifade etmek için de kullanılabilir. Hareketli bir basınç alanının teorik formülasyonunu incelemek, yüzen bir cisim istenilen formda elde edebilmek açısından oldukça önemlidir. Yüzey deformasyonu, serbest yüzeyden, tabandan ya da bu ikisinin arasında hareket eden bir cisimden ileri gelebilir. İlk durum, rüzgar kaynaklı yüksek ölçekli bir dalga oluşumuyla ilgili olabileceği gibi hareket halindeki bir tekne gövdesinin oluşturacağı yerel ölçekli bir gemi dalgasıyla da ilgili olabilir. Bu durumda, denklemler bir basınç gradyanı içerecek şekilde yeniden düzenlenmelidir. Dolayısıyla, değişik sayısal yöntemleri kullanarak, hareket eden bu basınç alanını ifade eden bir çok çalışma yapılmıştır. İkinci durum ise, yani yüzey kökenli olmayan basınç alanları su altındaki

yer kaymaları ya da depremler nedeniyle meydana gelen tsunami oluşumunu ifade eder.

Bu çalışmada, uygun basınç gradyanı terimlerinin momentum denklemlerine eklenmesiyle geliştirilmiş Boussinesq denklemleri kullanılmıştır. Bu sayede, yüzeyde oluşan görece kısa dalgalar için daha iyi dispersiyon karakteristiği elde edilebilir. Sayısal programın uzun dalga modunda veya Boussinesq modunda çalışabilmesi için, söz konusu denklemlerin ayrıklaştırılması buna uygun şekilde yapılmıştır. Uygulanan ayrıklaştırma, kullanıcının programı bir parametre tanımlayarak, hem dispersiyon terimleri olmadan uzun dalga modunda, hem de Boussinesq modunda çalıştırabilmesine olanak verir. Ayrıca, dispersiyon parametresinin uygun seçimiyle, Boussinesq modu kendi içinde, klasik Boussinesq modu veya geliştirilmiş Boussinesq modu olarak seçilebilir. Söz konusu tüm bu modlarda, yüzeyde hareket eden cisim, sabit ya da hareket eden yüzey basıncı olarak tanımlanabilmektedir. Böylece, yeni ayrıklaştırma yaklaşımıyla, tek bir bilgisayar kodu ile üç ayrı dalga denklemi çözülebilmektedir. Bu çok yönlülük, söz konusu dalga denklemlerinin performans karşılaştırmasına da olanak vermektedir.

Çalışmada öncelikle, bir boyutlu Boussinesq denkleminin ayrıklaştırılması ve programı test edilmiştir. Bir boyutlu Boussinesq modelinin ayrıklaştırılması Green'in teorik formülasyonu ile test edilmiştir. Lineerize edilmiş klasik ve geliştirilmiş Boussinesq denklemlerinin testi için sinüzoidal ve parabolik tipteki batimetriler kullanılmıştır. Yapılan karşılaştırmalarda, dalga genliklerinin Green'in teorik formülüyle uyum içersinde olduğu gözlemlenmiştir.

Bu testin yanı sıra, sayısal olarak modellenen solitary dalgaları analitik ifadeleri ile karşılaştırılmışlardır. Bunun sebebi, solitary dalgalarının Boussinesq denklemlerinin en temel analitik çözümü olmasıdır. Sayısal olarak modellenen solitary dalgalar, klasik ve geliştirilmiş Boussinesq modunda çalıştırılmış olup, farklı nonlinearite parametreleri baz alınarak incelenmiştir. Klasik Boussinesq modunda çalıştırılmış olan programdan elde edilen değerlerin bağıl hata yüzdeleri hesaplanarak programın güvenilirliği test edilmiştir.

Ayrıca, sayısal olarak iki boyutlu fakat gerçekte üç boyutlu olan model, açık (yansıtmayan) sınır koşullarının performansı açısından test edilmiştir. Bu sınırlar, modelin simetri özelliklerini ortaya çıkaran bir halka testine tabi tutulmuştur. Sayısal model, bütün modlarda (uzun dalga, klasik Boussinesq ve geliştirilmiş Boussinesq) çalıştırılmış olup, sadece geliştirilmiş Boussinesq modeline ait test sonuçlarına yer verilmiştir. Kontur grafikleri mükemmel yakın bir simetri göstererek açık sınır koşullarının iyi sonuçlar verdiğini ispatlamıştır.

Bahsedilmiş olan bu testler dışındaki diğer bir test ise, yine bütün modlar için (uzun dalga, klasik ve geliştirilmiş Boussinesq), hareket eden ve sabit duran basıncın, sayısal ve analitik çözümlerinin birbiriyle karşılaştırılmasıdır. Öncelikle, uzun dalga denklemleri için, Gauss tipinde basınç dağılımının analitik çözümleri, sabit ve hareketli durumlar için ele alınmıştır. Daha sonra, aynı Gauss tipi basınç dağılımı Boussinesq modelinin çözebileceği tüm modlar (uzun dalga, klasik ve gelişmiş Boussinesq) için sayısal çözümlerle kullanılarak analitik sonuçlarla karşılaştırılmıştır. Bağıl hata yüzdesi hesaplanarak, tüm bu modlarda çalıştırılan sayısal programın, belirlenen yüzey basıncı için doğru bir şekilde çalışıp çalışmadığı analitik çözümler ile karşılaştırma yapılarak kontrol edilmiştir. Yapılan tüm bu testler, programın güvenilirliğini desteklemektedir.

Bir sonraki aşamada, farklı formda yüzey basınç alanları ile istenilen cismin/cisimlerin etkilerinin yaratılıp tanımlandığı ve buna bağlı olarak yapılan simülasyonlar ile farklı durumlar incelenip birbiriyle karşılaştırılmıştır. Bu simülasyonlar, hareket halindeki bir gemi formunun yarattığı dalgalar ile bunların etkilerini anlayabilmek açısından oldukça önemlidir. Bunu gerçekleştirebilmek için, yüzey basınç terimleri, bir ve iki boyutlu (gerçekte iki ve üç boyutlu) olan Boussinesq sayısal modellerinin bir parçası haline getirilip uygulanmıştır. Bu çalışmada, yüzey basınç alanı literatürde genellikle kullanılan kosinüs formunda tanımlanmamıştır. Bunun yerine, daha yeni olarak, gemi benzeri bir form oluşturulmuştur. Yarımküre şeklindeki ilerleyen basınç dışında, narin gövde tipinde bir basınç alanı da, oluşan dalgaları modellemek için kullanılmıştır.

İlerleyen her iki basınç alanının oluşturduğu dalga şekillerinin, farklı derinlik Froude sayıları için değişik zaman aralıklarında simülasyonları yapılmıştır. Havelock'un analitik sonuçları hesaplanan giriş açılarıyla karşılaştırılmıştır. Bu karşılaştırmalar, özellikle bağıl derinliğin küçük olduğu, kritik üstü Froude bölgesi için çok iyi sonuçlar vermektedir. Ortalama hata yüzdelerinde ortaya çıkan fark, büyük ihtimalle Boussinesq denklemlerinin su derinliğine bağlı kısıtlayıcılığından ileri gelmektedir. Kritik altı bölge, görece daha derin suları temsil etmekte ve Froude sayısının sıfıra eşit olduğu durum ise, tamamen derin suya karşılık gelmektedir. Sayısal modelin, kritik altı bölgede görece daha kötü sonuç vermesi, oluşan dalgaların derin su özelliklerine bağlanabilir. Yapılmış olan bu simülasyonların hepsi, geliştirilmiş Boussinesq modunda elde edilen değerler kullanılarak yapılmıştır.

Nonlineeritenin etkisini gözlemleyebilmek için, narin gövde tipinde basıncın genliği önceki simülasyonlarda kullanılan değerın iki katına çıkartılmıştır. Sonuç olarak, nonlineeritenin giriş açıları üzerinde bir etkisi olmadığı fakat dalga şeklinin dikey simetrisini etkiliyor olduğu gözlemlenmiştir. Öte yandan, dalga şeklinin temel karakteristiğinin aynı kaldığı görülmüştür.

Klasik Boussinesq denklemlerinin uygulama alanlarından farklı olarak bu araştırma konusu, kıyı ve liman bölgelerindeki dalga hareketlerinin incelenmesinin dışında, yüzer bir cisim veya cisimler etkisi altında oluşacak dalga hareketlerini de inceleyebilmeyi mümkün kılmaktadır.

Örnek simülasyonlar olarak, birden fazla basınç alanı tanımlanarak, katamaran benzeri teknelerin oluşturacağı dalga şekilleri incelenmiştir. İleride yapılacak olan çalışmalarda, katamaran benzeri teknelerin oluşturacağı dalga şekilleri daha ayrıntılı bir şekilde incelenebileceği ve bunun yanı sıra, daha gerçekçi gemi benzeri cisimler kullanılarak, oluşacak olan dalgaların modellenebileceği düşünülmektedir. Katamaran ya da gemi benzeri bir cismin yaratacağı dalgaların incelenmesi özellikle hızın yüksek olduğu durumlarda önem kazanmaktadır. Yüksek hızlı teknelerin günümüzdeki popüleritesiyle birlikte, bu tip teknelerin yaratacağı büyük genlikli dalgalar, kıyılarda, deniz dibinde ve biyolojik çevrede erozyona neden olmaktadır. Öte yandan, bu dalgalar, insanların can güvenliği ve kıyıda bağlı bulunmakta olan teknelerin güvenliği bakımından da önemli bir etkiye sahiptir. Bu durum göz önüne alındığında, ileriki çalışmalarda, özellikle yüksek hızdaki teknelerin oluşturduğu dalgaların incelenmesi önem taşımaktadır.

1. INTRODUCTION

Waves are a common phenomenon in nature. By general definition, a wave is a movement with a certain periodic back-and-forth (longitudinal) or up-and-down (transverse) motion. A wave can also be defined as a disturbance that spreads in matter or space, obeying a certain "wave equation". The theoretical and numerical modelling of water waves has been extensively studied since the 16th century. In order to describe different wave phenomena, various water wave theories have been developed and these wave theories help us to understand the physical mechanisms of water waves and provide the basis for various water wave models. Coastal, marine and offshore engineers, naval architects, physical oceanographers and marine hydrodynamics have all been interested in water wave problems. Due to the increasing demand of sea transport and offshore oil exploration in the past few decades, research in water waves has been very active.

Ocean surface waves, or simply water waves, are mainly generated by wind. However, besides wind generated offshore and near shore waves, waves generated by moving bodies are also studied. General mathematical description of water wave phenomenon is given as Laplace's equation in 2-D or 3-D region (whichever is appropriate), bottom boundary condition, kinematic and dynamic boundary conditions on the free surface. Due to the nature of the free surface boundary conditions the problem is nonlinear. However, in most cases the problem is linearized by neglecting the nonlinear terms of the kinematic and dynamic boundary conditions. The linearized set of equations can be solved analytically to obtain a dispersion relationship, horizontal and vertical particle velocities, and the pressure field due to waves. This complete solution of the linearized problem is known under various names, such as Airy wave theory, the infinitesimal amplitude wave theory, the sinusoidal wave theory, or simply the linear wave theory.

If the nonlinear terms in the free surface boundary conditions are retained the solution of the complete problem must necessarily be numerical. Further, the numerical solution must also be iterative as the unknown free surface elevation appears both in

the kinematic and dynamic boundary conditions. Hence the general wave problem is a solution of the Laplace equation within a domain with a continuously deforming free surface, which itself is to be determined in time. For the numerical solution of this time-dependent complicated problem various numerical techniques such as finite-differences, finite-elements, boundary elements, etc. are in use. A somewhat different way of attacking the problem is to develop a vertically integrated set of equations from the general equations describing the problem. To achieve this goal, a definite assumption regarding the vertical variation of the kinematic variables (i.e., velocities) must be made. Following an appropriate assumption the vertical or depth integration may be performed, resulting in reduction of the dimension of the problem. The long wave equations or the shallow water wave theory, in which the horizontal velocities are taken constant over the entire water depth, is probably the most frequently used depth-integrated wave model. In terms of dispersion characteristics a better depth-integrated model is known as Boussinesq model.

In Boussinesq models [6], the horizontal velocities are allowed to vary parabolically over the water depth while the vertical velocity increases linearly from zero at the bottom. Boussinesq equations are normally valid from intermediate to shallow waters before the waves break. However, in engineering applications, the equations are often used beyond the breaking point, up to wave run-up in the swash zone. The original Boussinesq equations were derived for constant depth only. Later, Mei and LeMehaute [7], Peregrine [8] derived Boussinesq equations for variable depth. While Mei and LeMehaute used the velocity at the bottom as the dependent variable, Peregrine used the depth-averaged velocity and assumed the vertical velocity varying linearly over the depth. Due to wide popularity of the equations derived by Peregrine, these equations are often referred to as the standard Boussinesq equations for variable depth in the coastal engineering community.

The standard Boussinesq equations are valid only for relatively small kh and H/h values where kh and H/h represents the parameters indicating the relative depth (dispersion) and the wave steepness (nonlinearity), respectively. To extend the validity range of the equations, researchers have suggested various ways to improve the linear dispersion characteristics in relatively deeper water as well as including higher order wave nonlinearity. Witting [9] presented the first work on improving the dispersion

characteristics of these equations. These equations make use of full free surface boundary conditions hence are fully nonlinear, but are valid only for constant water depth. Madsen et. al [10] and Madsen and Sørensen [11] included higher order terms with adjustable coefficients into the standard Boussinesq equations for constant and variable water depth, respectively. Beji and Nadaoka [12] presented an alternative derivation of Madsen et. al's [11] improved Boussinesq equations.

By defining the dependent variable as the velocity at an arbitrary depth, Nwogu [13] introduced a new set of so-called extended Boussinesq equations, which are essentially akin to Witting's equations. To further extend the validity range of the Boussinesq equations to higher nonlinearity Kirby et. al. [14] proposed a higher order accurate Boussinesq model based on Nwogu's equations. Chen and Liu [15], [16] derived fully nonlinear and weakly dispersive Boussinesq equations using velocity potential and free surface elevation. Madsen et. al. [10] have proposed a series of new highly nonlinear Boussinesq models, in which either the mean velocity or the velocity at an arbitrary depth level was used to minimize the depth-integrated error of the linear velocity profile.

The Boussinesq equations are also employed to model wave generation and propagation by moving surface disturbances. The surface disturbance may come from a moving free surface object, bottom movement, or a moving object in between. Liu and Wu [17] presented a model with specific applications to ship waves generated by a moving pressure distribution in a rectangular and trapezoidal channel by using boundary integral method. Torsvik [18] made a numerical investigation on waves generated by a pressure disturbance moving at constant speed in a channel with a variable cross-channel depth profile by using Lynett et. al [19] and Liu and Wu [17]'s COULWAVE long wave model. Naschimento [20] et al. adapted Wei and Kirby's [21] FUNWAVE in order to include a specified moving pressure at the free surface. All these works use the same type of cosine function to represent the moving surface object.

The present work introduces three novel approaches in modelling the nonlinear waves due to moving surface pressure fields by Boussinesq equations. First, the improved Boussinesq equations of Beji and Nadaoka [12] with appropriate surface pressure gradient terms in the momentum equations are used so that better dispersion

characteristics could be achieved for relatively shorter waves generated on the surface. Secondly, the equations are manipulated in the discretization procedure such that the numerical scheme could be run either in the long wave mode or the Boussinesq mode. The Boussinesq mode could further be specified as the classical Boussinesq mode or the improved Boussinesq mode. Thus, the new discretization procedure makes it possible to use a single computer code for solving three different sets of equations in turn. Such a versatility allows performance comparisons of all these equations. Finally, the surface pressure field is not specified in the usually employed simple cosine form but in a much more shiplike form, which is constructed newly in this work. Also, more than a single pressure field is specified in sample simulations to investigate the combined wave patterns in catamaran-like surface vessels.

2. GENERAL MATHEMATICAL DESCRIPTION OF WATER WAVE PROBLEM

Wave theories are approximations to reality therefore they may describe only some phenomena under certain conditions that satisfy the assumptions made in their derivation. The same theory may not be adequate to describe other phenomena that violate those assumptions. One should be very careful while selecting the appropriate theory. It must be ensured that the wave phenomenon of interest is described well enough by the selected theory because the designs depend on the ability to predict wave surface profiles and water motion accurately.

The most elementary wave theory is the small-amplitude or linear wave theory. This theory, which usually is attributed to Airy [22], is easy to apply, and gives reasonable approximation of wave characteristics for a wide range of wave parameters. In 1847, the linear theory of Airy was extended by Stokes for non-linear deep water wave motion, correct up to third order in the wave steepness [23].

A more complete theoretical description of waves may be obtained as the sum of many successive approximations, where each additional term in the series is a correction to preceding terms. For some situations, waves are better described by these higher-order theories, which are usually referred to as finite-amplitude wave theories [2], [24]. Although there are limitations to its applicability, linear theory can still be useful if the assumptions made are valid. The assumptions made in linear wave theory are [1];

- The fluid is homogeneous and incompressible; therefore, the density is a constant.
- Surface tension can be neglected.
- The fluid is ideal or inviscid.
- Coriolis effect due to the earth's rotation can be neglected.
- Pressure at the free surface is uniform and constant.

- The particular wave being considered does not interact with any other water motions. The flow is irrotational so that water particles do not rotate (only normal forces are important and shearing forces are negligible).
- The bed is a horizontal, fixed, impermeable boundary, which implies that the velocity normal to the bed is zero.
- The wave amplitude is small and the waveform is invariant in time and space.
- Waves are plane or long-crested (two-dimensional).

The derivation of the theory, given the assumptions of small wave slope ($H/L \ll 1$) or a depth much greater than the wave height ($h/H \ll 1$), assumes for the fluid surface elevation η ,

$$\eta(x,t) = (H/2) \cos(kx - \omega t) \quad (2.1)$$

where H is the wave height, k the wave number, and ω the cyclic wave frequency. This theory is most often applied to ocean bodies and large lakes. An expression for the wave length has also been developed, although it must be solved iteratively. Simpler expressions are available for the limiting cases of deep and shallow water. The particles move generally in closed elliptical orbits that decrease in diameter with depth, reducing to limiting cases of circles and straight lines, respectively, in deep and shallow water.

Like finite-amplitude waves, linear waves are described by two dimensionless parameters, the wave steepness H/L and the relative water depth h/L . The relative depth determines whether waves are dispersive or nondispersive and whether the celerity, length, and height are influenced by water depth. Wave steepness is a tool to understand how large a wave is relative to its length and whether the linear wave theory assumption is applicable or not. For large values of the wave steepness one must question the assumption of small-amplitude theory.

Another dimensionless parameter is the ratio of wave steepness to relative water depth, which yields the definition "relative wave height", H/h for shallow water waves. Like the wave steepness, the large values of relative wave height indicates the question of

whether small-amplitude assumption is valid or not. Besides these parameters another parameter called Ursell number is used for shallow water waves to select a wave theory for a wave with given L and H (or T and H) in a given water depth h . The Ursell number is given as

$$U_R = \left(\frac{L}{H} \right)^2 \frac{H}{h} = \frac{L^2 H}{h^3} \quad (2.2)$$

High values of U_R indicates the necessity for using a nonlinear wave theory. Although the linear or small-amplitude wave theory provides a useful tool to understand wave motion, ocean waves are generally not small in amplitude. For a complete solution of ocean waves, a perturbation solution using successive approximations are developed to improve the linear theory solution of the hydrodynamic equations for gravity waves. Each order wave theory in the perturbation expansion serves as a correction and the net result is often a better agreement between theoretical and observed waves. These higher-order or extended solutions for gravity waves are often called nonlinear wave theories. Development of the nonlinear wave theories has evolved for a better description of surface gravity waves. These include Stokes theories, solitary and cnoidal waves [1].

After Stokes's pioneering studies, [23], [25], other studies such as De [26], Bretschneider [27], Skjelbreia and Hendrickson [28], Laitone [29], [30], [31], Chappellear [32] and Fenton [33] have assumed the wave slope ka is small where a is wave amplitude. The perturbation solution is developed as a power series in terms of $\varepsilon = ka$ and expected to converge as more terms are included in the expansion. However, convergence does not occur for steep waves unless a different perturbation parameter from that of Stokes is chosen as shown in the studies of Schwartz [34], Cokolet [35] and Williams [36], [37].

The most common theory is fifth-order Stokes finite-amplitude wave theory which is used in deep and shallow water wave studies [1]. Fenton [33] has formulated Stokes fifth-order theory with good convergence properties. In general, the perturbation expansion for velocity potential ϕ may be written as

$$\phi = \varepsilon \phi_1 + \varepsilon^2 \phi_2 + \dots \quad (2.3)$$

where $\varepsilon = ka$, the perturbation parameter. Each term in the series is smaller than the leading term by a factor of order ka . In this expansion, ϕ_1 yields the first-order theory (linear theory) and ϕ_2 is the second-theory order. Substituting Equation 2.3 and similar expressions for the surface elevation η , velocities u and v into the suitable governing equations and boundary conditions, yields a series of higher-order solutions for ocean waves. Equating the coefficients of equal powers of ka gives recurrence relations for each order solution [2], [24] and [38]. The first-order Stokes theory is the linear (Airy) theory [1].

In Stokes theory, the linear dispersion relation is still valid to second order, and both wavelength and celerity are independent of wave height to this order. At third and higher orders, wave celerity and wavelength depend on wave height, and therefore, for a given wave period, celerity and length are greater for higher waves. In addition, some limitations are imposed on the finite-amplitude Stokes theory in shallow water by means of the water depth and amplitude nonlinearities. The Stokes perturbation becomes invalid for steeper waves in shallow water because higher-order terms in Stokes expansion may increase in magnitude to become comparable or larger than the fundamental frequency component [33], [39]. Extension of the Stokes theory to higher orders has become common with computers. For example, Dean [40] substituted the stream function instead of velocity potential and developed the stream function theory. Dean [41] compared measured horizontal particle velocity in a wave tank with the tenth-order stream function theory and several other theories.

Stream function theory including currents has been developed using different numerical techniques by Dalrymple [42], Chaplin [43], Reinecker and Fenton [44]. For near-breaking waves, Cokelet [35] extended the method used by Schwartz [34] for steep waves for the full range of water depth and wave heights. Cokelet used a 110th-order theory for waves up to breaking and computed the wave profile, wave celerity, and various integral properties of waves, including the mean momentum, momentum flux, kinetic and potential energy, and radiation stress.

Since Stokes' finite amplitude wave theory is applicable for the cases where $h/L > 1/8$ or $kh > 0.78$ or $U_R < 79$, Peregrine [45] used a different method for longer waves. Portions of the wave travel faster as they reach into shallow water because of amplitude dispersion or waves travel faster because they are in deeper water. It can be said that in

shallow water, waves also feel the effects of frequency dispersion less. Mathematical representation for waves in shallow water needs a different perturbation parameter which expresses the combined influence of amplitude and frequency dispersion which are studied by Whitham [46], Miles [47], and Mei [24]. In Peregrine's study [48] he constructed two perturbation parameters whose ratio is equivalent to the Ursell parameters. The set of equations obtained in this manner are called the "nonlinear shallow-water wave equations".

2.1 Linear Wave Theory

A progressive wave is expressed by the variables x (spatial) and t (temporal) or by their combination (phase), defined as $\theta = kx - \omega t$. Values of θ vary between 0 and 2π . Figure 2.1 shows parameters that define a simple, progressive wave as it passes a fixed point in the ocean. A simple, periodic wave of permanent form propagating over a horizontal bottom is characterized by the wave height H , wavelength L and water depth h . As shown in Figure 2.1, the highest point of the wave is the *crest* and the

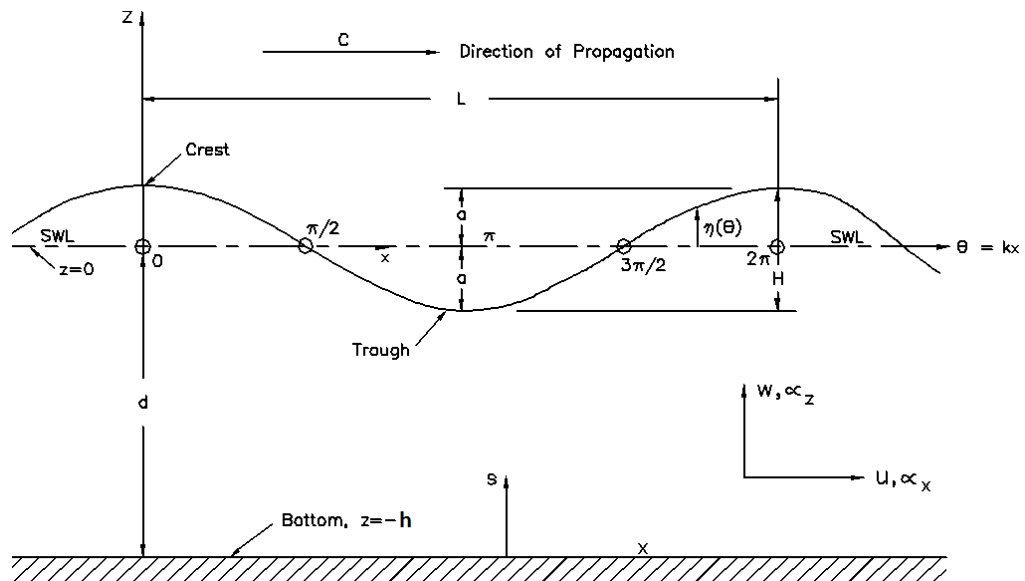


Figure 2.1: Schematic view of a simple progressive wave moving in the $+x$ direction, adapted from Coastal Engineering Manual [1].

lowest point is the *trough*. For linear or small-amplitude waves, the height of the crest above the still-water level (SWL) and the distance of the trough below the SWL are each equal to the wave amplitude a . Therefore $a = H/2$, where H is the wave height. The time interval between the passage of two successive wave crests or troughs at a

given point is the wave period T . The wavelength L is the horizontal distance between two identical points on two successive wave crests or two successive wave troughs. $\omega = 2\pi/T$ is the angular or radian frequency, the wave number is $k = 2\pi/L$, the phase velocity or wave celerity is $c = L/T = \omega/k$, the wave steepness is $\varepsilon = H/L$, the relative depth is h/L and the relative wave height is H/h .

The most fundamental description of a simple sinusoidal oscillatory wave is its length L , height H , period T and depth h (the distance from the bed to SWL). Figure 2.1 shows a two-dimensional, simple progressive wave propagating in the positive x direction. The symbol η denotes the displacement of the water surface relative to the SWL and is a function of x and time t . At the wave crest, η is equal to the amplitude of the wave a , or one-half the wave height $H/2$. Wave motion can be defined in terms of dimensionless parameters H/L , H/h and h/L . The dimensionless parameters ka and kh can be substituted for H/L and h/L , respectively, since these differ only by a constant factor π and 2π respectively from those preferred by engineers [1].

The assumption of irrotationality allows the use of a mathematical function termed the velocity potential Φ . The velocity potential is a scalar function whose gradient (i.e., the rate of change of Φ relative to the x - and z -coordinates in two dimensions where x = horizontal, z = vertical) at any point in fluid is the velocity vector. Thus, the fluid velocity in the x -direction is

$$u = \frac{\partial \Phi}{\partial x} \quad (2.4)$$

Similarly, the fluid velocity in the z -direction is

$$w = \frac{\partial \Phi}{\partial z} \quad (2.5)$$

Φ has the units of length squared divided by time. Consequently, if $\Phi(x, z, t)$ is known over the flow field, then fluid particle velocity components u and w can be determined.

Likewise, the irrotationality implies that there is another mathematical function termed the stream function Ψ . Some wave theories are formulated in terms of the stream function Ψ , which is orthogonal to the potential function Φ . Lines of constant values of the potential function (equipotential lines) and lines of constant values of the stream

function are mutually perpendicular or orthogonal. Consequently, if Ψ is known, Φ can be found, or vice versa, using the equations

$$\frac{\partial \Phi}{\partial x} = \frac{\partial \Psi}{\partial z} \quad (2.6)$$

$$\frac{\partial \Phi}{\partial z} = -\frac{\partial \Psi}{\partial x} \quad (2.7)$$

called as Cauchy-Riemann conditions [46]. Both Φ and Ψ satisfy the Laplace equation which governs the flow of an ideal fluid (inviscid and incompressible fluid). Thus, under these assumptions, the Laplace equation governs the flow beneath waves.

The Laplace equation in two dimensions with x being the horizontal and z the vertical axes in terms of velocity potential Φ is given by

$$\frac{\partial^2 \Phi}{\partial x^2} + \frac{\partial^2 \Phi}{\partial z^2} = 0 \quad (2.8)$$

In terms of stream function Ψ the Laplace equation becomes,

$$\frac{\partial^2 \Psi}{\partial x^2} + \frac{\partial^2 \Psi}{\partial z^2} = 0 \quad (2.9)$$

Since the distance traveled by a wave during one wave period is equal to one wavelength, wave celerity can be related to the wave period and length by

$$c = \frac{L}{T} \quad (2.10)$$

The dispersion relationship uses wave celerity, wavelength and water depth and is given by

$$c = \sqrt{\frac{gL}{2\pi} \tanh\left(\frac{2\pi h}{L}\right)} \quad (2.11)$$

Dispersion relationship indicates that waves with different periods travels at different speeds. For the case where there is more than one wave, the longer period wave will

travel faster. Hence the waves get separated or "disperse", using the expression $c = L/T$ the same relationship can also be written as

$$c = \frac{gT}{2\pi} \tanh\left(\frac{2\pi h}{L}\right) \quad (2.12)$$

Substituting wave number and wave angular frequency, an expression for wavelength as a function of water depth and wave period is obtained which is

$$L = \frac{gT^2}{2\pi} \tanh\left(\frac{2\pi h}{L}\right) = \frac{gT}{\omega} \tanh(kh) \quad (2.13)$$

In Equation (2.13) the wavelength L appears on both sides of the equation. Considering this difficulty, tabulated values of h/L and h/L_0 are used where L_0 is the deep water wavelength. An approximation to the expression (2.13) is given by Eckart [49] which is correct within about 10 %:

$$L \approx \frac{gT^2}{2\pi} \sqrt{\tanh\left(\frac{4\pi^2 h}{T^2 g}\right)} \quad (2.14)$$

Gravity waves may also be classified by the water depth in which they travel. Note that as the argument $kh = 2\pi h/L$ of the hyperbolic tangent gets large, the $\tanh(kh)$ approaches 1, and for small values of kh , $\tanh(kh) \approx kh$. According to the relative depth h/L , waves are classified as deep water waves when $\tanh(kh)$ approaches unity

Table 2.1: Classifications of water waves according to the relative depth h/L .

Classification	h/L	kh	$\tanh(kh)$
Deep water	1/2 to ∞	π to ∞	1
Transitional	1/20 to 1/2	$\pi/10$ to π	$\tanh(kh)$
Shallow water	0 to 1/20	0 to $\pi/10$	kh

thus equations (2.10) and (2.11) become

$$c_0 = \sqrt{\frac{gL_0}{2\pi}} = \frac{L_0}{T} \quad (2.15)$$

Similarly Equation (2.12) becomes

$$c_0 = \frac{gT}{2\pi} \quad (2.16)$$

When the relative depth h/L is greater than $1/2$, the wave characteristics are almost independent of depth. Deep water conditions can be expressed by the subscript 0 as in L_0 and c_0 except that the period T remains constant. Note that period, T is independent of depth for oscillatory waves, and therefore, the subscript for wave period is omitted [50]. In the SI system, the constant $g/2\pi$ is equal to 1.56 m/s^2 and therefore,

$$c_0 = \frac{gT}{2\pi} = \frac{9.8}{2\pi}T = 1.56T \quad (2.17)$$

$$L_0 = \frac{gT^2}{2\pi} = \frac{9.8}{2\pi}T^2 = 1.56T^2 \quad (2.18)$$

Using equations (2.17) and (2.18) for computing wave celerity when the relative depth is $h/L = 0.25$, the resulting error will be about 9 percent. It is shown that a relative depth (when the relative depth is between 0.5 and 0.04) of 0.5 is the limit of boundary separating deep water waves from waves in water of transitional depth. It has to be noted that if a wave is traveling in transitional depths, Equations (2.11) and (2.12) must be used without simplification. When the relative water depth becomes shallow, i.e., $2\pi h/L < 1/4$ or $h/L < 1/25$, Equation (2.11) becomes

$$c = \sqrt{gh} \quad (2.19)$$

The waves where Equation (2.19) may be applied are called long waves and this relation is attributed to Lagrange. Thus, when a wave travels in shallow water, wave celerity depends only on water depth.

In conclusion, as a wind wave moves over deep water its speed and length are only a function of its period (or frequency); then as the depth becomes intermediate relative to its length, the length and speed are dependent upon both depth and period; and finally

when the wave reaches shallow regions its length and speed are dependent only on depth (and not frequency) [1].

2.2 Particle Velocities

The horizontal component u and the vertical component w of the local fluid velocity are given as

$$u = \frac{H}{2} \frac{gT}{L} \frac{\cosh[2\pi(z+h)/L]}{\cosh(2\pi h/L)} \cos \theta \quad (2.20)$$

$$w = \frac{H}{2} \frac{gT}{L} \frac{\sinh[2\pi(z+h)/L]}{\cosh(2\pi h/L)} \sin \theta \quad (2.21)$$

where they express the local fluid velocity components any distance $(z+h)$ above the bottom. The velocities are periodic in both x and t . For a given value of the phase angle $\theta = (2\pi x/L - 2\pi t/T)$, the hyperbolic functions \cosh and \sinh , as functions of z result in an approximate exponential decay of the magnitude of velocity components with increasing distance below the free surface. The maximum positive horizontal velocity occurs when $\theta = 0, 2\pi$, etc., while the maximum horizontal velocity in the negative direction occurs when $\theta = \pi, 3\pi$, etc. On the other hand, the maximum positive vertical velocity occurs when $\theta = \pi/2, 5\pi/2$, etc., and the maximum vertical velocity in the negative direction occurs when $\theta = 3\pi/2, 7\pi/2$, etc. Fluid particle velocities under a wave train are shown in Figure 2.2 by differentiating each equation with respect to t , the local fluid particle accelerations are obtained from Equations (2.20) and (2.21) which yields,

$$a_x = \frac{\partial u}{\partial t} = \frac{Hg\pi}{L} \frac{\cosh[2\pi(z+h)/L]}{\cosh(2\pi h/L)} \sin \theta \quad (2.22)$$

$$a_z = \frac{\partial w}{\partial t} = -\frac{Hg\pi}{L} \frac{\cosh[2\pi(z+h)/L]}{\cosh(2\pi h/L)} \cos \theta \quad (2.23)$$

Figure 2.2 shows that the fluid under the crest moves in the direction of wave propagation and returns during passage of the trough. Since linear theory does not predict any net mass transport, this schematic presentation shows only an oscillatory

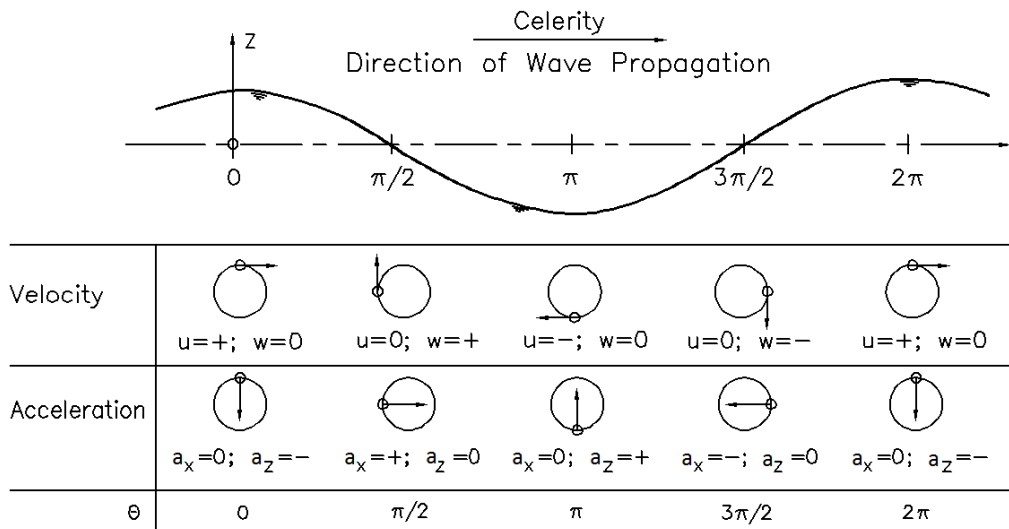


Figure 2.2: Local fluid velocities and accelerations under a sinusoidal progressive wave, adapted from Coastal Engineering Manual [1].

fluid motion. However, Figure 2.3 depicts profiles of the surface elevation, particle velocities, and accelerations by the linear wave theory [1].

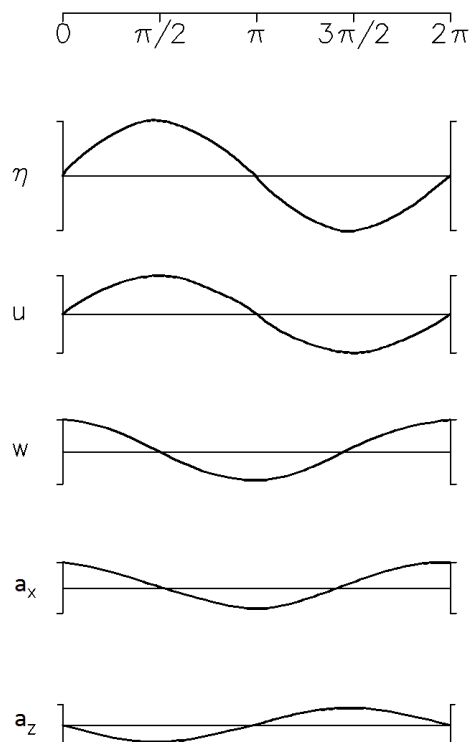


Figure 2.3: Profiles of particle velocity and acceleration by Airy theory in relation to the surface elevation, adapted from Coastal Engineering Manual [1].

Linear wave theory deals with the displacement of individual water particles within the wave. Water particles generally move in elliptical paths in shallow or transitional depth water and in circular paths in deep water as it can be seen in Figure 2.4.

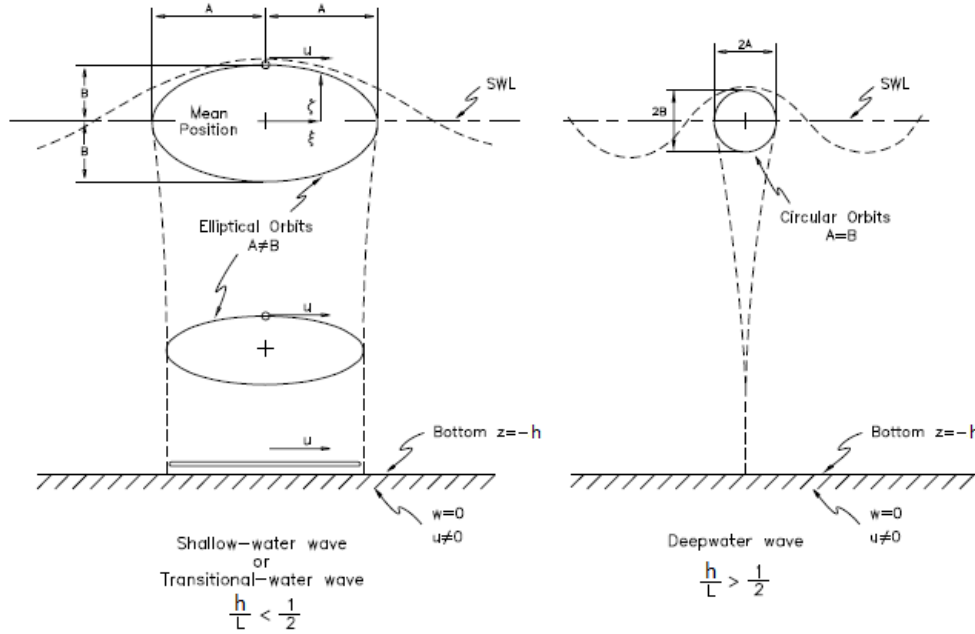


Figure 2.4: Water particle displacements from mean position for shallow-water and deep water waves, adapted from Coastal Engineering Manual [1].

If the mean particle position is considered to be at the center of the ellipse or circle, then vertical particle displacement with respect to the mean position cannot exceed one-half the wave height. Thus, since the wave height is assumed to be small, the displacement of any fluid particle from its mean position must be small. Figure 2.4 shows that the integration of Equations (2.20) and (2.21) gives the horizontal and vertical particle displacements from the mean position, respectively. Fluid particle displacements are,

$$\xi = -\frac{HgT^2}{4\pi L} \frac{\cosh\left[\frac{2\pi(z+h)}{L}\right]}{\cosh\left(\frac{2\pi h}{L}\right)} \sin\theta \quad (2.24)$$

$$\zeta = \frac{HgT^2}{4\pi L} \frac{\sinh\left[\frac{2\pi(z+h)}{L}\right]}{\cosh\left(\frac{2\pi h}{L}\right)} \cos\theta \quad (2.25)$$

where ξ is the horizontal displacement of the water particle from its mean position and ζ is the vertical displacement of the water particle from its mean position. However,

these equations can be simplified by using the expression,

$$\left(\frac{2\pi}{T}\right)^2 = \frac{2\pi g}{L} \tanh \frac{2\pi h}{L} \quad (2.26)$$

Equations (2.24) and (2.25) become,

$$\xi = -\frac{H}{2} \frac{\cosh \left[\frac{2\pi(z+h)}{L} \right]}{\sinh \left(\frac{2\pi h}{L} \right)} \sin \theta \quad (2.27)$$

$$\zeta = \frac{H}{2} \frac{\sinh \left[\frac{2\pi(z+h)}{L} \right]}{\sinh \left(\frac{2\pi h}{L} \right)} \cos \theta \quad (2.28)$$

Rewriting Equations (2.27) and (2.28)

$$\sin^2 \theta = \left[\frac{\xi}{a} \frac{\sinh \left(\frac{2\pi h}{L} \right)}{\cosh \left[\frac{2\pi(z+h)}{L} \right]} \right]^2 \quad (2.29)$$

$$\cos^2 \theta = \left[\frac{\zeta}{a} \frac{\sinh \left(\frac{2\pi h}{L} \right)}{\sinh \left[\frac{2\pi(z+h)}{L} \right]} \right]^2 \quad (2.30)$$

Adding these equations leads

$$\frac{\xi^2}{A^2} + \frac{\zeta^2}{B^2} = 1 \quad (2.31)$$

where A and B are

$$A = \frac{H}{2} \frac{\cosh \left[\frac{2\pi(z+h)}{L} \right]}{\sinh \left[\frac{2\pi h}{L} \right]} \quad (2.32)$$

$$B = \frac{H}{2} \frac{\sinh \left(\frac{2\pi(z+h)}{L} \right)}{\sinh \left(\frac{2\pi h}{L} \right)} \quad (2.33)$$

Remembering that Equation (2.31) is the equation of an ellipse with a major- (horizontal) semi-axis equal to A and a minor (vertical) semi-axis equal to B . The lengths of A and B are measures of the horizontal and vertical displacements of the

water particles as shown in Figure 2.4. Hence, the water particles are predicted to move in closed orbits by linear wave theory; i.e., a fluid particle returns to its initial position after each wave cycle. However, comparing laboratory measurements of particle orbits with this theory shows that particle orbits are not completely closed. This difference between linear theory and observations is due to the mass transport which means that linear theory is insufficient to explain wave motion completely [1].

For deep water case ($h/L > 1/2$), Equation (2.32) and Equation (2.33) are equal to each other as

$$A = B = \frac{H}{2} e^{\left(\frac{2\pi z}{L}\right)} \quad (2.34)$$

and paths of the particle is circular as seen in Figure 2.4. For shallow-water case ($h/L < 1/25$), the same equations become

$$A = \frac{H}{2} \frac{L}{2\pi h} \quad (2.35)$$

$$B = \frac{H}{2} \left(1 + \frac{z}{h}\right) \quad (2.36)$$

As indicated by Equation (2.34), in deep water, the water particle orbits are circular. Meanwhile, Equations (2.35) and (2.36) show that in transitional and shallow water, the orbits are elliptical. The more shallow the water, the flatter the ellipse and the amplitude of the water particle displacement decreases exponentially with depth. In deep water regions the amplitude of the water particle displacement becomes small relative to the wave height, H , at a depth equal to one-half the wavelength below the free surface; i.e., when $z = L_0/2$. For shallow regions, horizontal particle displacement near the bottom can be large and the vertical displacement of water particles varies from a minimum of zero at the bottom to a maximum equal to one-half the wave height at the surface.

2.3 Dynamic Pressure

Subsurface pressure under a wave is the sum of dynamic and static pressures which is

$$p' = \frac{\rho g H \cosh \left[\frac{2\pi(z+h)}{L} \right]}{2 \cosh \left(\frac{2\pi h}{L} \right)} \cos \theta - \rho g z + p_a \quad (2.37)$$

where p' is the total pressure, p_a is the atmospheric pressure, and ρ is the mass density of water. The first term represents a dynamic component due to vertical acceleration and the second term is the static component of pressure. For convenience, the pressure is usually taken as the gauge pressure defined as

$$p = p' - p_a = \frac{\rho g H \cosh \left[\frac{2\pi(z+h)}{L} \right]}{2 \cosh \left(\frac{2\pi h}{L} \right)} \cos \theta - \rho g z \quad (2.38)$$

Noting that $\eta = \frac{H}{2} \cos \left(\frac{2\pi x}{L} - \frac{2\pi t}{T} \right) - \rho g z$ the above equation can be rewritten

$$p = \rho g \eta \frac{\cosh \left[\frac{2\pi(z+h)}{L} \right]}{\cosh \left(\frac{2\pi h}{L} \right)} - \rho g z \quad (2.39)$$

The pressure response factor is defined as

$$K_z = \frac{\cosh \left[\frac{2\pi(z+h)}{L} \right]}{\cosh \left(\frac{2\pi h}{L} \right)} \quad (2.40)$$

Substituting this expression into the Equation (2.39) leads

$$p = \rho g (\eta K_z - z) \quad (2.41)$$

For the pressure at the bottom $z = -h$ the response factor becomes

$$K_z = K = \frac{1}{\cosh \left(\frac{2\pi h}{L} \right)} \quad (2.42)$$

In Figure 2.5 the pressure response factors are given as the functions of h/L_0 . One can easily determine intermediate and shallow water values and choose the appropriate bottom pressure response factor K . Besides determining the ratios, c/c_0 , L/L_0 or k_0/k , other variables necessary for water wave calculations can be found. For determining

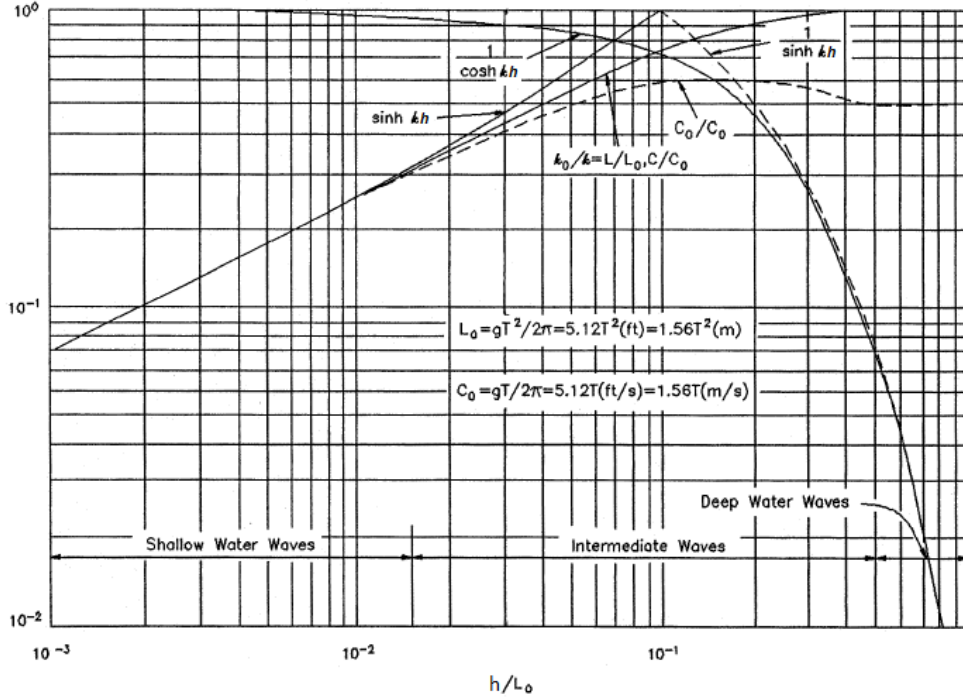


Figure 2.5: Variation of wave parameters with h/L_0 , adapted from Dean and Dalrymple [2].

the height of surface waves based on subsurface measurements of pressure, it is convenient to rewrite Equation (2.41)

$$\eta = \frac{N(p + \rho gz)}{\rho g K_z} \quad (2.43)$$

where z is the depth below the still water line of the pressure gauge and N is a correction factor equal to the unity if the linear theory applies [1]. Chakrabarti [39] presented experimental measurements that correlate dynamic pressure in the water column with linear wave theory. Although these laboratory measurements include a number of water depths, wave periods, and wave heights, the best agreement between the theory and these measurements occurs in deep water. Moreover, shallow water pressure measurements for steep water waves deviate significantly from the linear wave theory predictions.

2.4 Wave Groups

Speed of wave groups is an important tool to determine the propagation of wave energy in time and space. The speed of a group of waves or a wave train is generally not identical to the speed with which individual waves within the group travel. The group speed is termed the group velocity C_g ; the individual wave speed is the phase velocity or wave celerity.

For waves propagating in deep or transitional water with gravity as the primary restoring force, the group velocity will be less than the phase velocity. For those waves, propagated primarily under the influence of surface tension (i.e., capillary waves), the group velocity may exceed the velocity of an individual wave [1]. Interaction of two sinusoidal wave trains moving in the same direction with slightly different wavelengths and periods might be used to understand group velocity phenomena. The equation of the water surface of two components, η_1 and η_2 is

$$\eta = \eta_1 + \eta_2 = \frac{H}{2} \cos\left(\frac{2\pi x}{L_1} - \frac{2\pi t}{T_1}\right) + \frac{H}{2} \cos\left(\frac{2\pi x}{L_2} - \frac{2\pi t}{T_2}\right) \quad (2.44)$$

The surface profile which is developed can be seen in Figure 2.6. It is possible to sum up the two water surface elevation because superposition of solutions is permissible since the linear wave theory is used. For simplicity the heights of both wave components have been assumed to be equal. Since the wavelengths of the two component waves, L_1 and L_2 , have been assumed slightly different for some values of x at a given time, the two components will be in phase and the wave height observed will be $2H$; for some other values of x , the two waves will be completely out of phase and the resultant wave height will be zero.

The waves described in Figure 2.6 can be expressed by

$$\eta_{envelope} = \pm \cos\left[\pi\left(\frac{L_2 - L_1}{L_1 L_2}\right)x - \pi\left(\frac{T_2 - T_1}{T_1 T_2}\right)T\right] \quad (2.45)$$

The group velocity is represented by the speed of these groups. The limiting speed of the wave groups as they become large (i.e., as the wavelength L_1 approaches L_2

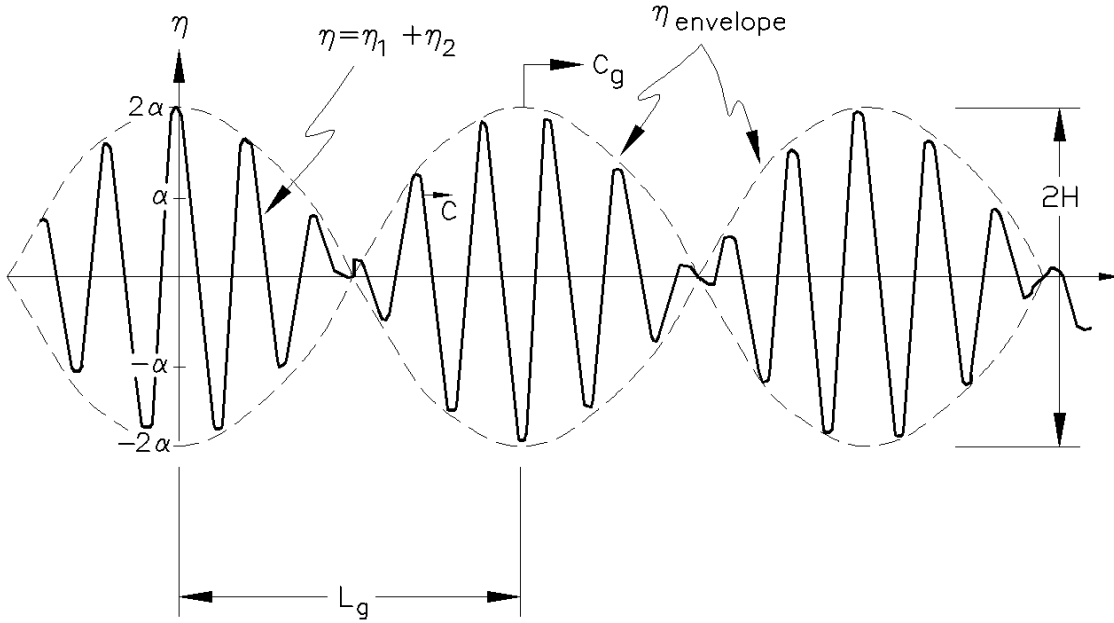


Figure 2.6: Wave group formed by the addition of two sinusoidal waves with slightly different periods, adapted from Coastal Engineering Manual [1].

and consequently the wave period T_1 approaches T_2) is the group velocity and can be shown to be equal to [1].

$$c_g = \frac{1}{2} \frac{L}{T} \left[1 + \frac{\frac{4\pi h}{L}}{\sinh\left(\frac{4\pi h}{L}\right)} \right] = nc \quad (2.46)$$

and n is

$$n = \frac{1}{2} \left[1 + \frac{\frac{4\pi h}{L}}{\sinh\left(\frac{4\pi h}{L}\right)} \right] \quad (2.47)$$

For the deep water case, the term $(4\pi h/L)/\sinh(4\pi h/L)$ approximately equals to zero hence $n = 1/2$, which leads

$$c_{g0} = \frac{1}{2} c_0 = \frac{1}{2} \sqrt{\frac{gL}{2\pi}} \quad (2.48)$$

or briefly one can say that group velocity is half of the phase velocity, $c_{g0} = c_0/2$. For the shallow water case in which the term is $\sinh(4\pi h/L \approx 4\pi h/L)$ which leads

$$c_{g_s} = c = \sqrt{gh} \quad (2.49)$$

in which the group velocity is equal to the phase velocity. Hence, in shallow water, since the wave celerity is determined by the water depth, all component waves in a wave train will travel at the same speed excluding the alternate reinforcing and canceling of components.

In deep and transitional waters, wave celerity depends on wavelength; hence, slightly longer waves travel slightly faster and produce the small phase differences resulting in wave groups. These waves are said to be dispersive or propagating in a dispersive medium; i.e., in a medium where their celerity is dependent on wavelength [1].

The ratios of group and phase velocities to the deep water phase velocity c_g/c_0 and c/c_0 respectively are given as a function of the depth relative to the deep water wavelength h/L_0 in Figure 2.7. In Figure 2.7, for small values of depth the two curves merge together and c_g reaches a maximum point before tending asymptotically toward $c/2$. Outside of shallow water zone, the phase velocity of gravity waves is greater than the group velocity. An observer who follows a group of waves at group velocity will see waves that originate at the back of the group move forward through the group traveling at the phase velocity and disappear at the front of the wave group.

The importance of group velocity is that it is the group velocity at which the wave energy is propagated. On the other hand Lamb [51] expressed that the group velocity can be obtained rigorously from the interference of two or more waves mathematically. However, the physical significance is not as obvious as it is in the method based on the consideration of wave energy. Therefore, wave energy and energy transmission is used for the additional explanation of group velocity.

2.5 Wave Energy and Energy Flux

The sum of kinetic energy and its potential energy gives the total energy of a wave system. The kinetic energy is that part of the total energy due to water particle

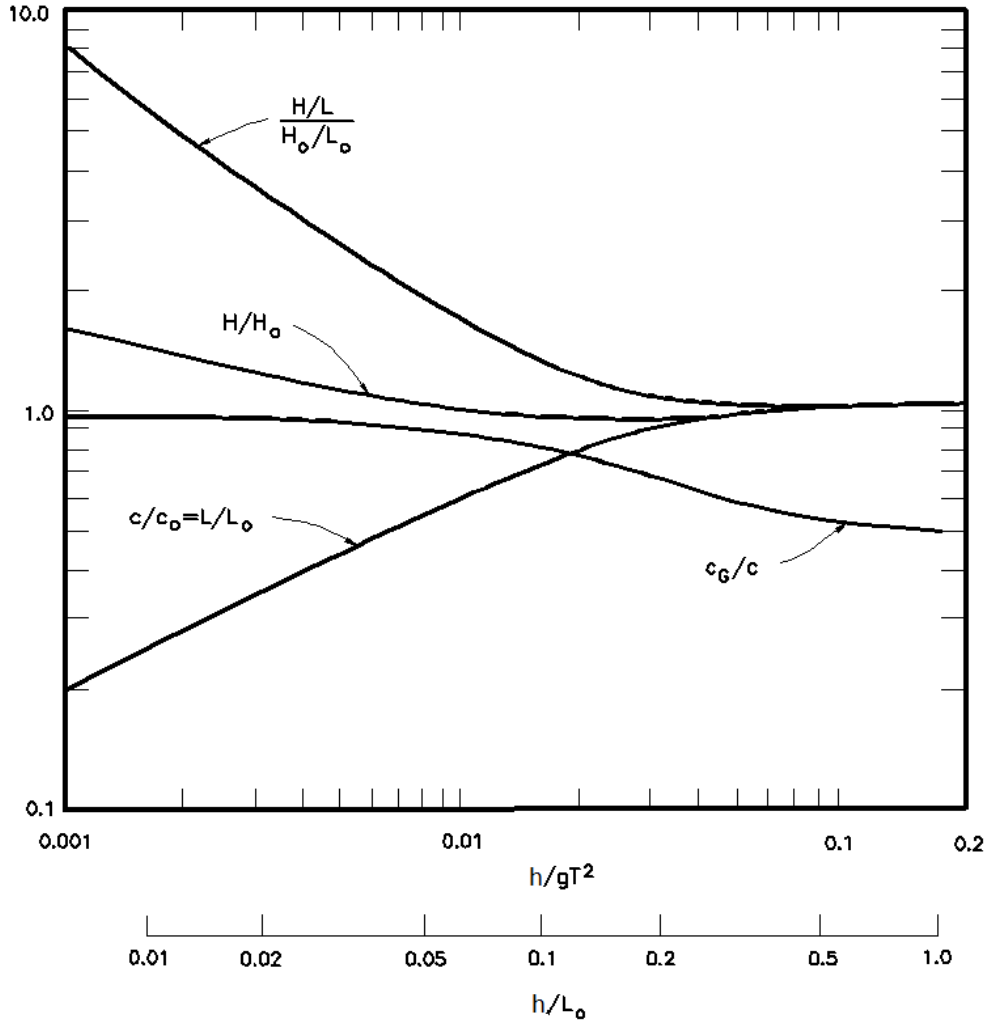


Figure 2.7: Variation of the ratios of group and phase velocities to deepwater phase speed using linear theory, adapted from Sarpkaya and Isaacson [3].

velocities associated with wave motion. The kinetic energy per unit length of wave crest for a wave defined with the linear theory can be found from

$$\bar{E}_k = \int_x^{x+L} \int_{-h}^{\eta} \rho \left(\frac{u^2 + w^2}{2} \right) dz dx \quad (2.50)$$

which is

$$\bar{E}_k = \frac{1}{16} \rho g H^2 L \quad (2.51)$$

Potential energy is that part of the energy resulting from part of the fluid mass being above the trough: the wave crest. The potential energy per unit length of wave crest

for a linear wave is given by

$$\bar{E}_p = \frac{1}{16} \rho g H^2 L \quad (2.52)$$

Thus, Airy theory says that if the potential energy is determined relative to still water level, and all waves are propagated in the same direction, potential and kinetic energy components are equal to each other and the total wave energy in one wavelength per unit crest width is given by

$$E = E_k + E_p = \frac{\rho g H^2 L}{16} + \frac{\rho g H^2 L}{16} = \frac{\rho g H^2 L}{8} \quad (2.53)$$

Total average wave energy per unit surface area which is called the specific energy or energy density is given by

$$\bar{E} = \frac{E}{L} = \frac{\rho g H^2}{8} \quad (2.54)$$

Wave energy flux is the rate at which energy is transmitted in the direction of wave propagation across a vertical plan perpendicular to the direction of wave advance and extending down the entire depth [1]. Assuming that linear theory is valid, the average energy flux per unit wave crest width transmitted across a vertical plane perpendicular to the direction of wave advance is

$$\bar{P} = \frac{1}{T} \int_t^{t+r} \int_{-h}^{\eta} p u dz dt \quad (2.55)$$

After integration,

$$\bar{P} = \bar{E} n c = \bar{E} c_g \quad (2.56)$$

where \bar{P} is wave power and the variable n was given in Equation (2.47). If a vertical plane is taken other than perpendicular to the direction of wave advance, $P = E c_g \sin \theta$, where θ is the angle between the plane across which the energy is being transmitted

and the direction of wave advance. For deep water Equation (2.56) becomes

$$\bar{P}_0 = \frac{1}{2} \bar{E}_0 c_0 \quad (2.57)$$

Likewise, for shallow water Equation (2.56) becomes

$$\bar{P} = \bar{E} c_g = \bar{E} c \quad (2.58)$$

For steady state, an energy balance for a region through which waves are passing will reveal that amount of energy entering the region will equal the amount leaving the region provided no energy is added or removed. Therefore, when the waves are moving so that their crests are parallel to the bottom contours

$$\bar{E}_0 n_0 c_0 = \bar{E} n c \quad (2.59)$$

or since $n_0 = \frac{1}{2}$, it can be rewritten as

$$\frac{1}{2} \bar{E}_0 c_0 = \bar{E} n c \quad (2.60)$$

When the wave crests are not parallel to the bottom contours, some parts of the wave will be traveling at different speeds and the wave will be refracted; in this case Equation (2.60) does not apply. The rate of energy transmission is important for coastal design, and it requires knowledge of c_g to determine how fast waves move toward shore. The mean rate of energy transmission associated with waves propagating into an area of calm water provides a different physical description of the concept of group velocity. Equation (2.60) establishes a relationship between the ratio of the wave height at some arbitrary depth and the deep water wave height. This ratio, known as the shoaling coefficient which is dependent on the wave steepness [1].

3. BOUSSINESQ EQUATIONS

Compared to the long wave equations the idea of Boussinesq formulation is to add in the effects of non-hydrostatic pressure, while eliminating the vertical coordinate. The procedure reduces the computational effort relative to a full three-dimensional solution. This principle was initially introduced by Boussinesq [6] who derived the new equations under the assumption that the magnitude of the vertical velocity increases parabolically from the bottom to the free surface. This assumption inevitably leads to a relative depth limitation in the accuracy of the embedded dispersive and nonlinear properties. This is the reason why Boussinesq-type equations are conventionally associated with somewhat shallow waters. As the water depth increases the errors modeling linear dispersion relationship increases and the classical Boussinesq equations are limited to relatively shallow waters. On the other hand, the increasing availability of the computer resources to run the numerical models and the development of variants of the theory which could be optimized to obtain better dispersion properties at larger values triggered further developments in Boussinesq models. For making Boussinesq equations applicable to relatively intermediate water depths, many researchers developed several ways to extend the validity of these equations. These extended Boussinesq equations have adjustable parameters to provide a better match with the exact dispersion relationship [52].

After Boussinesq's [6] depth-averaged model that included both weakly dispersive and nonlinear effects, Mei and LeMehaute [7] and Peregrine [8] derived Boussinesq equations for variable depth. While Mei and LéMehauté [7] used the velocity at the bottom as the dependent variable Peregrine [8] used the depth-averaged velocity. In the following years Peregrine's derivation is referred to as the standard Boussinesq equations. In general, Peregrine described the nonlinear transformation of irregular and multidirectional waves in shallow water where the vertical velocity is assumed to

vary linearly over the depth. However, the standard Boussinesq equations derived by Peregrine [8] are applicable to relatively shallow water depths.

3.1 Nonlinear Long Waves in Shallow Water: Derivation and Classification of Approximate Equations

The linearized shallow-water approximation is useful only if the two length ratios are small; $\mu \equiv kh \ll 1$ and $\varepsilon \equiv a/h \ll 1$ where a typical free surface amplitude and h is depth. A nonlinear theory of shallow water waves is necessary for dealing with coastal engineering problems. The presence of two small parameters (three length scales) add extra challenges into the approximation process since the magnitude of one ratio relative to the other is now important. Airy, Boussinesq [6] with Korteweg and de Vries [53] separately developed two theories which led to opposite conclusions regarding wave breaking on constant depth. Ursell [54] resolved this confusion by introducing a ratio which is used to decide which theory should be chosen. This ratio is referred to as Ursell parameter and given as,

$$U_r = \frac{a}{h} \frac{1}{(kh)^2} = \frac{ka}{(kh)^3} = \frac{aL^2}{h^3(2\pi)^2} \quad (3.1)$$

For long waves ($L \gg h$) with small Ursell number, $U_r \ll 32\pi^2/3 \approx 100$, linear wave theory is applicable. Otherwise, a nonlinear theory for fairly long waves ($L > 7h$), like the Korteweg-de Vries equation or Boussinesq equations has to be used. The approximation procedure for constant depth is demonstrated by using the formalism of Benney [55] and Peregrine [8]. Since there are two small parameters, it is useful to utilize dimensionless variables where the scales of these variables are suggested by the linearized theory:

$$\begin{aligned} (x', y') &= k(x, y), & z' &= \frac{z}{h}, & t' &= k(gh)^{1/2}t \\ \eta' &= \frac{\eta}{a}, & \Phi' &= \Phi \left[\frac{a}{kh} (gh)^{1/2} \right]^{-1} \end{aligned} \quad (3.2)$$

The normalizations on velocity components are shown as,

$$(u, v) = \left(\frac{\partial}{\partial x}, \frac{\partial}{\partial y} \right) \Phi = \frac{a}{h} (gh)^{1/2} \left(\frac{\partial}{\partial x'}, \frac{\partial}{\partial y'} \right) \Phi' = \frac{a}{h} (gh)^{1/2} (u', v')$$

$$w = \frac{\partial \Phi}{\partial z} = \frac{1}{kh} \frac{a}{h} (gh)^{1/2} \frac{\partial \Phi'}{\partial z'} = \frac{1}{kh} \frac{a}{h} (gh)^{1/2} (w') \quad (3.3)$$

Scaling horizontal and vertical components are different and is required by continuity.

The normalized equations are,

$$\mu^2 (\Phi'_{x'x'} + \Phi'_{y'y'}) + \Phi'_{z'z'} = 0, \quad -1 < z' < \varepsilon \eta' \quad (3.4)$$

$$\mu^2 [\eta'_{z'} + \varepsilon \Phi'_{x'} \eta'_{x'} + \varepsilon \Phi'_{y'} \eta'_{y'}] = \Phi'_{z'}, \quad z' = \varepsilon \eta' \quad (3.5)$$

$$\mu^2 [\Phi'_{z'} + \eta'] + \frac{1}{2} \varepsilon [\mu^2 (\Phi'^2_{x'} + \Phi'^2_{y'}) + \Phi'^2_{z'}], \quad z' = \varepsilon \eta' \quad (3.6)$$

$$\Phi'_{z'} = 0, \quad z = -1 \quad (3.7)$$

Note that the primes will be ignored after this step and $\mu = kh$ is assumed to be small and ε is left to be arbitrary for the time being. Remembering that Φ is analytic, it can be expanded as a power series in the vertical coordinate,

$$\Phi(x, y, z, t) = \sum_{n=0}^{\infty} (z+1)^n \Phi_n \quad (3.8)$$

where $\Phi_n = \Phi_n(x, y, t), n = 0, 1, 2, 3, \dots$, whose orders of magnitude are yet unknown.

To denote horizontal gradient $(\frac{\partial}{\partial x}, \frac{\partial}{\partial y})$, ∇ is used and derivatives are evaluated as,

$$\nabla \Phi = \sum_0^{\infty} (z+a)^n \nabla \Phi_n \quad (3.9)$$

$$\nabla^2 \Phi = \sum_0^{\infty} (z+1)^n \nabla^2 \Phi_n \quad (3.10)$$

$$\frac{\partial \Phi}{\partial z} = \sum_0^{\infty} (z+1)^{n-1} \Phi_n = \sum_0^{\infty} (z+1)^n (n+1) \Phi_{n+1} \quad (3.11)$$

$$\frac{\partial^2 \Phi}{\partial z^2} = \sum_0^{\infty} (z+1)^{n-1} (n+1)n \Phi_{n+1} = \sum_0^{\infty} (z+1)^n (n+2)(n+1) \Phi_{n+2} \quad (3.12)$$

Substituting Equations (3.10) and (3.12) into the Laplace equation leads to

$$\mu^2 \nabla^2 \Phi + \frac{\partial^2}{\partial z^2} \Phi = \sum_{n=0}^{\infty} (z+1)^n [\mu^2 \nabla^2 \Phi_n + (n+2)(n+1) \Phi_{n+2}] = 0 \quad (3.13)$$

The coefficient of each power of $(z+1)$ vanishes since z is arbitrary within $(-1, \varepsilon \eta)$ and this yields a recursive relation which is,

$$\Phi_{n+2} = \frac{-\mu^2 \nabla^2 \Phi_n}{(n+2)(n+1)}, \quad n = 0, 1, 2, \dots \quad (3.14)$$

Equation (3.7) leads to $\Phi_1 \equiv 0$ on the horizontal bottom which implies from Equation (3.14) that all Φ_n 's with odd n vanish

$$\Phi_1 = \Phi_3 = \Phi_5 = \dots = 0 \quad (3.15)$$

For even n ,

$$\begin{aligned} \Phi_2 &= \frac{-\mu^2}{2 \cdot 1} \nabla^2 \Phi_0 = \frac{-\mu^2}{2!} \nabla^2 \Phi_0 \\ \Phi_4 &= \frac{-\mu^2}{4 \cdot 3} \nabla^2 \Phi_2 = \frac{\mu^4}{4!} \nabla^2 \nabla^2 \Phi_0 \\ \Phi_6 &= \frac{-\mu^2}{6 \cdot 5} \nabla^2 \Phi_4 = \frac{-\mu^6}{6!} \nabla^2 \nabla^2 \nabla^2 \Phi_0 \end{aligned} \quad (3.16)$$

Noting that $\Phi_0 = O(\phi) = O(1)$ yields $\Phi_2 = O(\mu^2)$ and $\Phi_4 = O(\mu^4)$ and so on. The potential with an error of $O(\mu^6)$ is,

$$\Phi = \Phi_0 - \frac{\mu^2}{2} (z+1)^2 \nabla^2 \Phi_0 + \frac{\mu^4}{24} (z+1)^4 \nabla^2 \nabla^2 \Phi_0 + O(\mu^6) \quad (3.17)$$

Using the boundary conditions on the free surface and keeping $O(\mu^4)$ terms in Φ_t , Φ_x and Φ_y because of the multiplier μ^2 ,

$$\mu^2 \left[\frac{H_t}{\varepsilon} + \nabla H \cdot \left(\nabla \Phi_0 - \frac{\mu^2}{2} H^2 \nabla^2 \nabla \Phi_0 \right) \right] = -\mu^2 H \nabla^2 \Phi_0 + \frac{\mu^4}{6} H^3 \nabla^2 \nabla^2 \Phi_0 + O(\mu^6) \quad (3.18)$$

$$\begin{aligned} \mu^2 \left[\Phi_{0t} - \frac{\mu^2}{2} H^2 \nabla^2 \Phi_{0t} + \eta \right] &+ \frac{1}{2} \varepsilon \mu^2 [(\nabla \Phi_0)^2 - \mu^2 H^2 \nabla \Phi_0 \cdot \nabla^2 (\nabla \Phi_0)] \\ &+ \frac{1}{2} \varepsilon \mu^4 H^2 (\nabla^2 \Phi_0)^2 = O(\mu^6) \end{aligned} \quad (3.19)$$

where H is total depth and equals to $H = 1 + \varepsilon \eta$. Defining horizontal velocity at the bottom as $u_0 = \nabla \Phi_0$, equation (3.18) can be rewritten,

$$\frac{1}{\varepsilon} H_t + \nabla H \cdot \left(u_0 - \frac{\mu^2}{2} H^2 \nabla^2 u_0 \right) + H \nabla \cdot u_0 - \frac{\mu^2}{6} H^3 \nabla^2 (\nabla \cdot u_0) = O(\mu^4) \quad (3.20)$$

The gradient of equation (3.19) yields,

$$u_{0t} + \varepsilon u_0 \cdot \nabla u_0 + \frac{\nabla H}{\varepsilon} + \mu^2 \nabla \left[-\frac{\varepsilon}{2} H^2 u_0 \cdot \nabla^2 u_0 + \frac{\varepsilon}{2} H^2 (\nabla \cdot u_0)^2 - \frac{1}{2} H^2 \nabla \cdot u_{0t} \right] = O(\mu^4) \quad (3.21)$$

Solving η and u_0 , the actual velocity components are,

$$(u, v) = \nabla \Phi = u_0 - \frac{\mu^2}{2} (z+1)^2 \nabla \nabla \cdot u_0 + O(\mu^4) \quad (3.22)$$

$$w = \frac{\partial \Phi}{\partial z} = -\mu^2 (z+1) \nabla^2 \Phi_0 = \mu^2 (z+1) \nabla \cdot u_0 + O(\mu^4) \quad (3.23)$$

From the Bernoulli equation, the dimensionless form of the pressure field is which is normalized by ρgh is,

$$-P = z + \varepsilon \left\{ \Phi_t + \frac{\varepsilon}{2} \left[(\nabla \Phi)^2 + \frac{1}{\mu^2} \Phi_z^2 \right] \right\} \quad (3.24)$$

Substituting equations (3.22) and (3.23) into equation (3.24) one gets,

$$\begin{aligned} -P = z &+ \varepsilon \left\{ \left[\Phi_{0t} - \frac{\mu^2}{2} (z+1)^2 \nabla \cdot u_{0t} \right] \right. \\ &+ \left. \frac{\varepsilon}{2} [u_0^2 - \mu^2 (z+1)^2 u_0 \cdot \nabla^2 u_0 + \mu^2 (z+1)^2 (\nabla \cdot u_0)^2] \right\} + O(\mu^4) \end{aligned} \quad (3.25)$$

For eliminating Φ_0 , Equation (3.19) is used which yields,

$$P = (\varepsilon\eta - z) - \frac{\varepsilon\mu^2}{2}[H^2 - (z+1)^2] \times \{\nabla \cdot u_{0t} + \varepsilon[u_0 \cdot \nabla^2 u_0 - (\nabla \cdot u_0)^2]\} + O(\mu^4) \quad (3.26)$$

However, instead of using u_0 a depth averaged horizontal velocity \bar{u} can be introduced such as,

$$\begin{aligned} \bar{u} &= \frac{1}{H} \int_{-1}^{\varepsilon\eta} dz \nabla \Phi \\ &= \frac{1}{H} \int_{-1}^{\varepsilon\eta} dz \left(u_0 - \frac{\mu^2}{2} (z+1)^2 \nabla \nabla \cdot u_0 + \dots \right) \\ &= u_0 - \frac{\mu^2}{6} H^2 \nabla^2 u_0 + O(\mu^4) \end{aligned} \quad (3.27)$$

which can be inverted to give

$$u_0 = \bar{u} + \frac{\mu^2}{6} H^2 \nabla^2 \bar{u} + O(\mu^4) \quad (3.28)$$

Substituting Equation (3.28) into Equation (3.20) yields,

$$H_t + \varepsilon \nabla \cdot (H\bar{u}) = 0 \quad (3.29)$$

Note that this equation is just the depth averaged law of continuity and is exact to all orders of μ^2 . If u_0 is expressed in terms of \bar{u} ,

$$\begin{aligned} \bar{u}_t &+ \varepsilon \bar{u} \cdot \bar{u} + \frac{\nabla H}{\varepsilon} + \frac{\mu^2}{6} \left(\frac{H^2}{2} \nabla^2 \bar{u} \right)_t \\ &+ \mu^2 \nabla \left\{ -\frac{\varepsilon}{3} H^2 \bar{u} \cdot \nabla^2 \bar{u} + \frac{\varepsilon}{2} H^2 (\nabla \cdot \bar{u})^2 - \frac{H^2}{2} \nabla \cdot \bar{u}_t \right\} = O(\mu^4) \end{aligned} \quad (3.30)$$

Note that all the equations thus far are valid for arbitrary ε and extension to higher orders in μ^2 is unnecessary. Expressing Equations (3.29), (3.30) and (3.26) in physical variables leads,

$$H_t + \nabla \cdot (H\bar{u}) = 0 \quad (3.31)$$

$$\bar{u}_t + \bar{u} \cdot \nabla \bar{u} + g \nabla H + \frac{1}{6} (H^2 \nabla^2 \bar{u})_t + \nabla \left\{ -\frac{1}{3} H^2 \bar{u} \cdot \nabla^2 \bar{u} + \frac{H^2}{2} (\nabla \cdot \bar{u})^2 - \frac{H^2}{2} \nabla \cdot \bar{u}_t \right\} = 0 \quad (3.32)$$

$$P = \rho g (\eta - z) - \frac{1}{2} [H^2 - (z+h)^2] \{ \nabla \cdot u_t + [u \cdot \nabla^2 u - (\nabla \cdot u)^2] \} \quad (3.33)$$

There are two limiting cases; namely, long wave equations and Boussinesq equations.

3.1.1 Airy's theory for very long waves

As it is mentioned before, Airy's theory is proper approximation for very long waves of finite amplitude and within this approximation the pressure is hydrostatic. The limiting case is when $\rho \rightarrow 0$ and $\varepsilon = O(1)$. Neglecting the terms proportional to μ^2 from Equations (3.26) and (3.30), the physical variables are obtained as,

$$\eta_t + \nabla \cdot [(\eta + h)\bar{u}] = 0 \quad (3.34)$$

$$\bar{u}_t + \bar{u} \cdot \nabla \bar{u} + g \nabla \eta = 0 \quad (3.35)$$

$$P = \rho g (\eta - z) \quad (3.36)$$

The previous equations are actually valid for variable $h(x, y)$.

3.1.2 Boussinesq theory

The limiting case is when $O(\varepsilon) = O(\mu^2) < 1$. For weakly nonlinear and moderately long waves in shallow water, Equations (3.29), (3.30) and (3.26) are approximated in order to include the terms of order $O(\varepsilon)$ and $O(\mu^2)$ by obtaining,

$$\eta_t + \nabla \cdot [(\varepsilon \eta + 1)\bar{u}] = 0 \quad (3.37)$$

$$\bar{u}_t + \varepsilon \bar{u} \cdot \nabla \bar{u} + \nabla \eta - \frac{\mu^2}{3} \nabla \nabla \cdot \bar{u}_t = 0 \quad (3.38)$$

$$P = \varepsilon \eta - z + \frac{\varepsilon \mu^2}{2} (z^2 + 2z) \nabla \cdot \bar{u}_t \quad (3.39)$$

The corresponding physical variables are,

$$\eta_t + \nabla \cdot [(\eta + h)\bar{u}] = 0 \quad (3.40)$$

$$\bar{u}_t + \bar{u} \cdot \nabla \bar{u} + g \nabla \eta - \frac{h^2}{3} \nabla \nabla \cdot \bar{u}_t = 0 \quad (3.41)$$

$$P = \rho g(\eta - z) + \frac{\rho}{2} (2zh + z^2) \nabla \cdot \bar{u}_t \quad (3.42)$$

Equations (3.37) and (3.38) or their equivalents Equations (3.40) and (3.41) are called Boussinesq equations. Note that the pressure is not hydrostatic. Airy's and Boussinesq's theories differ by the linear term multiplied by μ^2 in Equation (3.38). However, this term has a significant importance. For instance, using the linearized forms of Equations (3.40) and (3.41) for one-dimensional infinitesimal waves,

$$\eta = Ae^{i(kx - \omega t)}, \quad \bar{u} = Ue^{i(kx - \omega t)} \quad (3.43)$$

After neglecting the exponential factor,

$$-i\omega A + ikhU = 0 \quad (3.44)$$

$$i\omega U + ikgA - \frac{h^2}{3} (ik)^2 (-i\omega)U = 0 \quad (3.45)$$

which is a homogeneous set of equations for A and U . For a nontrivial solution the discriminant must vanish,

$$\begin{aligned} & \begin{vmatrix} -i\omega & ikh \\ igk & -i\omega \left(1 + \frac{k^2 h^2}{3}\right) \end{vmatrix} = 0 \\ \omega^2 &= \frac{ghk^2}{1 + \frac{1}{3}k^2 h^2} = ghk^2 \left(1 - \frac{k^2 h^2}{3} + \dots\right) \\ c &\cong (gh)^{1/2} \left(1 - \frac{k^2 h^2}{3}\right)^{1/2} \end{aligned} \quad (3.46)$$

where c is the phase velocity. The terms $\frac{1}{3}(kh)^2 = \frac{1}{3}\mu^2$ represents the frequency dispersion and arises from the term $\left(\frac{1}{3}h^2\right)u_{xxt}$. Note that Equation (3.46) is the regular

dispersion relation which is expanded with two-term. Boussinesq equations includes the effects of nonlinearity with ε and dispersion μ^2 to the leading order. When $\varepsilon \gg \mu^2$ they reduce to Airy equations which are valid for all ε . When $\varepsilon \ll \mu^2$, they reduce to the linearized approximation with weak dispersion. As $\varepsilon \rightarrow 0$ and $\mu^2 \rightarrow 0$ the classical linearized wave equation is obtained.

3.1.3 Variable depth

The procedure beginning from Equation (3.8) may be extended, if the horizontal scale of depth variation is not greater than the typical wavelength. The bottom boundary condition by means of physical variables is,

$$\Phi_z = -h_x \Phi_x - h_y \Phi_y, \quad z = -h(x, y) \quad (3.47)$$

In dimensionless variables the same condition becomes

$$\Phi_z = -\mu^2 (h_x \Phi_x + h_y \Phi_y), \quad z = -h(x, y) \quad (3.48)$$

in which the variable depth is normalized by the typical depth h_0 . It is also used in defining the dimensionless variables of Equations (3.2) and (3.3). Instead of Equation (3.8) one may assume,

$$\Phi = \sum_{n=0}^{\infty} [z + h(x, y)]^n \Phi_n(x, y) \quad (3.49)$$

Substituting Equation (3.49) into the Laplace equation and applying Equation (3.48), a set of recursive relations among Φ_n are obtained. For odd n , the Φ_n 's do not vanish. According to the similar arguments Mei and LèMehautè [7] obtained the Boussinesq equations for one-dimensional waves. For two dimensions the following equations were deduced by Peregrine [8] in terms of \bar{u} and η .

$$\eta_t + \nabla \cdot [(h + \eta)\bar{u}] = 0 \quad (3.50)$$

$$\frac{\partial \bar{u}}{\partial t} + \bar{u} \cdot \nabla \bar{u} + g \nabla \eta = \frac{h}{2} \nabla [\nabla \cdot (h \bar{u}_t)] - \frac{h^2}{6} \nabla [\nabla \cdot \bar{u}_t] \quad (3.51)$$

3.2 The Mathematical Framework for Nonlinear, Dispersive Shallow Water Waves

Based on the initial assumptions of an inviscid, incompressible Newtonian fluid, the mathematical framework for the analysis of nonlinear, dispersive shallow-water waves is outlined in this section and the non-dimensionalisation and scaling of the equations are described. Note that the derivation procedure for Boussinesq-type shallow water equations is not unique and a variety of different equation systems have been proposed, for instance [10], [12], [13] and [48]. The derivation of classical form of the Boussinesq equations are given in this chapter where the derivation procedure followed Peregrine's work but includes the effect of a spatially varying depth to derive the variable depth equation system.

The incompressible Navier-Stokes equations are capable of modeling water waves. However, the numerical solution of these equations is very complex since the wave phenomenon is a three-dimensional problem with unknown free surface boundary conditions. Since the viscosity is negligible in wave motion the Euler equations may be used instead of the Navier-Stokes equations.

The Euler equations for an inviscid, incompressible, irrotational flow with a free surface over a horizontal bottom are used for deriving Boussinesq equations describing shallow water flows by Peregrine [48]. Vorticity can diffuse from the boundary once the fluid is in motion but for a finite time the effects will not be felt throughout the fluid. The Boussinesq equations describing shallow water flow are derived from the incompressible, irrotational Euler equations as it is been indicated in Peregrine's study [48]. There are two spatial dimensions are considered; (x, z) being horizontal and vertical respectively. The z coordinate varies between the free surface $\eta(x, t)$ and the sea bed $-h(x)$ with the origin taken at the still-water depth. The governing equations are horizontal momentum, vertical momentum, incompressibility and irrotationality equations respectively. These equations are written in terms of the two-dimensional velocity field (u, w) , pressure p , constant density ρ and acceleration due to gravity g

with respect to the coordinate system (x, z) and time t .

$$\frac{\partial u}{\partial t} + u \frac{\partial u}{\partial x} + w \frac{\partial u}{\partial z} + \frac{1}{\rho} \frac{\partial p}{\partial x} = 0 \quad (3.52)$$

$$\frac{\partial w}{\partial t} + u \frac{\partial w}{\partial x} + w \frac{\partial w}{\partial z} + \frac{1}{\rho} \frac{\partial p}{\partial z} + g = 0 \quad (3.53)$$

$$\frac{\partial u}{\partial x} + \frac{\partial w}{\partial z} = 0 \quad (3.54)$$

$$\frac{\partial u}{\partial z} - \frac{\partial w}{\partial x} = 0 \quad (3.55)$$

At the free surface $z = \eta(x, t)$ the particles are free to move with the fluid velocity, hence there is a kinematic boundary condition,

$$w - u \frac{\partial \eta}{\partial x} - \frac{\partial \eta}{\partial t} = 0 \quad (3.56)$$

At the surface it is also assumed that surface tension is negligible and that there are no applied stresses [48], hence there is a simple constant pressure boundary condition where the constant pressure is set to a reference level zero at the free surface.

$$p = 0 \quad (3.57)$$

The bottom boundary $z = -h(x)$ is assumed to be fixed and impermeable and hence the kinematic boundary condition reduces to,

$$w + u \frac{\partial h}{\partial x} = 0 \quad (3.58)$$

3.2.1 Non-dimensionalization and scaling

The parameters ρ , g , and H are chosen to non-dimensionalize the system variables, where H is a typical water depth eg. the average depth. This choice follows the work

of Peregrine [8], but is not unique.

$$\begin{aligned} \tilde{x} = \frac{x}{H}, \quad \tilde{z} = \frac{z}{H}, \quad \tilde{h} = \frac{h}{H}, \quad \tilde{\eta} = \frac{\eta}{H}, \quad \tilde{t} = \sqrt{\frac{g}{H}}t & \quad (3.59) \\ \tilde{u} = \frac{u}{\sqrt{gH}}, \quad \tilde{w} = \frac{w}{\sqrt{gH}}, \quad \tilde{p} = \frac{p}{\rho gH} & \end{aligned}$$

For examining the magnitude of each term, scaling the individual variables is necessary so that every aspect of the problem has variation $O(1)$. The physical system can be characterized by the typical water depth H , a typical wavelength L and a typical wave amplitude a . The nonlinearity and dispersion present in the system are parameterized by the ratios ε and μ respectively [48].

$$\varepsilon = \frac{a}{H} \quad (3.60)$$

$$\mu = \frac{H}{L} \quad (3.61)$$

As explained in Chapter 2, Ursell [54] established a correlation number known as Ursell number,

$$Ur = \frac{\varepsilon}{\mu^2} = \frac{aL^2}{H^3} \quad (3.62)$$

where it predicts which wave theory is applicable. The Boussinesq wave theory requires $\varepsilon \ll 1$, $\mu \ll 1$ and Ur to be $O(1)$ [54]. Afterwards, the equation system can be derived from the suitably scaled and non-dimensionalised fluid flow equations by integrating through the depth and then expanding in terms of the small parameters μ and ε . Terms up to and including $O(\varepsilon, \mu^2)$ are retained. In order to change scaled coordinate \hat{x} as $O(1)$ over one wavelength, the horizontal coordinate is scaled. Time is also scaled considering this situation since the flow will be horizontal to first order and this choice will produce an $O(1)$ horizontal velocity. The free surface elevation is scaled similarly as to be $O(1)$ compared to a typical wave amplitude.

$$\hat{x} = \mu\tilde{x}, \quad \hat{t} = \mu\tilde{t}, \quad \hat{\eta} = \frac{\tilde{\eta}}{\varepsilon} \quad (3.63)$$

Considering the free surface boundary condition (3.56) and the continuity equation (3.54) yields the following scaled velocities.

$$\hat{u} = \frac{\tilde{u}}{\varepsilon}, \quad \hat{w} = \frac{\tilde{w}}{\varepsilon\mu} \quad (3.64)$$

All the other variables are assumed to have scaling factors 1. Substituting these new variables into the equations (3.52)-(3.55) gives,

$$\varepsilon \frac{\partial \hat{u}}{\partial \hat{t}} + \varepsilon^2 \hat{u} \frac{\partial \hat{u}}{\partial \hat{x}} + \varepsilon^2 \hat{w} \frac{\partial \hat{u}}{\partial \hat{z}} + \frac{\partial \tilde{p}}{\partial \hat{x}} = 0 \quad (3.65)$$

$$\varepsilon\mu^2 \frac{\partial \hat{w}}{\partial \hat{t}} + \varepsilon^2\mu^2 \hat{u} \frac{\partial \hat{w}}{\partial \hat{x}} + \varepsilon^2\mu^2 \hat{w} \frac{\partial \hat{w}}{\partial \hat{z}} + \frac{\partial \hat{p}}{\partial \hat{z}} + 1 = 0 \quad (3.66)$$

$$\frac{\partial \hat{u}}{\partial \hat{x}} + \frac{\partial \hat{w}}{\partial \hat{z}} = 0 \quad (3.67)$$

$$\frac{\partial \hat{u}}{\partial \hat{z}} - \mu^2 \frac{\partial \hat{w}}{\partial \hat{x}} = 0 \quad (3.68)$$

At the free surface $\hat{z} = \varepsilon \hat{\eta}$, the boundary conditions equations (3.56) and (3.57) become,

$$\hat{w} - \varepsilon \hat{u} \frac{\partial \hat{\eta}}{\partial \hat{x}} - \frac{\partial \hat{\eta}}{\partial \hat{t}} = 0 \quad (3.69)$$

$$\tilde{p} = 0 \quad (3.70)$$

At the bed $\hat{z} = -\tilde{h}$ the kinematic bottom boundary condition (3.58) becomes,

$$\hat{w} + \hat{u} \frac{\partial \tilde{h}}{\partial \hat{x}} = 0 \quad (3.71)$$

These equations shows a non-dimensionalised, scaled system for small amplitude nonlinear water waves and are the basis for the derivation of all the Boussinesq-type shallow water equations.

3.3 The Classical Form of the Boussinesq Equations for Constant Depth

Peregrine's study [48] includes a precise mathematical framework for the rigorous derivation of water wave equations. In his study one-dimensional system of Boussinesq equation is described by means of small amplitude nonlinear water waves in a constant depth environment which are derived by expanding equations (3.65)-(3.71) in terms of the small parameters ε and μ . Peregrine's derivation of one-dimensional Boussinesq equations is shown here in detail with the effects of a variable depth. Although the depth is assumed constant at the beginning, terms including a variation in depth are not neglected and the extension to the depth variable equations, stated by Peregrine [48], follows straightforwardly afterwards.

Integrating equation (3.67) with respect to \tilde{z} and applying Leibniz Rule gives,

$$\begin{aligned}\int_{-\tilde{h}}^{\tilde{z}} \frac{\partial \hat{w}}{\partial \tilde{z}} d\tilde{z} &= - \int_{-\tilde{h}}^{\tilde{z}} \frac{\partial \hat{u}}{\partial \hat{x}} d\tilde{z} \\ \hat{w}|_{\tilde{z}} - \hat{w}|_{-\tilde{h}} &= - \frac{\partial}{\partial \hat{x}} \int_{-\tilde{h}}^{\tilde{z}} \hat{u} d\tilde{z} - \hat{u}|_{-\tilde{h}} \frac{\partial(-\tilde{h})}{\partial \hat{x}} + \hat{u}|_{\tilde{z}} \frac{\partial(\tilde{z})}{\partial \hat{x}}\end{aligned}$$

Considering that the coordinates \hat{x} and \hat{z} are independent and using the boundary condition (3.71) at $\tilde{z} = -\tilde{h}$ gives,

$$\hat{w} = - \frac{\partial}{\partial \hat{x}} \int_{-\tilde{h}}^{\tilde{z}} \hat{u} d\tilde{z} \quad (3.72)$$

Noting that the vertical velocity $\hat{w}|_{\tilde{z}}$ is denoted by \hat{w} . Substituting equation (3.72) into equation (3.68) and integrating with respect to \tilde{z} gives,

$$\begin{aligned}\frac{\partial \hat{u}}{\partial \tilde{z}} &= \mu^2 \frac{\partial \hat{w}}{\partial \hat{x}} \\ &= -\mu^2 \frac{\partial^2}{\partial \hat{x}^2} \int_{-\tilde{h}}^{\tilde{z}} \hat{u} d\tilde{z}\end{aligned} \quad (3.73)$$

$$\hat{u} = \hat{u}_0(\tilde{x}, \tilde{t}) + O(\mu^2) \quad (3.74)$$

where $\hat{u}_0(\hat{x}, \hat{t})$ is an arbitrary function of \hat{x} and \hat{t} . Hence, equation (3.74) implies that \hat{u} is independent of \tilde{z} to $O(\mu^2)$. Noting that \hat{u} is independent from \tilde{z} to evaluate the integral and substituting equation (3.74) into equation (3.72) one obtains an expression for the vertical velocity \hat{w} .

$$\begin{aligned}\hat{w} &= -\frac{\partial}{\partial \hat{x}} \int_{-\tilde{h}}^{\tilde{z}} \hat{u}_0(\hat{x}, \hat{t}) + O(\mu^2) \\ &= -\frac{\partial}{\partial \hat{x}} ((\tilde{z} + \tilde{h})\hat{u}_0) + O(\mu^2) \\ &= -\tilde{z} \frac{\partial \hat{u}_0}{\partial \hat{x}} - \frac{\partial(\tilde{h}\hat{u}_0)}{\partial \hat{x}} + O(\mu^2)\end{aligned}\quad (3.75)$$

Substituting equation (3.75) into equation (3.68) and integrating with respect to \tilde{z} , an expression for \hat{u} is obtained.

$$\frac{\partial \hat{u}}{\partial \tilde{z}} = -\mu^2 \left(\tilde{z} \frac{\partial^2 \hat{u}_0}{\partial \hat{x}^2} + \frac{\partial^2(\tilde{h}\hat{u}_0)}{\partial \hat{x}^2} \right) + O(\mu^4) \quad (3.76)$$

$$\hat{u} = \hat{u}_0(\hat{x}, \hat{t}) - \mu^2 \left(\frac{\tilde{z}^2}{2} \frac{\partial^2 \hat{u}_0}{\partial \hat{x}^2} + \tilde{z} \frac{\partial^2(\tilde{h}\hat{u}_0)}{\partial \hat{x}^2} \right) + O(\mu^4) \quad (3.77)$$

The expression for pressure is rewritten by using equations (3.66) and (3.75).

$$\begin{aligned}-\frac{\partial \tilde{p}}{\partial \tilde{z}} &= \varepsilon \mu^2 \frac{\partial \hat{w}}{\partial \hat{t}} + 1 + O(\varepsilon^2 \mu^2) \\ &= -\varepsilon \mu^2 \left(\tilde{z} \frac{\partial^2 \hat{u}_0}{\partial \hat{x} \partial \hat{t}} + \frac{\partial^2(\tilde{h}\hat{u}_0)}{\partial \hat{x} \partial \hat{t}} \right) + 1 + O(\varepsilon^2 \mu^2, \varepsilon \mu^4)\end{aligned}\quad (3.78)$$

where it is integrated with respect to \tilde{z} from an arbitrary depth \tilde{z} to the free surface $\varepsilon \hat{\eta}$ which yields,

$$-\int_{\tilde{z}}^{\varepsilon \hat{\eta}} \frac{\partial \tilde{p}}{\partial \tilde{z}} d\tilde{z} = -\varepsilon \mu^2 \left[\frac{\tilde{z}^2}{2} \frac{\partial^2 \hat{u}_0}{\partial \hat{x} \partial \hat{t}} + \tilde{z} \frac{\partial^2(\tilde{h}\hat{u}_0)}{\partial \hat{x} \partial \hat{t}} \right]_{\tilde{z}}^{\varepsilon \hat{\eta}} + [\tilde{z}]_{\tilde{z}}^{\varepsilon \hat{\eta}} + O(\varepsilon^2 \mu^2, \varepsilon \mu^4) \quad (3.79)$$

The boundary condition (3.70) gives $\tilde{p}|_{\varepsilon \hat{\eta}} = 0$. By redefining $\tilde{p}|_{\tilde{z}}$ as \tilde{p} and expanding both sides of the terms, noting that evaluation at $\varepsilon \hat{\eta}$ introduces only $O(\varepsilon^2 \mu^2)$ terms

give,

$$\bar{p} = \varepsilon\mu^2 \left(\frac{\tilde{z}^2}{2} \frac{\partial^2 \hat{u}_0}{\partial \hat{x} \partial \hat{t}} + \tilde{z} \frac{\partial^2 (\tilde{h} \hat{u}_0)}{\partial \hat{x} \partial \hat{t}} \right) + \varepsilon \hat{\eta} - \tilde{z} + O(\varepsilon^2 \mu^2, \varepsilon \mu^4) \quad (3.80)$$

The expressions for \hat{w} , \hat{u} and \bar{p} which are given in equations (3.75), (3.77) and (3.80) are substituted into the horizontal momentum equation (3.65) in which the terms are rearranged and higher order terms in ε and μ on the right hand side are collected gives,

$$\frac{\partial \hat{u}_0}{\partial \hat{t}} + \varepsilon \hat{u}_0 \frac{\partial \hat{u}_0}{\partial \hat{x}} + \frac{\partial \hat{\eta}}{\partial \hat{x}} = O(\varepsilon \mu^2, \mu^4) \quad (3.81)$$

Peregrine [48] defined the depth averaged velocity, $\hat{u}(\hat{x}, \hat{t})$ in terms of the velocity field $\hat{u}(\hat{x}, \tilde{z}, \hat{t})$ which is,

$$\hat{u} = \frac{1}{\tilde{h} + \varepsilon \hat{\eta}} \int_{-\tilde{h}}^{\varepsilon \hat{\eta}} \hat{u} d\tilde{z} \quad (3.82)$$

Although Mei and Le Méhauté [7] used the bottom velocity $\hat{u}(\hat{x}, -\tilde{h}, \hat{t})$ in order to derive the set of Boussinesq equations, the choice of velocity variable is not unique. However, the choice of depth averaged velocity allows a simpler form of continuity equation in Boussinesq model. Substituting from equation (3.77) and rearranging the terms ignoring the higher order terms in ε and μ gives,

$$\begin{aligned} \hat{u} &= \frac{1}{\tilde{h} + \varepsilon \hat{\eta}} \left\{ \hat{u}_0 (\tilde{h} + \varepsilon \hat{\eta}) - \mu^2 \left(\left(\frac{(\varepsilon \hat{\eta})^3 + \tilde{h}^3}{6} \right) \frac{\partial^2 \hat{u}_0}{\partial \hat{x}^2} + \left(\frac{(\varepsilon \hat{\eta})^2 - \tilde{h}^2}{2} \right) \frac{\partial^2 (\tilde{h} \hat{u}_0)}{\partial \hat{x}^2} \right) \right\} \\ &\quad + O(\mu^4) \\ &= \hat{u}_0 - \frac{\mu^2}{\tilde{h} \left(1 + \varepsilon \frac{\hat{\eta}}{\tilde{h}} \right)} \left(\frac{\tilde{h}^3}{6} \frac{\partial^2 \hat{u}_0}{\partial \hat{x}^2} - \frac{\tilde{h}^2}{2} \frac{\partial^2 (\tilde{h} \hat{u}_0)}{\partial \hat{x}^2} + O(\varepsilon \mu^2, \mu^4) \right) \\ &= \hat{u}_0 - \mu^2 \left(\frac{\tilde{h}^2}{6} \frac{\partial^2 \hat{u}_0}{\partial \hat{x}^2} - \frac{\tilde{h}}{2} \frac{\partial^2 (\tilde{h} \hat{u}_0)}{\partial \hat{x}^2} \right) + O(\varepsilon \mu^2, \mu^4) \end{aligned} \quad (3.83)$$

Noting that $\hat{u}_0 = \hat{u} + O(\mu^2)$ the above expression is rearranged to give an expression for $\hat{u}(\hat{x}, \hat{t})$.

$$\hat{u}_0 = \hat{u} + \mu^2 \left(\frac{\tilde{h}^2}{6} \frac{\partial^2 \hat{u}}{\partial \hat{x}^2} - \frac{\tilde{h}}{2} \frac{\partial^2 (\tilde{h} \hat{u})}{\partial \hat{x}^2} \right) + O(\varepsilon \mu^2, \mu^4) \quad (3.84)$$

Substituting the above expression into equation (3.81) yields the momentum equation which is

$$\frac{\partial \hat{u}}{\partial \hat{t}} + \varepsilon \hat{u} \frac{\partial \hat{u}}{\partial \hat{x}} + \frac{\partial \hat{\eta}}{\partial \hat{x}} + \mu^2 \left(\frac{\tilde{h}^2}{6} \frac{\partial^2}{\partial \hat{x}^2} \left(\frac{\partial \hat{u}}{\partial \hat{t}} \right) - \frac{\tilde{h}}{2} \frac{\partial^2}{\partial \hat{x}^2} \left(\tilde{h} \frac{\partial \hat{u}}{\partial \hat{t}} \right) \right) = O(\varepsilon \mu^2, \mu^4) \quad (3.85)$$

By integrating equation (3.67) by depth,

$$\int_{-\tilde{h}}^{\varepsilon \hat{\eta}} \left(\frac{\partial \hat{u}}{\partial \hat{x}} + \frac{\partial \hat{w}}{\partial \hat{z}} \right) d\hat{z} = 0 \quad (3.86)$$

Applying Leibniz rule and using the boundary conditions (3.69) and (3.71) considering the depth averaged velocity defined in equation (3.82) yields,

$$\begin{aligned} \frac{\partial}{\partial \hat{x}} \int_{-\tilde{h}}^{\varepsilon \hat{\eta}} \hat{u} d\hat{z} - \hat{u}|_{\varepsilon \hat{\eta}} \frac{\partial(\varepsilon \hat{\eta})}{\partial \hat{x}} + \hat{u}|_{-\tilde{h}} \frac{\partial(-\tilde{h})}{\partial \hat{x}} + \hat{w}|_{\varepsilon \hat{\eta}} - \hat{w}|_{-\tilde{h}} = 0 \\ \frac{\partial}{\partial \hat{x}} [(\tilde{h} + \varepsilon \hat{\eta}) \hat{u}] + \frac{\partial \hat{\eta}}{\partial \hat{t}} = 0 \end{aligned} \quad (3.87)$$

Reusing the dimensional and unscaled forms of the expressions gives the Boussinesq equations,

$$\frac{\partial \bar{u}}{\partial t} + \bar{u} \frac{\partial \bar{u}}{\partial x} + g \frac{\partial \eta}{\partial x} + \frac{h^2}{6} \frac{\partial^3 \bar{u}}{\partial x^2 \partial t} - \frac{h}{2} \frac{\partial^3 (h \bar{u})}{\partial x^2 \partial t} = 0 \quad (3.88)$$

$$\frac{\partial \eta}{\partial t} + \frac{\partial}{\partial x} [(h + \eta) \bar{u}] = 0 \quad (3.89)$$

As Peregrine [8] used a constant depth, H , the Boussinesq equations (3.88) and (3.89) are simplified to,

$$\frac{\partial \bar{u}}{\partial t} + \bar{u} \frac{\partial \bar{u}}{\partial x} + g \frac{\partial \eta}{\partial x} - \frac{H^2}{3} \frac{\partial^3 \bar{u}}{\partial x^2 \partial t} = 0 \quad (3.90)$$

$$\frac{\partial \eta}{\partial t} + \frac{\partial}{\partial x} [(H + \eta) \bar{u}] = 0 \quad (3.91)$$

3.4 The Classical Form of the Boussinesq Equations for Varying Depth

Peregrine [48] introduced an extra scaling parameter over the spatial domain for a variable depth environment which characterize the variation in depth.

$$\alpha_h = \max \left(\frac{\partial \tilde{h}}{\partial \tilde{x}} \right) \quad (3.92)$$

This new scaling leads the bottom boundary condition 3.58 as,

$$\mu \hat{w} + \alpha_h \hat{u} \left(\frac{\partial \tilde{h}}{\partial \tilde{x}} \right) = 0 \quad (3.93)$$

It shows that requiring $\alpha_h = O(\mu)$ leads the same set of equations when compared with the original scaling equation (3.71). This suggests that the depth must not vary rapidly over the scale of a typical wavelength and especially in sudden changes of depth, such as a step, leads inconsistencies in this formulation. Following the procedure given by Peregrine the derivation of Boussinesq equations is shown here which includes the effect of a variable depth. For long waves there are two important parameters which are, the nonlinearity parameter, ε (ratio of amplitude to depth) and the dispersion parameter μ (ratio of depth to wavelength). $\mu \ll 1$ for all long wave theories and $\varepsilon = O(1)$ for small amplitude theory but there is an assumption made for solitary wave and the Boussinesq equations that ε and μ^2 are of the same order. By choosing a suitable horizontal length scale, it can be assumed that $\varepsilon \approx \mu^2$.

The variables η , p , \mathbf{u} and $\int_{-h}^{\eta} \mathbf{u} dz$ are expanded as follows.

$$f = f_0 + \varepsilon f_1 + \varepsilon^2 f_2 + \dots \quad (3.94)$$

while w is expanded as,

$$w = \mu (w_0 + \varepsilon w_1 + \dots) \quad (3.95)$$

The independent variables can be scaled as follows,

$$\frac{\partial}{\partial t} = \mu \left(\frac{\partial}{\partial t_1} \right), \quad \frac{\partial}{\partial x} = \mu \left(\frac{\partial}{\partial x_1} \right), \quad \frac{\partial}{\partial y} = \mu \left(\frac{\partial}{\partial y_1} \right) \quad (3.96)$$

To make the order of magnitude of terms in the equations appear explicitly the variables η_i , p_i , \mathbf{u}_i and $(\int_{-h}^{\eta} \mathbf{u} dz)_i$ their derivatives with respect to x_1 , y_1 , z and t_1 are all assumed to be $O(1)$ when the equations (3.94), (3.95), (3.96) are substituted. Noting that here the index i corresponds to 1 and 2. The first order form of the irrotationality condition $\partial u/\partial z = \nabla w$ becomes,

$$\frac{\partial \mathbf{u}_1}{\partial z} = 0$$

hence $\left(\int_{-h}^{\eta} \mathbf{u} dz \right)_1 = h \mathbf{u}_1$

Equation (3.53) shows that $\partial p_1/\partial z = 0$ and when this is combined with the boundary condition $p_0 + \varepsilon p_1 = 0$ at $z = \varepsilon \eta_1$, it gives $p_1 = \rho g \eta_1$. Then, Euler's equation of motion and the vertically integrated continuity equation where the kinematic free surface and bottom boundary conditions are applied, become linearized long wave equations.

$$\frac{\partial \mathbf{u}_1}{\partial t_1} + g \nabla_1 \eta_1 = 0 \quad (3.97)$$

$$\frac{\partial \eta_1}{\partial t_1} + \nabla_1 \cdot (h \mathbf{u}_1) = 0 \quad (3.98)$$

Integrating the first order form of continuity equation over the depth by using Leibniz rule and applying the boundary conditions at $z = -h$ yields,

$$w_1 = -\nabla_1 \cdot (h \mathbf{u}_1) - z \nabla_1 \cdot \mathbf{u}_1$$

For the second order terms the integration of the irrotationality condition $\frac{\partial \mathbf{u}_2}{\partial z} = \nabla_1 w_1$ gives

$$\mathbf{u}_2 = \mathbf{U}_2(x_1, t_1) - z \nabla_1 [\nabla_1 \cdot (h \mathbf{u}_1)] - \frac{1}{2} z^2 \nabla_1 (\nabla_1 \mathbf{u}_1)$$

where $\mathbf{U}_2(x_1, t_1)$ is an arbitrary function arises from the integration. Equation (3.53) including the vertical acceleration is;

$$\frac{\partial w_1}{\partial t_1} + \frac{1}{\rho} \frac{\partial p_2}{\partial z} = 0$$

and using the boundary conditions at $z = \varepsilon \eta_1 + \varepsilon^2 \eta_2$ this integrates to,

$$p_2 = \rho g \eta_2(x_1, t_1) + z \frac{\partial}{\partial t_1} \nabla_1 \cdot (h \mathbf{u}_1) + \frac{1}{2} z^2 \frac{\partial}{\partial t_1} \nabla_1 \cdot \mathbf{u}_1$$

From equation (3.52) substituting \mathbf{u}_2 and p_2 the second order momentum becomes,

$$\frac{\partial \mathbf{U}_2}{\partial t} + (\mathbf{u}_1 \cdot \nabla_1) \mathbf{u}_1 + g \nabla_1 \eta_2 = 0 \quad (3.99)$$

The higher derivatives cancel out when the undisturbed free surface is taken as $z = 0$. In continuity equation there are equivalent terms which also depend on the origin of z . From $\varepsilon^2 \left(\int_{-h}^{\eta} \mathbf{u} dz \right)_2 = \int_{-h}^0 \varepsilon^2 \mathbf{u}_2 dz + \int_0^{\varepsilon \eta_1} \varepsilon \mathbf{u}_1 dz$; it is possible to define second order $\int_{-h}^{\eta} \mathbf{u} dz$ as follows,

$$\left(\int_{-h}^{\eta} \mathbf{u} dz \right)_2 = \eta_1 \mathbf{u}_1 + h \mathbf{U}_2 + \frac{1}{2} h^2 \nabla_1 [\nabla_1 \cdot (h \mathbf{u}_1)] - \frac{1}{6} h^3 \nabla_1 (\nabla_1 \cdot \mathbf{u}_1)$$

The second order terms of the continuity equation are;

$$\frac{\partial \eta_2}{\partial t_1} + \nabla_1 \cdot \left(\int_{-h}^{\eta} \mathbf{u} dz \right)_2 = 0 \quad (3.100)$$

Since the second order terms have first order effects over moderate times, it is necessary to include these effects. Hence, first order variables incorporating the second order terms are used. The mean velocity can be defined as follows,

$$\bar{\mathbf{u}} = \frac{\int_{-h}^{\eta} \mathbf{u} dz}{h + \eta} = \varepsilon \mathbf{u}_1 + \varepsilon^2 \mathbf{U}_2 + \frac{1}{2} h \nabla_1 [\nabla_1 \cdot (h \mathbf{u}_1)] - \frac{1}{6} h^2 \nabla_1 (\nabla_1 \cdot \mathbf{u}_1) \quad (3.101)$$

By adding ε times equations (3.99) and (3.100) to equations (3.97) and (3.98) respectively and by changing back to the variables x , y and t , the momentum and

continuity equations in terms of $\bar{\mathbf{u}}$ are,

$$\frac{\partial \bar{\mathbf{u}}}{\partial t} + (\bar{\mathbf{u}} \cdot \nabla) \bar{\mathbf{u}} + g \nabla \eta = \frac{1}{2} h \frac{\partial}{\partial t} \nabla [\nabla \cdot (h \bar{\mathbf{u}})] - \frac{1}{6} h^2 \frac{\partial}{\partial t} \nabla (\nabla \cdot \bar{\mathbf{u}}) \quad (3.102)$$

$$\frac{\partial \eta}{\partial t} + \nabla \cdot [(h + \eta) \bar{\mathbf{u}}] = 0 \quad (3.103)$$

where $\bar{\mathbf{u}}(x, y, t)$ is the two-dimensional depth averaged velocity field, and ∇ is the two-dimensional gradient operator with respect to horizontal coordinates x and y . These equations have been derived by assuming that the wave amplitude is small compared to the depth and the depth is small compared to the wavelength. By introducing ε and μ into these equations, these statements have been made precise.

3.5 Improved Boussinesq Equations

Dispersion relation of Peregrine's system is an accurate approximation to Stokes first order wave theory for very small values of the dispersion parameter μ . Witting [9] used a different form of the exact, fully nonlinear, depth-integrated momentum equation for one horizontal dimension in which velocity at the free surface is used. An expansion of Padé series was used to relate the different velocity variables in the governing equations, with the coefficients of the expansion determined to yield the best linear dispersion characteristics [52]. By retaining terms up to the fourth order in dispersion, Witting [9] obtained relatively accurate result for both deep and shallow water waves. However, the model presented by Witting is only valid in water of constant depth [52].

Murray [56] and Madsen et al. [10] examined the dispersion properties of various forms of the Boussinesq equations as well as Witting's [9] Pade approximation of the linear dispersion relation for Airy waves [52]. They have introduced an additional third-order term to the momentum equation to improve the dispersion properties of the Boussinesq equations. The third-order is derived from the long wave equations and reduces to zero in shallow water, resulting in the standard form of the equations for shallow water. The equations assume a constant water depth and, thus, are not applicable to shoaling waves.

Beji and Nadaoka introduced a slightly different method to improve the dispersion characteristics by a simple algebraic manipulation of Peregrine's work for variable

depth [12], [57]. On the other hand, Nwogu [13] defined the dependent variable as the velocity at an arbitrary depth with a rational polynomial approximation to the exact linear dispersion relationship without the need to add higher order terms to the equations. Although the arbitrary location could be chosen to give a Pade approximation to the linear dispersion relationship, Nwogu [13] chose an alternative value which minimized the error in the linear phase speed over certain depth range [52]. Liu [16] and Wei et al. [58] presented a set of highly nonlinear Boussinesq-type equations that not only can be applied to intermediate water depth but also are capable of simulating wave propagation with strong nonlinear interaction. Wei et al. [58] have also developed a high-order numerical scheme to solve these equations. Although the higher-order Boussinesq equations for the improvement of the nonlinear and dispersive properties in water waves have been successful in certain aspects, most of them involved numerous additional derivatives and hence made the accurate numerical solution increasingly difficult to obtain.

Although several studies has been done in order to use Boussinesq-type equation model such that wave evolution from relatively deep water to the breaking point could be accurately captured, the processes of runup and rundown are not included. In Figure 3.1 the validity zones of standard and improved Boussinesq equations can be seen.

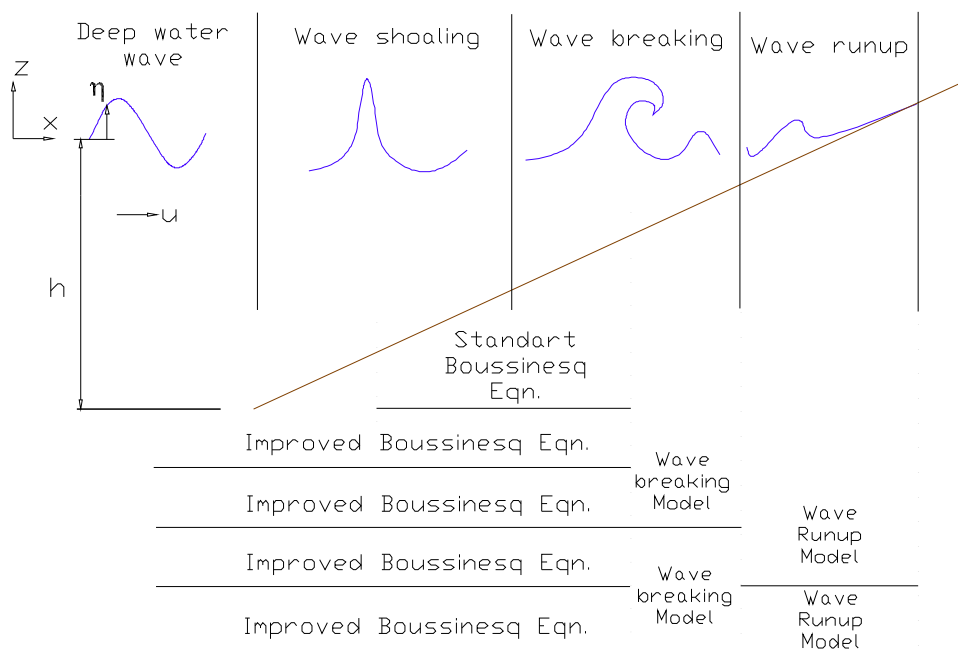


Figure 3.1: Validity zone of different type of Boussinesq equations.

3.5.1 Derivation of Beji and Nadaoka's improved Boussinesq equations

According to Beji and Nadaoka the second order terms are replaced with their equivalents in the Boussinesq type equations as these equations are the result of an ordering process with respect to two parameters, which are ε and μ^2 . As given by Beji and Nadaoka [12] a simple addition and subtraction in equation (3.102) gives

$$\begin{aligned} \mathbf{u}_t + (\mathbf{u} \cdot \nabla)\mathbf{u} + g\nabla\eta &= (1 + \beta)\frac{h}{2}\nabla[\nabla \cdot (h\mathbf{u}_t)] - \beta\frac{h}{2}\nabla[\nabla \cdot (h\mathbf{u}_t)] \\ &\quad - (1 + \beta)\frac{h^2}{6}\nabla(\nabla \cdot \mathbf{u}_t) + \beta\frac{h^2}{6}\nabla(\nabla \cdot \mathbf{u}_t) \end{aligned} \quad (3.104)$$

where β is a scalar to be determined from the dispersion relation. Instead of a full replacement, a partial replacement of the dispersion terms are made so a form with better dispersion characteristics is obtained.

Using $\mathbf{u}_t = -g\nabla\eta$ for replacing the terms proportional to β gives

$$\begin{aligned} \mathbf{u}_t + (\mathbf{u} \cdot \nabla)\mathbf{u} + g\nabla\eta &= (1 + \beta)\frac{h}{2}\nabla[\nabla \cdot (h\mathbf{u}_t)] + \beta g\frac{h}{2}\nabla[\nabla \cdot (h\nabla\eta)] \\ &\quad - (1 + \beta)\frac{h^2}{6}\nabla(\nabla \cdot \mathbf{u}_t) - \beta g\frac{h^2}{6}\nabla(\nabla^2\eta) \end{aligned} \quad (3.105)$$

which is a momentum equation with mixed dispersion terms. Setting $\beta = 0$ recovers the original equation, while $\beta = -1$ corresponds to replacing \mathbf{u}_t with $-g\nabla\eta$ in equation (3.102). Equations (3.103) and (3.105) constitute the improved Boussinesq Equations.

3.5.2 Specification of dispersion parameter

Linearized 1-D Boussinesq Equations for mildly varying depth is formulated as follows. The continuity equation in expanded form

$$\frac{\partial \eta}{\partial t} + \frac{\partial h}{\partial x}u + h\frac{\partial u}{\partial x} = 0 \quad (3.106)$$

The momentum equation can be expanded as

$$\frac{\partial u}{\partial t} + g \frac{\partial \eta}{\partial x} = h \frac{\partial h}{\partial x} \frac{\partial^2 u}{\partial x \partial t} + \frac{h^2}{3} \frac{\partial^3 u}{\partial x^2 \partial t} \quad (3.107)$$

where $h \frac{\partial h}{\partial x} \frac{\partial^2 u}{\partial x \partial t}$ is the linear shoaling term while $\frac{h^2}{3} \frac{\partial^3 u}{\partial x^2 \partial t}$ is the linear dispersing term. Linearized 1-D Boussinesq Equations for constant depth simplify to the following equations.

$$\frac{\partial \eta}{\partial t} + h \frac{\partial u}{\partial x} = 0 \quad (3.108)$$

$$\frac{\partial u}{\partial t} + g \frac{\partial \eta}{\partial x} = \frac{h^2}{3} \frac{\partial^3 u}{\partial x^2 \partial t} \quad (3.109)$$

In order to obtain the combined form of the 1-D Boussinesq Equations, linearized relations $u_x = -\frac{1}{h} \eta_t$, $u_{xxt} = -\frac{1}{h} \eta_{xxt}$, $u_{xxxxt} = -\frac{1}{h} \eta_{xxxxt}$ and $u_{xt} = -\frac{1}{h} \eta_{tt}$ are considered. Partial differentiation of momentum equation with respect to x gives;

$$u_{xt} + g \eta_{xx} = \frac{h^2}{3} \left(-\frac{1}{h} \eta_{xxtt} \right) \quad (3.110)$$

Substituting the above expressions into equation (3.110) leads to,

$$\begin{aligned} -\frac{1}{h} \eta_{tt} + g \eta_{xx} &= \frac{h^2}{3} \left(-\frac{1}{h} \eta_{xxtt} \right) \\ \eta_{tt} - gh \eta_{xx} &= \frac{h^2}{3} \eta_{xxtt} \end{aligned} \quad (3.111)$$

Finally, combined form of the 1-D Boussinesq Equations for constant depth is obtained as,

$$\frac{\partial^2 \eta}{\partial t^2} - gh \frac{\partial^2 \eta}{\partial x^2} = \frac{h^2}{3} \frac{\partial^4 \eta}{\partial x^2 \partial t^2} \quad (3.112)$$

where $\frac{h^2}{3} \frac{\partial^4 \eta}{\partial x^2 \partial t^2}$ is the linear dispersion depth. Water waves of different wave lengths travel with different phase speeds, a phenomenon known as frequency dispersion. For the case of infinitesimal wave amplitude, the terminology is linear frequency

dispersion. The frequency dispersion characteristics of a Boussinesq-type of equation can be used to determine the range of wavelengths for which it is a valid approximation. Assume $\eta = \eta_0 e^{i(kx \pm \omega t)}$ so that $\eta_{tt} = -\omega^2 \eta_0 e^{i(kx \pm \omega t)}$, $\eta_{xx} = -k^2 \eta_0 e^{i(kx \pm \omega t)}$ and $\eta_{xxt} = k^2 \omega^2 \eta_0 e^{i(kx \pm \omega t)}$. If we substitute the above expressions into (3.112) it becomes

$$-\omega^2 - gh(-k^2) = \frac{h^2}{3} (k^2 \omega^2) \quad (3.113)$$

Rearranging this equation yields

$$\omega^2 \left(1 + \frac{k^2 h^2}{3} \right) = ghk^2 \quad (3.114)$$

which can be rewritten as,

$$\omega^2 = \frac{k^2}{1 + \frac{k^2 h^2}{3}} gh \simeq k^2 \left(1 - \frac{k^2 h^2}{3} \right) gh \quad (3.115)$$

since $(1 + \mu^2)^{-1} \approx 1 - \mu^2$ for small values of μ^2 . For not so shallow water waves $\tanh(kh) \approx kh - \frac{k^3 h^3}{3}$ which yields

$$\omega^2 = gk \left(kh - \frac{k^3 h^3}{3} \right)$$

$$\omega^2 = gk^2 h \left(1 - \frac{k^2 h^2}{3} \right)$$

Since $\omega = kc$,

$$k^2 c^2 = gk^2 h \left(1 - \frac{k^2 h^2}{3} \right)$$

$$c = \frac{\sqrt{gh}}{\sqrt{1 + \frac{k^2 h^2}{3}}} \approx \sqrt{gh} \sqrt{\left(1 - \frac{k^2 h^2}{3} \right)} \quad (3.116)$$

Here $\frac{k^2 h^2}{3}$ shows the correction to the wave celerity due to the inclusion of the weak dispersion effect. Considering the improved Boussinesq equations, in linearized forms

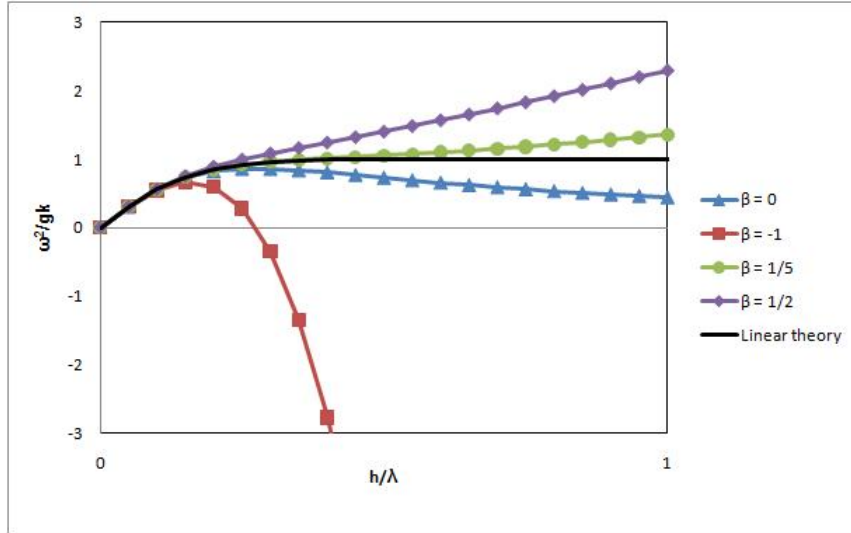


Figure 3.2: Dispersion curves for various values of dispersion parameter β compared with linear theory.

equations (3.103) and (3.105) yield the following dispersion relation evaluated by Beji and Nadaoka [12]:

$$\frac{\omega^2}{gk} = \frac{kh(1 + \beta k^2 h^2/3)}{[1 + (1 + \beta)k^2 h^2/3]} \quad (3.117)$$

where ω is the wave frequency, $k^2 = k_x^2 + k_y^2$ and k_x, k_y are the components of the wave number vector. Equation (3.117) is specified according to matching the resulting dispersion relation with a second order Padé expansion of the linear theory dispersion and β is determined from this second order Padé expansion of the linear theory dispersion relation $\omega^2/gk = \tanh kh$:

$$\frac{\omega^2}{gk} = \frac{kh + k^3 h^3/15}{1 + 2k^2 h^2/5} \quad (3.118)$$

In order that Equation (3.117) be identical with Equation (3.118) β should be set to 1/5. Figure (3.2) compares various values of dispersion parameters with the exact expression of linear theory. Among these asymptotic expansions, the one corresponding the Padé type expansion is the best. Thus, when $\beta = 1/5$, the model may propagate relatively shorter waves ($h/L = 1$) with acceptable errors in amplitude and celerity.

4. A NEW DISCRETIZATION SCHEME FOR 1-D and 2-D IMPROVED BOUSSINESQ EQUATIONS

The finite difference method is the most natural way of solving a PDE directly in an approximate manner. The idea behind this method is to discretize the continuous space and time into a finite number of discrete grid points and time steps, and then to approximate the local derivatives at these grid points with finite difference schemes. There are two approaches used in numerical analysis for obtaining numerical solutions of time-dependent ordinary and partial differential equations: explicit and implicit methods. Explicit methods calculate the state of a system at a later time directly from the state of the system at the current time, while implicit methods do the same by requiring the solution of a matrix equation at each new time level. The advantages and disadvantages of these two approaches are summarized as follows.

- **Explicit Approach**

- *Advantage*: Relatively simple to set up and program
- *Disadvantage*: For a given Δx , Δt must be less than some limit imposed by stability constraints. In many cases, Δt must be very small to maintain stability; this can result in long computer running times to make calculations over a given interval of t .

- **Implicit Approach**

- *Advantage*: Stability can be maintained over much larger values of Δt , hence using considerably fewer time steps to make calculations over a given interval of t . This result in less computer time.
- *Disadvantage*: More complicated to set up and program.
- *Disadvantage*: Since matrix manipulations are usually required at each time step, the computer time *per time step* is much larger than in the explicit approach.

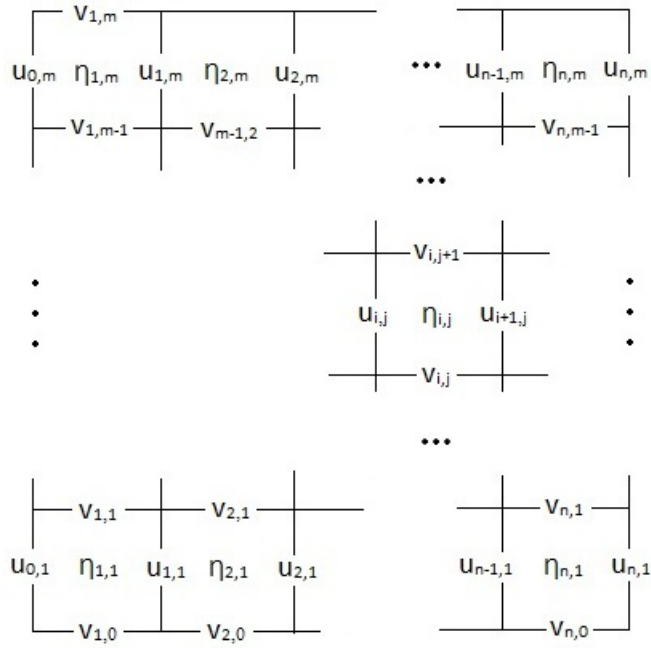


Figure 4.1: The Arakawa-C grid.

- *Disadvantage:* Since large Δt can be taken, truncation error is larger, and the use of implicit methods to follow the exact transients (time variations of the independent variable) may not be as accurate as an explicit approach. However, for a time-dependent solution in which the steady state is the desired result, this relative time-wise inaccuracy is not important.

For numerical modeling, the discretization of the variables u , v and η are necessary in order to solve momentum and continuity equations. Arakawa C grid which is shown in Figure (4.1), is the most appropriate system for wave problems since it enables the discretization of the continuity equation in the most accurate manner. Here, u , v and η represent the velocity vectors and the free surface displacement, respectively.

4.1 A New Discretization Scheme for 1-D Improved Boussinesq Equations

The surface displacement is obtained from a semi-explicit discretization of the continuity equation which is,

$$\eta_t + \frac{\partial}{\partial x}[(h + \eta)u] = 0 \quad (4.1)$$

Rearranging and discretizing the continuity equation gives,

$$\begin{aligned} \frac{\eta_i^{k+1} - \eta_i^k}{\Delta t} + \frac{1}{2}h \left[\left(\frac{\partial u}{\partial x} \right)^{k+1} + \left(\frac{\partial u}{\partial x} \right)^k \right]_{i-\frac{1}{2}} \\ = -h_x u_{i-\frac{1}{2}}^{k+\frac{1}{2}} - \frac{\partial}{\partial x} \left(\eta_i u_{i-\frac{1}{2}} \right)^{k+\frac{1}{2}} \end{aligned} \quad (4.2)$$

where i is the spatial increment index and k denotes the time level. It should be noted that the discretization is centered at $\eta_i^{k+1/2}$. Multiplying both sides of the continuity equation by Δt and differentiating with respect to x gives:

$$\begin{aligned} \left(\frac{\partial \eta}{\partial x} \right)_i^{k+1} = \left(\frac{\partial \eta}{\partial x} \right)_i^k - \frac{1}{2}h \left[\left(\frac{\partial^2 u}{\partial x^2} \right)^{k+1} + \left(\frac{\partial^2 u}{\partial x^2} \right)^k \right]_{i-\frac{1}{2}} \Delta t \\ - 2h_x \left(\frac{\partial u}{\partial x} \right)_{i-\frac{1}{2}}^{k+\frac{1}{2}} \Delta t - \frac{\partial^2}{\partial x^2} \left(\eta_i u_{i-\frac{1}{2}} \right)^{k+\frac{1}{2}} \Delta t \end{aligned} \quad (4.3)$$

The momentum equation which is solved for u is

$$u_t + uu_x + g\eta_x = (1 + \beta) \frac{h^2}{3} u_{xxt} + (1 + \beta) h h_x u_{xt} + g\beta \frac{h^2}{3} \eta_{xxx} + g\beta h h_x \eta_{xx} \quad (4.4)$$

Discretization of the momentum equation is given as follows with all spatial derivatives being centered at the grid point where u_i^k is located.

$$\begin{aligned}
& \frac{u_i^{k+1} - u_i^k}{\Delta t} + \frac{1}{2}g \left[\left(\frac{\partial \eta}{\partial x} \right)_{i+\frac{1}{2},j}^{k+1} + \left(\frac{\partial \eta}{\partial x} \right)_{i+\frac{1}{2},j}^k \right] \\
& = (1 + \beta) \frac{h^2}{3} \\
& \quad \left[\frac{(u_{i+1}^{k+1} - 2u_i^{k+1} + u_{i-1}^{k+1}) - (u_{i+1}^k - 2u_i^k + u_{i-1}^k)}{\Delta x^2 \Delta t} \right] \\
& \quad + (1 + \beta) hh_x \left[\frac{(u_{i+1}^{k+1} - u_{i-1}^{k+1}) - (u_{i+1}^k - u_{i-1}^k)}{2\Delta x \Delta t} \right] \\
& \quad - u_i^{k+\frac{1}{2}} \left(\frac{\partial u_i}{\partial x} \right)^{k+\frac{1}{2}} \\
& \quad + g\beta \frac{h^2}{3} \left[\frac{\eta_{i+1}^{k+\frac{1}{2}} - 3\eta_i^{k+\frac{1}{2}} + 3\eta_{i-1}^{k+\frac{1}{2}} - \eta_{i-2}^{k+\frac{1}{2}}}{\Delta x^3} \right] \\
& \quad + g\beta hh_x \left[\frac{\eta_{i-2}^{k+\frac{1}{2}} - \eta_{i+1}^{k+\frac{1}{2}} - \eta_i^{k+\frac{1}{2}} - \eta_{i-1}^{k+\frac{1}{2}}}{2\Delta x^2} \right] \tag{4.5}
\end{aligned}$$

Substituting $\left(\frac{\partial \eta}{\partial x}\right)_{i,j}^{k+1}$ from equation (4.3) into the discretized x -momentum equation (4.5) and multiplying by Δt gives

$$\begin{aligned}
& - \left[\frac{1}{4}gh \frac{\Delta t^2}{\Delta x^2} + \frac{(1+\beta)}{3} \frac{h^2}{\Delta x^2} - \frac{(1+\beta)}{2} \frac{hh_x}{\Delta x} - \frac{1}{4}gh_x \frac{\Delta t^2}{\Delta x} \right] u_{i-1}^{k+1} \\
& + \left[1 + \frac{1}{2}gh \frac{\Delta t^2}{\Delta x^2} + \frac{2(1+\beta)}{3} \frac{h^2}{\Delta x^2} \right] u_i^{k+1} \\
& - \left[\frac{1}{4}gh \frac{\Delta t^2}{\Delta x^2} + \frac{(1+\beta)}{3} \frac{h^2}{\Delta x^2} + \frac{(1+\beta)}{2} \frac{hh_x}{\Delta x} + \frac{1}{4}gh_x \frac{\Delta t^2}{\Delta x} \right] u_{i+1}^{k+1} \\
= & \left[\frac{1}{4}gh \frac{\Delta t^2}{\Delta x^2} - \frac{(1+\beta)}{3} \frac{h^2}{\Delta x^2} + \frac{(1+\beta)}{2} \frac{hh_x}{\Delta x} - \frac{1}{4}gh_x \frac{\Delta t^2}{\Delta x} \right] u_{i-1}^k \\
& + \left[1 - \frac{1}{2}gh \frac{\Delta t^2}{\Delta x^2} + \frac{2(1+\beta)}{3} \frac{h^2}{\Delta x^2} \right] u_i^k \\
& + \left[\frac{1}{4}gh \frac{\Delta t^2}{\Delta x^2} - \frac{(1+\beta)}{3} \frac{h^2}{\Delta x^2} - \frac{(1+\beta)}{2} \frac{hh_x}{\Delta x} + \frac{1}{4}gh_x \frac{\Delta t^2}{\Delta x} \right] u_{i+1}^k \\
& - g \left(\frac{\partial \eta_{i+\frac{1}{2}}}{\partial x} \right)^k \Delta t + \frac{1}{2}g \frac{\partial^2}{\partial x^2} (\eta_{i+\frac{1}{2}}^{k+\frac{1}{2}} u_i^{k+\frac{1}{2}}) \Delta t^2 - u_i^{k+\frac{1}{2}} \left(\frac{\partial u_i}{\partial x} \right)^{k+\frac{1}{2}} \Delta t \\
& + \frac{1}{2}g\beta hh_x \frac{\Delta t}{\Delta x^2} (\eta_{i+2}^{k+\frac{1}{2}} - \eta_{i+1}^{k+\frac{1}{2}} - \eta_i^{k+\frac{1}{2}} + \eta_{i-1}^{k+\frac{1}{2}}) \\
& + \frac{1}{3}g\beta h^2 \frac{\Delta t}{\Delta x^3} (\eta_{i+2}^{k+\frac{1}{2}} - 3\eta_{i+1}^{k+\frac{1}{2}} + 3\eta_i^{k+\frac{1}{2}} - \eta_{i-1}^{k+\frac{1}{2}}) \tag{4.6}
\end{aligned}$$

which is essentially a tridiagonal matrix system for u_{i-1}^{k+1} , u_i^{k+1} and u_{i+1}^{k+1} .

The numerical tests presented in Figure 4.2 are done using the above discretization scheme. Figure 4.2 shows computations using two different bathymetries for linearized original Boussinesq equations ($\beta = 0$) and the linearized improved Boussinesq equations ($\beta = 1/5$). For varying bathymetries Green's formula [51] predicts an amplitude variation for long waves according to

$$a(x) = a_0 \sqrt{\sqrt{h_0/h(x)}} \tag{4.7}$$

where a_0 is the wave amplitude and h_0 is the water depth at $x = 0$.

In Figure 4.2 all the wave profiles are compared with the theoretical formula of Green. The computational wave amplitudes are almost perfectly matching with Green's formula.

4.2 A New Discretization Scheme for 2-D Improved Boussinesq Equations

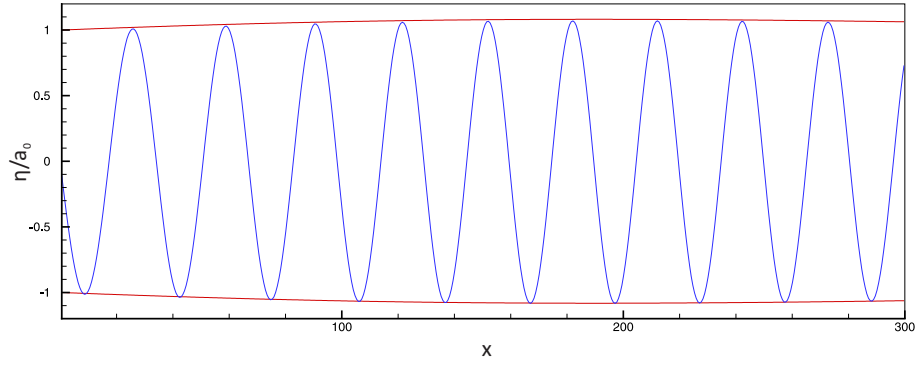
For 2-D Boussinesq equations the x -momentum equation is solved for u , while the y -momentum equation is solved for v . The surface displacement is obtained from a semi-explicit discretization of the continuity equation. Consider the continuity equation for 2-D case:

$$\eta_t + \frac{\partial}{\partial x}[(h + \eta)u] + \frac{\partial}{\partial y}[(h + \eta)v] = 0 \quad (4.8)$$

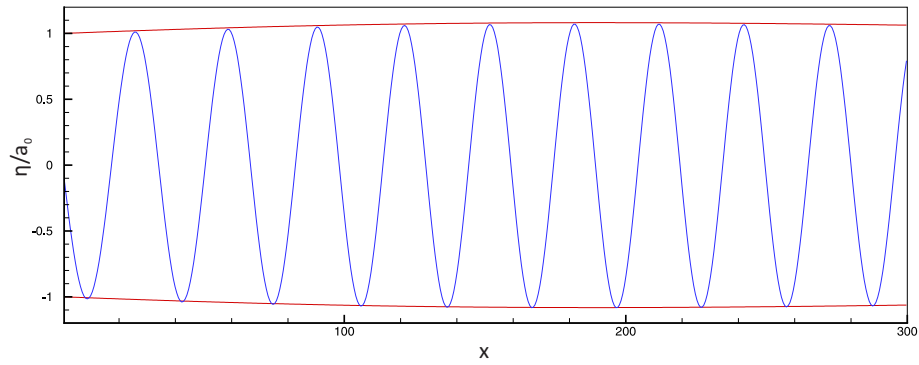
Rearranging and discretizing the continuity equation in time only gives,

$$\begin{aligned} & \frac{\eta_{i,j}^{k+1} - \eta_{i,j}^k}{\Delta t} + \frac{1}{2}h \left[\left(\frac{\partial u}{\partial x} \right)^{k+1} + \left(\frac{\partial u}{\partial x} \right)^k \right]_{i-\frac{1}{2},j} \\ = - & \left[h_x u_{i-\frac{1}{2},j}^{k+\frac{1}{2}} + h_y v_{i,j-\frac{1}{2}}^{k+\frac{1}{2}} + \frac{\partial}{\partial x} (\eta u)^{k+\frac{1}{2}} + \frac{\partial}{\partial y} (\eta v)^{k+\frac{1}{2}} + h \frac{\partial v_{i,j-\frac{1}{2}}^{k+\frac{1}{2}}}{\partial y} \right] \end{aligned} \quad (4.9)$$

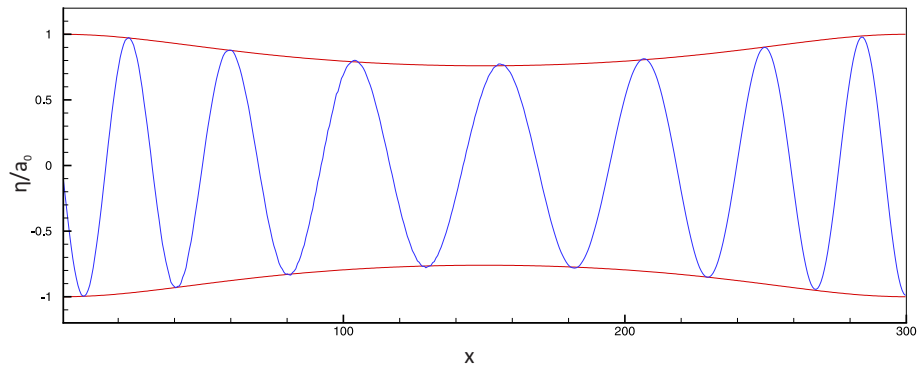
where i is the spatial incremental index in the x -direction, j is the spatial incremental index in the y -direction and k is the incremental index in time.



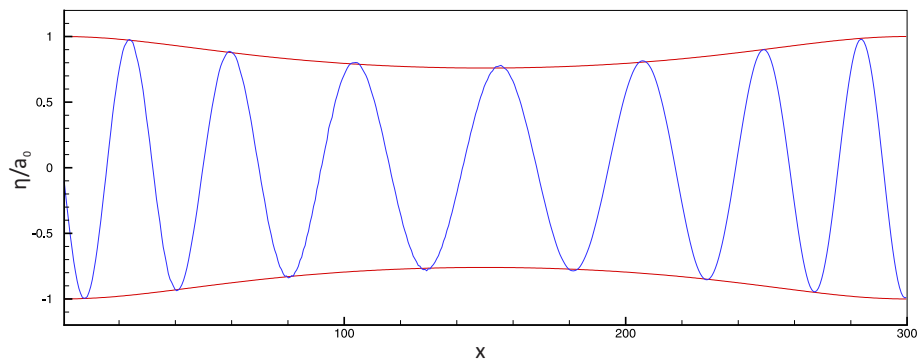
(a) Parabolic bathymetry for $\beta = 0$



(b) Parabolic bathymetry for $\beta = 1/5$



(c) Sinusoidally changing bathymetry for $\beta = 0$



(d) Sinusoidally changing bathymetry for $\beta = 1/5$

Figure 4.2: Numerical tests for 1-D Boussinesq equations for varying bathymetries.

For later use, multiplying both sides of the continuity equation by Δt and differentiating with respect to x gives

$$\begin{aligned}
\left(\frac{\partial \eta}{\partial x}\right)_{i,j}^{k+1} &= \left(\frac{\partial \eta}{\partial x}\right)_{i,j}^k - \frac{1}{2}h \left[\left(\frac{\partial^2 u}{\partial x^2}\right)^{k+1} + \left(\frac{\partial^2 u}{\partial x^2}\right)^k \right]_{i-\frac{1}{2},j} \Delta t \\
&\quad - 2h_x \left(\frac{\partial u}{\partial x}\right)_{i-\frac{1}{2},j}^{k+\frac{1}{2}} \Delta t - h_y \left(\frac{\partial v}{\partial x}\right)_{i,j-\frac{1}{2}}^{k+\frac{1}{2}} \Delta t \\
&\quad - h_x \left(\frac{\partial v}{\partial y}\right)_{i,j-\frac{1}{2}}^{k+\frac{1}{2}} - h \left(\frac{\partial^2 v}{\partial x \partial y}\right)_{i,j-\frac{1}{2}}^{k+\frac{1}{2}} \Delta t \\
&\quad - \frac{\partial^2}{\partial x^2} (\eta u)_{i-\frac{1}{2},j}^{k+\frac{1}{2}} \Delta t - \frac{\partial^2}{\partial x \partial y} (\eta v)_{i,j-\frac{1}{2}}^{k+\frac{1}{2}} \Delta t \tag{4.10}
\end{aligned}$$

Likewise, multiplying both sides of the continuity equation by Δt and differentiating with respect to y gives

$$\begin{aligned}
\left(\frac{\partial \eta}{\partial y}\right)_{i,j}^{k+1} &= \left(\frac{\partial \eta}{\partial y}\right)_{i,j}^k - \frac{1}{2}h \left[\left(\frac{\partial^2 v}{\partial y^2}\right)^{k+1} + \left(\frac{\partial^2 v}{\partial y^2}\right)^k \right]_{i-\frac{1}{2},j} \Delta t \\
&\quad - 2h_y \left(\frac{\partial v}{\partial y}\right)_{i-\frac{1}{2},j}^{k+\frac{1}{2}} \Delta t - h_x \left(\frac{\partial u}{\partial y}\right)_{i,j-\frac{1}{2}}^{k+\frac{1}{2}} \Delta t \\
&\quad - h_y \left(\frac{\partial u}{\partial x}\right)_{i,j-\frac{1}{2}}^{k+\frac{1}{2}} \Delta t - h \left(\frac{\partial^2 u}{\partial x \partial y}\right)_{i,j-\frac{1}{2}}^{k+\frac{1}{2}} \Delta t \\
&\quad - \frac{\partial^2}{\partial x \partial y} (\eta u)_{i-\frac{1}{2},j}^{k+\frac{1}{2}} \Delta t - \frac{\partial^2}{\partial y^2} (\eta v)_{i,j-\frac{1}{2}}^{k+\frac{1}{2}} \Delta t \tag{4.11}
\end{aligned}$$

The x momentum equation in 2-D form is given by

$$\begin{aligned}
u_t + uu_x + vu_y + g\eta_x &= (1 + \beta) \frac{h^2}{3} u_{xxt} + (1 + \beta) hh_x u_{xt} \\
&+ (1 + \beta) \frac{h^2}{3} v_{xyt} + \frac{1}{2} (1 + \beta) hh_x v_{yt} \\
&+ \frac{1}{2} (1 + \beta) hh_y v_{xt} + g\beta \frac{h^2}{3} \eta_{xxx} \\
&+ g\beta hh_x \eta_{xx} + g\beta \frac{h^2}{3} \eta_{xyy} \\
&+ \frac{1}{2} g\beta hh_x \eta_{yy} + \frac{1}{2} g\beta hh_y \eta_{xy}
\end{aligned} \tag{4.12}$$

Discretization of the x momentum equation in time reads

$$\begin{aligned}
\frac{u_{i,j}^{k+1} - u_{i,j}^k}{\Delta t} &+ \frac{1}{2} g \left[\left(\frac{\partial \eta}{\partial x} \right)^{k+1} + \left(\frac{\partial \eta}{\partial x} \right)^k \right]_{i+\frac{1}{2},j} \\
&= (1 + \beta) \frac{h^2}{3} \left[\left(\frac{\partial^2 u}{\partial x^2} \right)^{k+1} - \left(\frac{\partial^2 u}{\partial x^2} \right)^k \right] \frac{1}{\Delta t} \\
&+ (1 + \beta) hh_x \left[\left(\frac{\partial u}{\partial x} \right)^{k+1} - \left(\frac{\partial u}{\partial x} \right)^k \right] \frac{1}{\Delta t} \\
&- (uu_x)^{k+\frac{1}{2}} - (vu_y)^{k+\frac{1}{2}} + (1 + \beta) \frac{h^2}{3} v_{xyt} \\
&+ \frac{1}{2} (1 + \beta) hh_x v_{yt} + \frac{1}{2} (1 + \beta) hh_y v_{xt} \\
&+ g\beta \frac{h^2}{3} \eta_{xxx} + g\beta hh_x \eta_{xx} + g\beta \frac{h^2}{3} \eta_{xyy} + \frac{1}{2} g\beta hh_x \eta_{yy} \\
&+ \frac{1}{2} g\beta hh_y \eta_{xy}
\end{aligned} \tag{4.13}$$

Substituting $\left(\frac{\partial \eta}{\partial x}\right)_{i,j}^{k+1}$ from equation (4.10) into the time discretized x -momentum equation (4.13) and multiplying by Δt gives,

$$\begin{aligned}
u_{i,j}^{k+1} &= u_{i,j}^k - \frac{1}{4}gh \left[\left(\frac{\partial^2 u}{\partial x^2}\right)^{k+1} + \left(\frac{\partial^2 u}{\partial x^2}\right)^k \right] \Delta t^2 + g \left(\frac{\partial \eta}{\partial x}\right)^k \Delta t \\
&= (1 + \beta) \frac{h^2}{3} \left[\left(\frac{\partial^2 u}{\partial x^2}\right)^{k+1} - \left(\frac{\partial^2 u}{\partial x^2}\right)^k \right] + (1 + \beta)hh_x \left[\left(\frac{\partial u}{\partial x}\right)^{k+1} + \left(\frac{\partial u}{\partial x}\right)^k \right] \\
&\quad + \frac{1}{2}gh_x \left[\left(\frac{\partial u}{\partial x}\right)^{k+1} + \left(\frac{\partial u}{\partial x}\right)^k \right] \Delta t^2 + \frac{1}{4}gh_y \left[\left(\frac{\partial v}{\partial x}\right)^{k+1} + \left(\frac{\partial v}{\partial x}\right)^k \right] \Delta t^2 \\
&\quad + \frac{1}{4}gh_x \left[\left(\frac{\partial v}{\partial y}\right)^{k+1} + \left(\frac{\partial v}{\partial y}\right)^k \right] \Delta t^2 + \frac{1}{4}gh\Delta t^2 \left[\left(\frac{\partial^2 v}{\partial x\partial y}\right)^{k+1} + \left(\frac{\partial^2 v}{\partial x\partial y}\right)^k \right] \\
&\quad + (1 + \beta) \frac{h^2}{3} + \left[\left(\frac{\partial^2 v}{\partial x\partial y}\right)^{k+1} - \left(\frac{\partial^2 v}{\partial x\partial y}\right)^k \right] \\
&\quad + \frac{1}{2}(1 + \beta)hh_x \left[\left(\frac{\partial v}{\partial y}\right)^{k+1} - \left(\frac{\partial v}{\partial y}\right)^k \right] + \frac{1}{2}(1 + \beta)hh_y \left[\left(\frac{\partial v}{\partial x}\right)^{k+1} - \left(\frac{\partial v}{\partial x}\right)^k \right] \\
&\quad + g\beta h\Delta t \left[\frac{h}{3}(\eta_{xxx} + \eta_{xyy}) + h_x \left(\eta_{xx} + \frac{1}{2}\eta_{yy} \right) + \frac{1}{2}h_y\eta_{xy} \right] \\
&\quad + \frac{1}{2}g\Delta t^2 \left[\frac{\partial^2}{\partial x^2}(\eta u)^{k+\frac{1}{2}} + \frac{\partial^2}{\partial x\partial y}(\eta v)^{k+\frac{1}{2}} \right] - [(uu_x)^{k+\frac{1}{2}} + (vu_y)^{k+\frac{1}{2}}] \Delta t \quad (4.14)
\end{aligned}$$

Rearranging the equation (4.14) gives,

$$\begin{aligned}
& h \left[\frac{1}{3}(1+\beta)h + \frac{1}{4}g\Delta t^2 \right] \left(\frac{\partial^2 u}{\partial x^2} \right)^{k+1} \\
& + h_x \left[(1+\beta)h + \frac{1}{2}g\Delta t^2 \right] \left(\frac{\partial u}{\partial x} \right)^{k+1} - u_{i,j}^{k+1} \\
= & h \left[\frac{1}{3}(1+\beta)h - \frac{1}{4}g\Delta t^2 \right] \left(\frac{\partial^2 u}{\partial x^2} \right)^k + h_x \left[(1+\beta)h - \frac{1}{2}g\Delta t^2 \right] \left(\frac{\partial u}{\partial x} \right)^k \\
& - u_{i,j}^k + g \left(\frac{\partial \eta}{\partial x} \right)^k \Delta t - \frac{1}{2}h_x \left[(1+\beta)h + \frac{1}{2}g\Delta t^2 \right] \left(\frac{\partial v}{\partial y} \right)^{k+1} \\
& + \frac{1}{2}h_x \left[(1+\beta)h - \frac{1}{2}g\Delta t^2 \right] \left(\frac{\partial v}{\partial y} \right)^k - \frac{1}{2}h_y \left[(1+\beta)h + \frac{1}{2}g\Delta t^2 \right] \left(\frac{\partial v}{\partial x} \right)^{k+1} \\
& + \frac{1}{2}h_y \left[(1+\beta)h - \frac{1}{2}g\Delta t^2 \right] \left(\frac{\partial v}{\partial x} \right)^k - h \left[\frac{1}{3}(1+\beta)h + \frac{1}{4}g\Delta t^2 \right] \left(\frac{\partial^2 v}{\partial x \partial y} \right)^{k+1} \\
& + h \left[\frac{1}{3}(1+\beta)h - \frac{1}{4}g\Delta t^2 \right] \left(\frac{\partial^2 v}{\partial x \partial y} \right)^k \\
& - g\beta h \Delta t \left[\frac{h}{3}(\eta_{xxx} + \eta_{xyy}) + h_x \left(\eta_{xx} + \frac{1}{2}\eta_{yy} \right) + \frac{1}{2}h_y \eta_{xy} \right] \\
& - \frac{1}{2}g\Delta t^2 \left[\frac{\partial^2}{\partial x^2}(\eta u)^{k+\frac{1}{2}} + \frac{\partial^2}{\partial x \partial y}(\eta v)^{k+\frac{1}{2}} \right] + [(uu_x)^{k+\frac{1}{2}} + (vu_y)^{k+\frac{1}{2}}] \Delta t \quad (4.15)
\end{aligned}$$

The y momentum equation in 2-D form is given by

$$\begin{aligned}
v_t + uv_x + vv_y + g\eta_y &= (1+\beta)\frac{h^2}{3}v_{yyt} + (1+\beta)hh_y v_{yt} \\
& + (1+\beta)\frac{h^2}{3}u_{xyt} + \frac{1}{2}(1+\beta)hh_x u_{yt} \\
& + \frac{1}{2}(1+\beta)hh_y u_{xt} + g\beta\frac{h^2}{3}\eta_{yyy} \\
& + g\beta hh_y \eta_{yy} + g\beta\frac{h^2}{3}\eta_{xxy} \\
& + \frac{1}{2}g\beta hh_y \eta_{xx} + \frac{1}{2}g\beta hh_x \eta_{xy} \quad (4.16)
\end{aligned}$$

Discretization of the y momentum equation reads

$$\begin{aligned}
& \frac{v_{i,j}^{k+1} - v_{i,j}^k}{\Delta t} + \frac{1}{2}g \left[\left(\frac{\partial \eta}{\partial y} \right)^{k+1} + \left(\frac{\partial \eta}{\partial y} \right)^k \right]_{i+\frac{1}{2},j} \\
&= (1+\beta) \frac{h^2}{3} \left[\left(\frac{\partial^2 v}{\partial y^2} \right)^{k+1} - \left(\frac{\partial^2 v}{\partial y^2} \right)^k \right] \frac{1}{\Delta t} \\
&+ (1+\beta) hh_y \left[\left(\frac{\partial v}{\partial y} \right)^{k+1} - \left(\frac{\partial v}{\partial y} \right)^k \right] \frac{1}{\Delta t} \\
&- (uv_x)^{k+\frac{1}{2}} - (vv_y)^{k+\frac{1}{2}} + (1+\beta) \frac{h^2}{3} u_{xyt} \\
&+ \frac{1}{2} (1+\beta) hh_x u_{yt} + \frac{1}{2} (1+\beta) hh_y u_{xt} \\
&+ g\beta \frac{h^2}{3} \eta_{yyy} + g\beta hh_y \eta_{yy} + g\beta \frac{h^2}{3} \eta_{xxy} + \frac{1}{2} g\beta hh_y \eta_{xx} \\
&+ \frac{1}{2} g\beta hh_x \eta_{xy} \tag{4.17}
\end{aligned}$$

Substituting $\left(\frac{\partial \eta}{\partial y}\right)_{i,j}^{k+1}$ from equation (4.11) into the discretized y-momentum equation (4.17) and multiplying by Δt gives,

$$\begin{aligned}
v_{i,j}^{k+1} &= v_{i,j}^k - \frac{1}{4}gh \left[\left(\frac{\partial^2 v}{\partial y^2}\right)^{k+1} + \left(\frac{\partial^2 v}{\partial y^2}\right)^k \right] \Delta t^2 + g \left(\frac{\partial \eta}{\partial y}\right)^k \Delta t \\
&= (1 + \beta) \frac{h^2}{3} \left[\left(\frac{\partial^2 v}{\partial y^2}\right)^{k+1} - \left(\frac{\partial^2 v}{\partial y^2}\right)^k \right] + (1 + \beta)hh_y \left[\left(\frac{\partial v}{\partial y}\right)^{k+1} + \left(\frac{\partial v}{\partial y}\right)^k \right] \\
&\quad + \frac{1}{2}gh_y \left[\left(\frac{\partial v}{\partial y}\right)^{k+1} + \left(\frac{\partial v}{\partial y}\right)^k \right] \Delta t^2 + \frac{1}{4}gh_x \left[\left(\frac{\partial u}{\partial y}\right)^{k+1} + \left(\frac{\partial u}{\partial y}\right)^k \right] \Delta t^2 \\
&\quad + \frac{1}{4}gh_y \left[\left(\frac{\partial u}{\partial x}\right)^{k+1} + \left(\frac{\partial u}{\partial x}\right)^k \right] \Delta t^2 + \frac{1}{4}gh\Delta t^2 \left[\left(\frac{\partial^2 u}{\partial x \partial y}\right)^{k+1} + \left(\frac{\partial^2 u}{\partial x \partial y}\right)^k \right] \\
&\quad + (1 + \beta) \frac{h^2}{3} + \left[\left(\frac{\partial^2 u}{\partial x \partial y}\right)^{k+1} - \left(\frac{\partial^2 u}{\partial x \partial y}\right)^k \right] \\
&\quad + \frac{1}{2}(1 + \beta)hh_x \left[\left(\frac{\partial u}{\partial y}\right)^{k+1} - \left(\frac{\partial u}{\partial y}\right)^k \right] + \frac{1}{2}(1 + \beta)hh_y \left[\left(\frac{\partial u}{\partial x}\right)^{k+1} - \left(\frac{\partial u}{\partial x}\right)^k \right] \\
&\quad + g\beta h\Delta t \left[\frac{h}{3}(\eta_{yyy} + \eta_{xxy}) + h_y \left(\eta_{yy} + \frac{1}{2}\eta_{xx} \right) + \frac{1}{2}h_x \eta_{xy} \right] \\
&\quad + \frac{1}{2}g\Delta t^2 \left[\frac{\partial^2}{\partial y^2}(\eta v)^{k+\frac{1}{2}} + \frac{\partial^2}{\partial x \partial y}(\eta u)^{k+\frac{1}{2}} \right] - [(uv_x)^{k+\frac{1}{2}} + (vvy)^{k+\frac{1}{2}}] \Delta t \quad (4.18)
\end{aligned}$$

Rearranging equation (4.18) given above,

$$\begin{aligned}
& h \left[\frac{1}{3}(1+\beta)h + \frac{1}{4}g\Delta t^2 \right] \left(\frac{\partial^2 v}{\partial y^2} \right)^{k+1} \\
& + h_y \left[(1+\beta)h + \frac{1}{2}g\Delta t^2 \right] \left(\frac{\partial v}{\partial y} \right)^{k+1} - v_{i,j}^{k+1} \\
= & h \left[\frac{1}{3}(1+\beta)h - \frac{1}{4}g\Delta t^2 \right] \left(\frac{\partial^2 v}{\partial y^2} \right)^k + h_y \left[(1+\beta)h - \frac{1}{2}g\Delta t^2 \right] \left(\frac{\partial v}{\partial y} \right)^k \\
& - v_{i,j}^k + g \left(\frac{\partial \eta}{\partial x} \right)^k \Delta t - \frac{1}{2}h_y \left[(1+\beta)h + \frac{1}{2}g\Delta t^2 \right] \left(\frac{\partial u}{\partial x} \right)^{k+1} \\
& + \frac{1}{2}h_y \left[(1+\beta)h - \frac{1}{2}g\Delta t^2 \right] \left(\frac{\partial u}{\partial x} \right)^k - \frac{1}{2}h_x \left[(1+\beta)h + \frac{1}{2}g\Delta t^2 \right] \left(\frac{\partial u}{\partial y} \right)^{k+1} \\
& + \frac{1}{2}h_x \left[(1+\beta)h - \frac{1}{2}g\Delta t^2 \right] \left(\frac{\partial u}{\partial y} \right)^k - h \left[\frac{1}{3}(1+\beta)h + \frac{1}{4}g\Delta t^2 \right] \left(\frac{\partial^2 u}{\partial x \partial y} \right)^{k+1} \\
& + h \left[\frac{1}{3}(1+\beta)h - \frac{1}{4}g\Delta t^2 \right] \left(\frac{\partial^2 u}{\partial x \partial y} \right)^k \\
& - g\beta h \Delta t \left[\frac{h}{3}(\eta_{yyy} + \eta_{xxy}) + h_y \left(\eta_{yy} + \frac{1}{2}\eta_{xx} \right) + \frac{1}{2}h_x \eta_{xy} \right] \\
& - \frac{1}{2}g\Delta t^2 \left[\frac{\partial^2}{\partial y^2}(\eta v)^{k+\frac{1}{2}} + \frac{\partial^2}{\partial x \partial y}(\eta u)^{k+\frac{1}{2}} \right] + [(uv_x)^{k+\frac{1}{2}} + (vv_y)^{k+\frac{1}{2}}] \Delta t \quad (4.19)
\end{aligned}$$

The numerical solution proceeds as follows. First, the provisional values of η are computed from the continuity equation (4.9) using the old time velocity values. The discretized x - and y -momentum equations (4.15) and (4.19) yield a tridiagonal matrix system for the velocities u and v at new time level. For the x -sweep, the new time level values of v^{k+1} s are treated as known by using the last computed values so that u^{k+1} s are the only unknowns. The resulting matrix system is solved by Thomas Algorithm. Similarly for the y -sweep, the v^{k+1} s are the only unknowns to be solved. Finally the continuity equation (4.9) is used again to obtain the improved values of η using the newly computed u^{k+1} and v^{k+1} values. At each time step the procedure is iterated thrice, which is found to be sufficient for reliable results. For a more precise approach the successive values of the variables may be compared according to a convergence criterium. Nevertheless the numerical experiments do not justify the

additional computational load as no appreciable improvement in the results is observed with increasing iteration number.

The performance of the non-reflective boundaries is checked by a ring test which reveals the symmetrical accuracy of the model. The ring test for all the modes (long wave, classical Boussinesq and Boussinesq with Padé (2,2)) of the numerical scheme are performed; however, only the test for the improved Boussinesq model is shown here. The computational domain is taken as 2×2 m with $h = 0.1$ m water depth. The region is discretized by 50 points along both x - and y -axes. Time step $\Delta t = 1/50$ s, and the simulations are shown for $t = 0.2$ s, 0.4 s and 0.5 s in Figure 4.3 and for $t = 0.6$ s, 0.8 s and 1.0 s in Figure 4.4. The contour plots show nearly perfect symmetry.

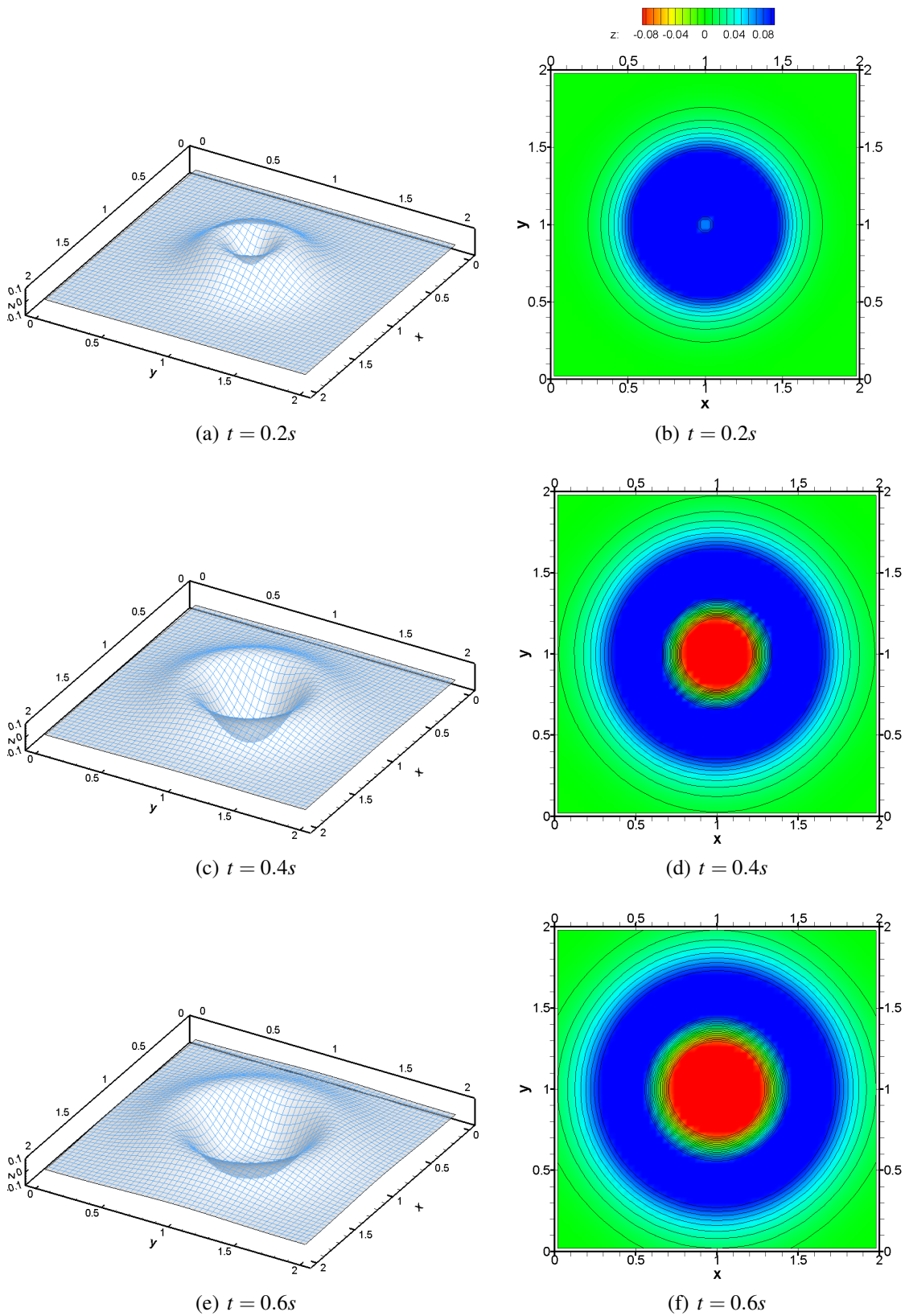


Figure 4.3: Ring test for 2-D Boussinesq equations with $\beta = 1/5$ at $t = 0.2$, $t = 0.4$ and $t = 0.6$ seconds. Left column: perspective views, right column: contour graphics.

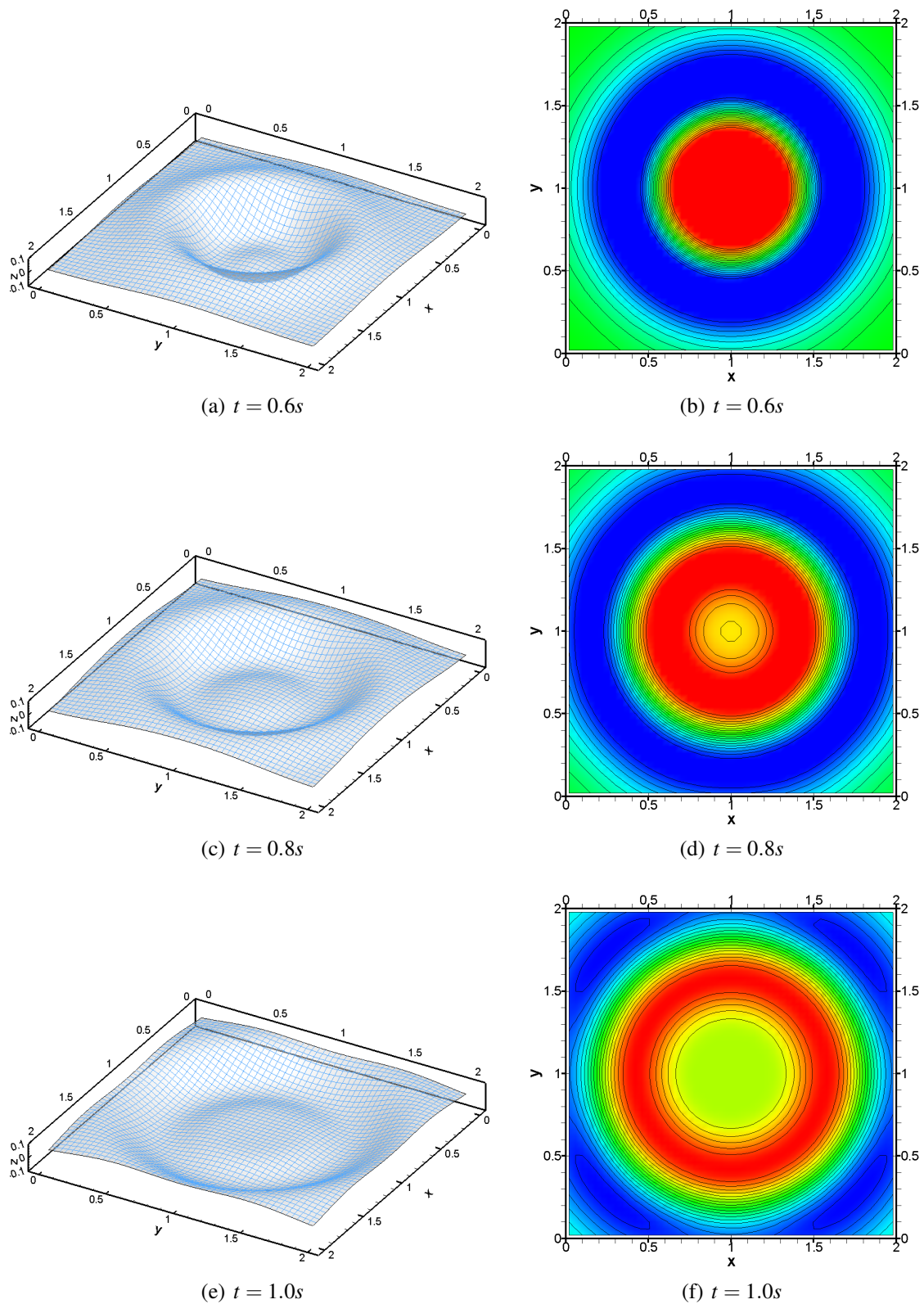


Figure 4.4: Ring test for 2-D Boussinesq equations with $\beta = 1/5$ at $t = 0.6$, $t = 0.8$ and $t = 1.0$ seconds. Left column: perspective views, right column: contour graphics.

5. SOLITARY WAVES AND CNOIDAL WAVES

5.1 Theoretical Description of Solitary Waves

The most elementary analytical solution of Boussinesq equations is the solitary wave [59], [60], [61]. A solitary wave is a wave with only crest and a surface profile lying entirely above the still water level. It is neither oscillatory nor does it exhibit a trough. The solitary wave can be defined as a wave of translation since the water particles are displaced at a distance in the direction of wave propagation as the wave passes [1]. The initial observation of a solitary wave in shallow water was made by John Scott Russell. In Russells [59] own words: "I was observing the motion of a boat which was rapidly drawn along a narrow channel by a pair of horses, when the boat suddenly stopped-not so the mass of water in the channel which it had put in motion; it accumulated round the prow of the vessel in a state of violent agitation, then suddenly leaving it behind, rolled forward with great velocity, assuming the form of a large solitary elevation, a rounded, smooth and well-defined heap of water, which continued its course along the channel apparently without change of form or diminution of speed. I followed it on horseback, and overtook it still rolling on at a rate of some eight or nine miles an hour, preserving its original figure some thirty feet long and a foot to a foot and a half in height. Its height gradually diminished, and after a chase of one or two miles I lost it in the windings of the channel. Such, in the month of August 1834, was my first chance interview with that singular and beautiful phenomenon which I have called the Wave of Translation." Russell built a water tank to visualize this wave and made research about the properties of the solitary waves.

Boussinesq [6] , Rayleigh [62], Keller [63] and Munk [64] performed pioneering theoretical studies of solitary waves [1]. In 1895, the Dutch professor Diederik Korteweg and his doctoral student Gustav de Vries [53] derived a partial differential equation which models the solitary wave that Russell had observed. So called the Korteweg-de Vries (KdV) equation had already appeared in studies on water waves

published by Boussinesq [6] and Rayleigh [62]. More recent analyses of solitary waves were performed by Fenton [60], Longuet-Higgins and Fenton [65], and Byatt-Smith and Longuet-Higgins [66]. In 1965, Zabusky and Kruskal [67] simulated the collision of solitary waves in a nonlinear crystal lattice and observed that they retain their shapes and speed after collision. Interacting solitary waves experience a phase shift, advancing the faster and retarding the slower. In analogy with colliding particles, the word "solitons" is used to describe these elastically colliding waves. A narrative of the discovery of solitons can be found in Zabusky [68]. A true solitary wave cannot be formed in nature because there are usually small dispersive waves at the trailing edge of the wave. On the other hand, long waves such as tsunamis and waves resulting from large displacements of water caused by such phenomena as landslides and earthquakes sometimes behave approximately like solitary waves. Also, when an oscillatory wave moves into shallow water, it may often be approximated by a solitary wave [64]. In this situation, the wave amplitude becomes progressively higher, the crests become shorter and more pointed, and the trough becomes longer and flatter. Fenton's solution gives the maximum solitary wave height, $H_{max} = 0.85h$ and maximum propagation speed $c_{max}^2 = 1.7gh$. Earlier research studies using the solitary waves obtained $H_{max} = 0.78h$ and $c_{max}^2 = 1.56gh$ where H is wave height, h is water depth, c is wave speed and g is gravity of acceleration. For calculating the height of breaking waves in shallow water, usually the maximum solitary-amplitude wave is used. However, other studies has shown that the highest solitary wave is not necessarily the most energetic [69].

Only one parameter, wave steepness, $\varepsilon = H/h$ is needed to specify a solitary wave because both wavelength and period of solitary waves are infinite. To lowest order, the solitary wave profile varies as $\text{sech}^2 q$ [70], where $q = (3H/h)^{1/2}(x - ct)/2h$. The free-surface elevation, particle velocities, and pressure may be expressed respectively as follows [1];

$$\frac{\eta}{H} = \frac{u}{\sqrt{gh} \frac{H}{h}} \quad (5.1)$$

$$\frac{u}{\sqrt{gh}} \frac{H}{h} = \frac{\Delta p}{\rho g H} \quad (5.2)$$

$$\frac{\Delta p}{\rho g H} = \text{sech}^2 q \quad (5.3)$$

where Δp is the difference in pressure at a point under the wave due to the presence of the solitary wave. To second approximation, this pressure difference is given by

$$\frac{\Delta p}{\rho g H} = 1 - \frac{3H}{4h} \left[1 - \left(\frac{Y_s}{h} \right)^2 \right] \quad (5.4)$$

where Y_s is the height of the surface profile above the bottom. Since the solitary wave has horizontal particle velocities only in the direction of wave advance, there is a net displacement of fluid in the direction of wave propagation.

The solitary wave is a limiting case of the cnoidal wave. Cnoidal waves may be viewed as the nonlinear counterparts of the sinusoidal waves in shallow water. When $k^2 = 1, K(k) = K(1) = \infty$, and the elliptic cosine reduces to the hyperbolic secant function and the water surface Y_s measured above the bottom reduces to

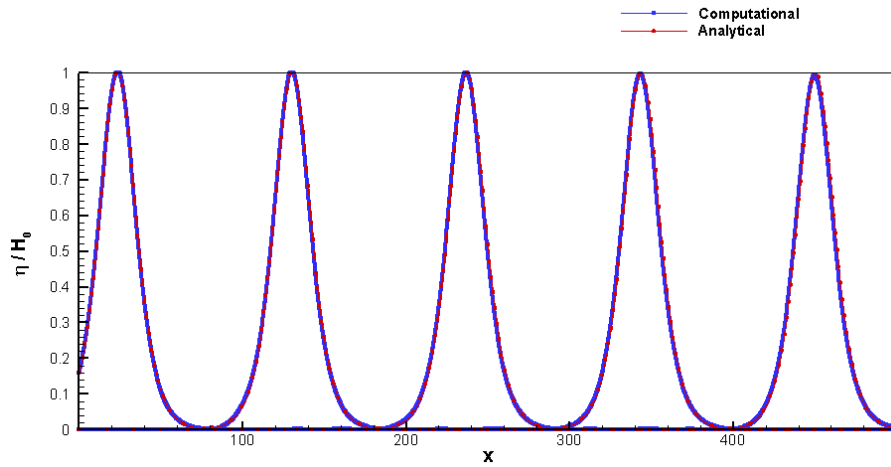
$$Y_s = h + H \operatorname{sech}^2 \left[\sqrt{\frac{3H}{4h^3}} (x - ct) \right] \quad (5.5)$$

and the free surface is given by,

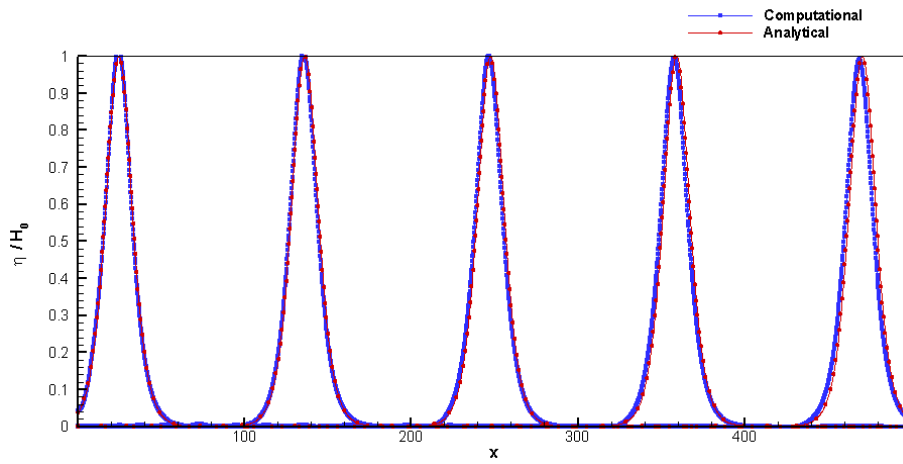
$$\eta = H \operatorname{sech}^2 \left[\sqrt{\frac{3H}{4h^3}} (x - ct) \right] \quad (5.6)$$

5.2 Numerical Simulations of Solitary Waves

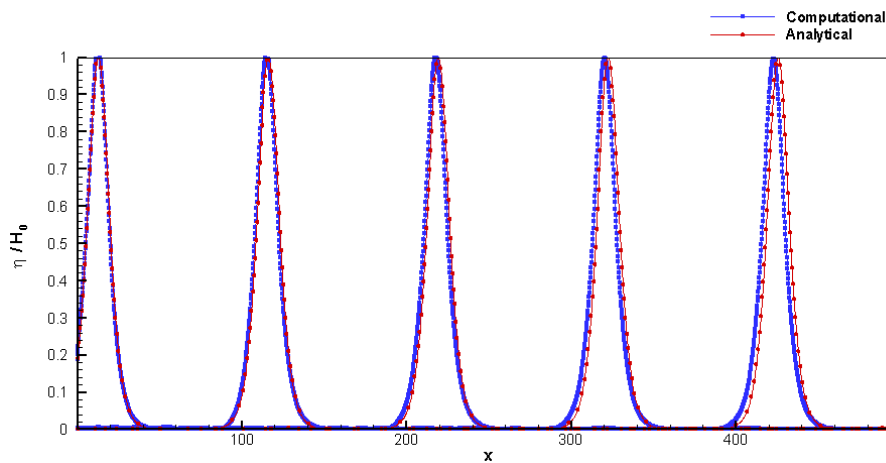
The numerical tests presented here are done using the numerical scheme developed in Section 3. The water depth is taken constant with $h = 1$ m and both the original ($\beta = 0$) and the improved Boussinesq equations ($\beta = 1/5$) are used for comparing the difference between analytical and numerical solutions. As it can be seen in Figures 5.1 and 5.2, except for a phase difference especially for steeper waves, the analytical and computational results agree fairly well for both $\beta = 0$ and $\beta = 1/5$. From analytical point of view, the solitary waves corresponding to the improved Boussinesq equations should be slightly different. Differences in height between analytical and computational results are shown in Figure 5.3 for $\beta = 0$ by calculating the relative error percentage for different ε values. It is observed that as nonlinearity parameter,



(a) $\beta = 0, \quad \varepsilon = 0.1$

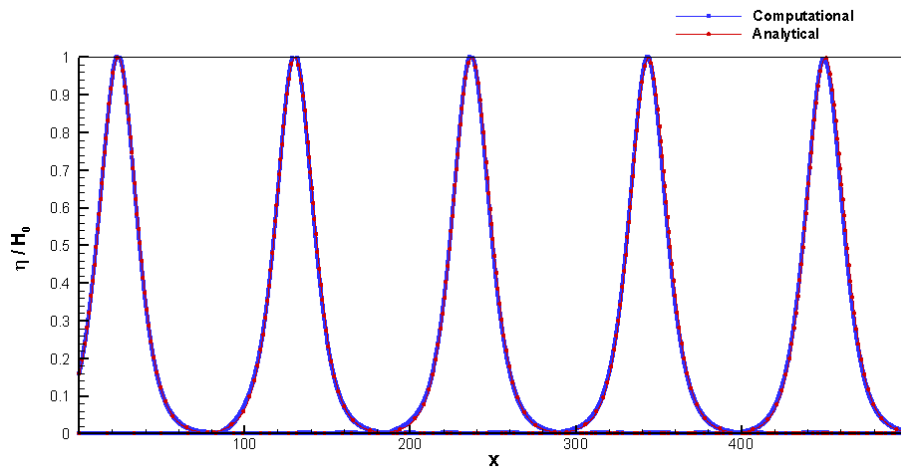


(b) $\beta = 0, \quad \varepsilon = 0.2$

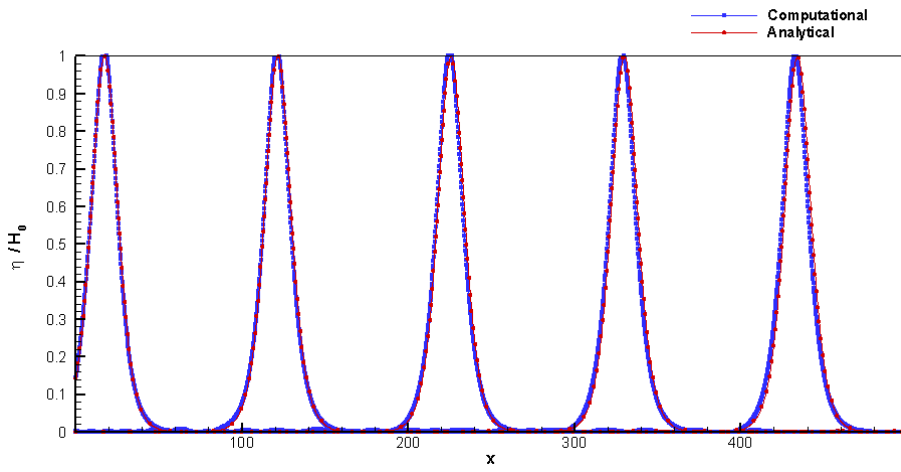


(c) $\beta = 0, \quad \varepsilon = 0.3$

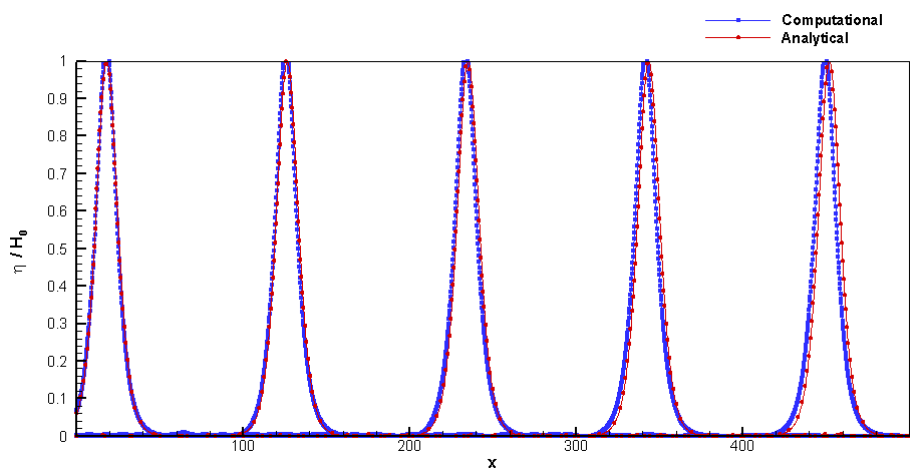
Figure 5.1: Solitary waves for different wave heights $\varepsilon = H/h = 0.1, 0.2, 0.3$ when $\beta = 0$.



(a) $\beta = 1/5, \quad \varepsilon = 0.1$



(b) $\beta = 1/5, \quad \varepsilon = 0.2$



(c) $\beta = 1/5, \quad \varepsilon = 0.3$

Figure 5.2: Solitary waves for different wave heights $\varepsilon = H/h = 0.1, 0.2, 0.3$ when $\beta = 1/5$.

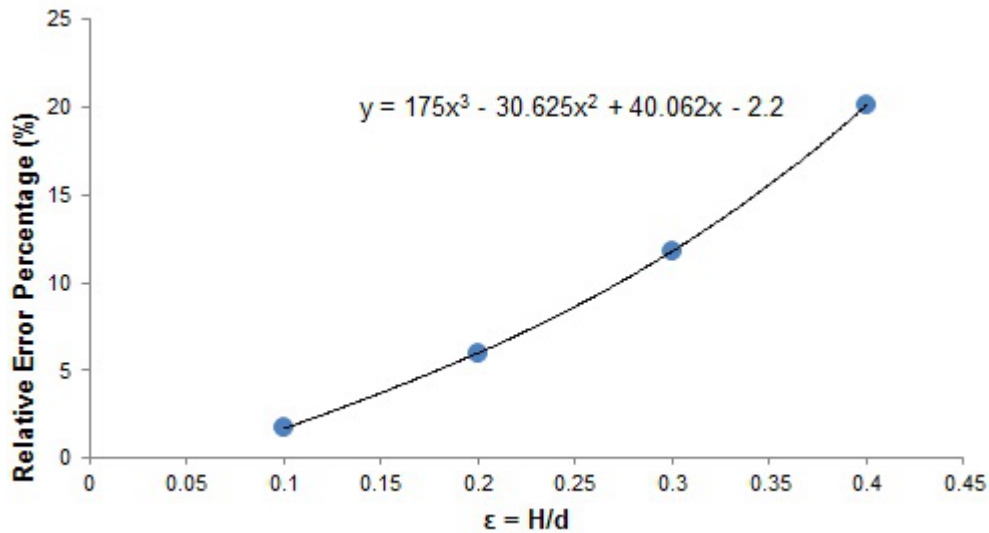


Figure 5.3: Relative error of the calculated wave height versus nonlinearity parameter.

ϵ , increases, the relative error percentage increases up to 20% for $\epsilon = 0.4$. Note that $\epsilon = 0.78$ is the theoretical wave breaking limit.

5.3 Theoretical Description of Cnoidal Waves

Long, finite-amplitude waves of permanent form propagating in shallow water may be described by cnoidal wave theory. The existence in shallow water of such long waves of permanent form may have first been recognized by Boussinesq [6]. However, the theory was originally developed by Korteweg and de Vries [53] and it is applicable to finite-amplitude shallow-water waves and includes both nonlinearity and dispersion effects [1]. Although cnoidal theory is based on the Boussinesq equations, it is restricted to waves progressing in only one direction. The theory is defined in terms of the Jacobian elliptic function, cn , thus it is called cnoidal waves. In Figure 5.4 the schematic comparisons are given for different wave theories. It is seen that the linear profile is symmetric about the still water level while the Stokes wave has higher more peaked crests and shorter, flatter troughs. The cnoidal wave crests are higher above the still water level than the troughs are below the still water level. Compared to Stokes waves, cnoidal troughs are longer and flatter and crests are sharper and steeper. The solitary wave which is describes in the previous section has all of its profile above the still water level. Validity range of cnoidal theory is approximately $h/L < 1/8$ when the Ursell number $U_R > 20$. As wavelength becomes long and approaches infinity, cnoidal wave theory reduces to the solitary wave theory. In addition, as H/h ratio

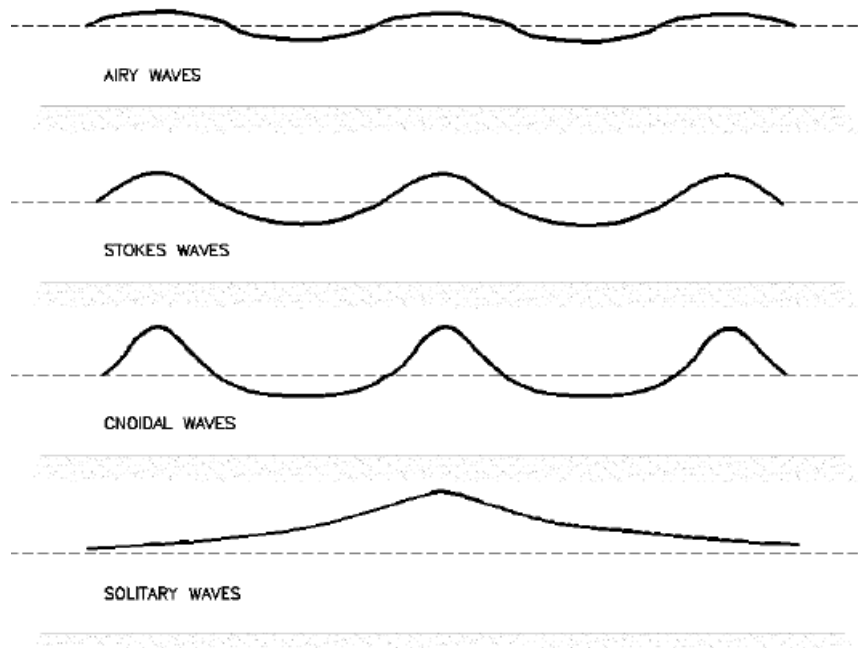


Figure 5.4: Wave profiles of different progressive waves, adapted from Coastal Engineering Manual [1].

decreases, the wave profile approaches the sinusoidal profile predicted by the linear theory [1]. Keulegan and Patterson [71], Keller [63], Laitone [30] developed first-through third-order approximations to the cnoidal wave theory. However, Wiegel's study [72] summarized the principal results in a more practical way by presenting such wave characteristics as length, celerity, and period in tabular and graphical form. Furthermore, Wiegel [70] simplified the previous works for engineering applications. Additional improvements to the theory have been made by Miles [47] and Fenton [60], [73]. Fenton [73] used a Rayleigh-Boussinesq series in order to develop a generalized recursion relationship for the KdV solution of any order. The theoretical representations are given by Fenton [73], Fenton and McKee [74] and Miles [47]. Wave characteristics are described in terms of the modules k of the elliptic integrals where k itself has no physical significance, it is used to express the relationships between various wave parameters. The ordinate of the water surface y_s measured above the bottom is given by

$$y_s = y_t + Hcn^2 \left[2K(k) \left(\frac{x}{L} - \frac{t}{T} \right), k \right] \quad (5.7)$$

where y_t is the distance from the bottom to the wave trough, H is wave height between trough and crest, cn is elliptic cosine function, $K(k)$ is complete elliptic integral of the first kind and k modulus of the elliptic integrals. The elliptic cosine function cn is a periodic function where $cn^2[2K(k)(x/L) - (t/T)]$ has a maximum amplitude equal to unity. The modulus k is defined within the range 0 and 1. Note that when $k = 0$, the wave profile becomes a sinusoid, as in the linear theory; when $k = 1$, the wave profile becomes that of a solitary wave [1]. The distance from the bottom to the wave trough y_t is,

$$\frac{y_t}{h} = \frac{y_c}{h} - \frac{H}{h} = \frac{16H^2}{3L^2} K(k)[K(k) - E(k)] + 1 - \frac{H}{h} \quad (5.8)$$

where y_c is the distance from the bottom to the crest, and $E(k)$ is the complete elliptic integral of the second kind. Wavelength, L is expressed as,

$$L = \sqrt{\frac{16H^3}{3H}} kK(k) \quad (5.9)$$

Similarly, the wave period, T is expressed by means of elliptic integrals.

$$T \sqrt{\frac{g}{h}} = \sqrt{\frac{16y_t}{3H}} \frac{h}{y_t} \left[\frac{kK(k)}{1 + \frac{H}{y_t k^2} \left(\frac{1}{2} - \frac{E(k)}{K(k)} \right)} \right] \quad (5.10)$$

6. 1-D LINEAR SHALLOW WATER WAVES FORCED BY A MOVING PRESSURE FIELD

There are different techniques for modeling a specific wave system; namely, analytical wave modeling, empirical wave modeling, physical wave modeling, and numerical wave modeling. Since every method has their own advantage and limitation, the purpose of their application should be chosen carefully. A physical wave system in nature is very complicated. However, it is possible to capture the most important characteristic of this wave system by analyzing it with a simplified theoretical model. Waves propagating in shallow water, $kh < \pi/10$, are often called long waves or shallow water waves. Tidal waves, tsunamis and other waves with extremely long periods and wave lengths are shallow water waves, even in the deep ocean [2]. Linearized continuity equation (2-D) without a moving pressure field can be written as,

$$\frac{\partial(uh)}{\partial x} + \frac{\partial(vh)}{\partial y} = -\frac{\partial\eta}{\partial t} \quad (6.1)$$

Linearized frictionless long wave equations of motion (2-D) are,

$$\frac{\partial u}{\partial t} = -g \frac{\partial \eta}{\partial x} \quad (6.2)$$

$$\frac{\partial v}{\partial t} = -g \frac{\partial \eta}{\partial y} \quad (6.3)$$

With the condition of bottom being horizontal, cross differentiating to eliminate u and v , the equations yield

$$c^2 \left(\frac{\partial^2 \eta}{\partial x^2} + \frac{\partial^2 \eta}{\partial y^2} \right) = \frac{\partial^2 \eta}{\partial t^2} \quad (6.4)$$

where $c = \sqrt{gh}$. This is known as the wave equation which is used in several fields such as membrane vibrations and planar sound waves [2]. The solution of this equation

for a progressive long wave is,

$$\eta = \frac{H}{2} \cos(kx - \omega t) \quad (6.5)$$

Substituting into the x - momentum equation into equation (6.2) yields,

$$\frac{\partial u}{\partial t} = g \frac{H}{2} k \sin(kx - \omega t) \quad (6.6)$$

or

$$u = g \frac{H}{2\omega} k \cos(kx - \omega t) = \frac{\eta}{h} c \quad (6.7)$$

Substituting into the continuity equation yields $c^2 = gh$ which corresponds to the long wave form of the dispersion relationship. The reason of considering linearized long wave equations is to facilitate analytical solutions. In this sense, it is assumed that u and η and their products are small.

6.1 Analytical Solution of 1-D Linear Shallow Water Waves Forced By A Moving Pressure Field

For testing the accuracy of numerically simulated waves due to a moving pressure field, a 1-D case with known analytical solution is considered. The analytical solution for the 1-D linearized long wave equations is recapitulated first and then comparisons with the numerical solutions are given. The linearized long wave equations for constant depth may be written as

$$\begin{aligned} \eta_t + hu_x &= 0 \\ u_t + g\eta_x &= -\frac{1}{\rho} p_x \end{aligned} \quad (6.8)$$

where p is the applied surface pressure. In absence of any forcing function ($p = 0$) the above equations have the free wave solutions

$$\begin{aligned}\eta_1 &= a_1 f(x - ct) \\ \eta_2 &= a_2 f(x + ct)\end{aligned}\tag{6.9}$$

$$\begin{aligned}u_1 &= \frac{c}{h} a_1 f(x - ct) \\ u_2 &= -\frac{c}{h} a_2 f(x + ct)\end{aligned}\tag{6.10}$$

where $f(x, t)$ is an arbitrary function, a_1 and a_2 are arbitrary constants and $c = \sqrt{gh}$ is the shallow water wave celerity. If the pressure field is defined as $p = p_0 f(x - vt)$ with v being the speed of the pressure field in the positive x -direction then the forced system has a solution of the form

$$\begin{aligned}\eta_3 &= a_3 f(x - vt) \\ u_3 &= b_3 f(x - vt)\end{aligned}\tag{6.11}$$

with a_3 and b_3 to be determined from the wave equations. Substituting η_3 , u_3 and p into equation (6.8) gives

$$\begin{aligned}a_3 &= \frac{-hp_0}{\rho(c^2 - v^2)} \\ b_3 &= \frac{-vp_0}{\rho(c^2 - v^2)}\end{aligned}\tag{6.12}$$

Finally, applying the initial condition that the total displacement and velocity must separately be zero at $t = 0$,

$$\begin{aligned}\eta_1 + \eta_2 + \eta_3 &= 0 \\ u_1 + u_2 + u_3 &= 0\end{aligned}\tag{6.13}$$

gives

$$\begin{aligned} a_1 &= \frac{(c+v)hp_0}{2\rho c(c^2-v^2)} \\ a_2 &= \frac{(c-v)hp_0}{2\rho c(c^2-v^2)} \end{aligned} \quad (6.14)$$

The final solution is then

$$\eta = \frac{hp_0}{2\rho c(c^2-v^2)} [(c+v)f(x-ct) + (c-v)f(x+ct) - 2cf(x-vt)] \quad (6.15)$$

and

$$u = \frac{p_0}{2\rho(c^2-v^2)} [(c+v)f(x-ct) - (c-v)f(x+ct) - 2vf(x-vt)] \quad (6.16)$$

Note that when $t = 0$ both η and u become identically zero.

6.2 Numerical Solution of 1-D Linear Shallow Water Waves Forced By A Moving Pressure Field

For the test case the pressure function f is selected in the form of a Gaussian distribution function as $f(\chi) = \exp\left[-(\chi/250)^2\right]$ where $\chi = x - vt$. $p_0 = -5000$ Pa, $\rho = 1000$ kg/m³, $g = 9.81$ m/s² and the water depth is $h = 20$ m so that $c = \sqrt{gh} = 14$ m/s. The length of the computational domain is taken 20000 m, grid size 20 m and time step 1 s. The initial location of the pressure field is in the middle of the computational domain, $x_0 = 10000$ m. Figure 6.1 compares the analytical solution with the numerical solution of long wave equations for $v = 0, 10,$ and 18 m/s cases, which corresponds to the depth-based Froude numbers $Fr = v/c = v/\sqrt{gh} = 0.0, 0.7,$ and 1.3 approximately.

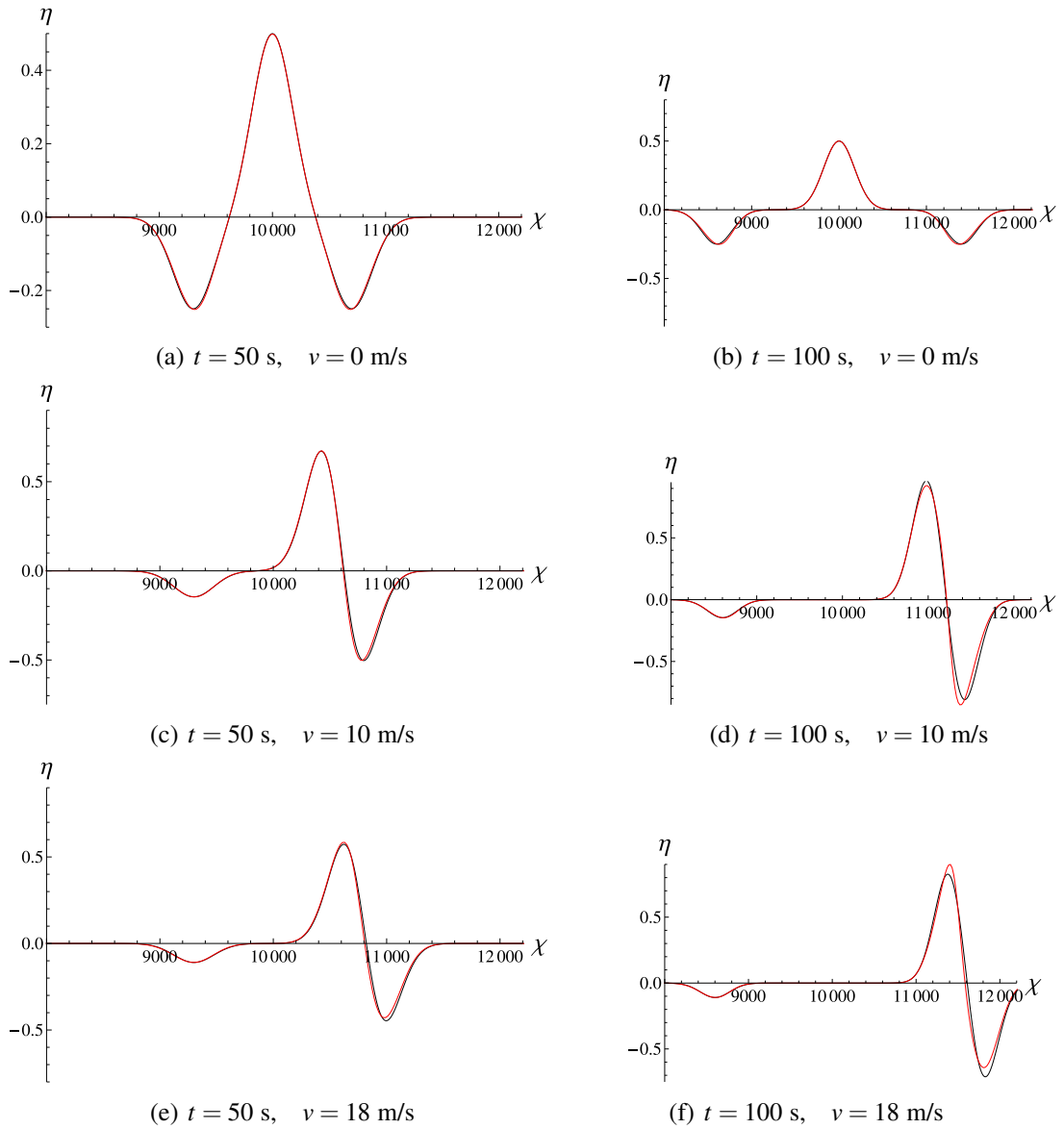


Figure 6.1: Comparison of numerical and analytical solutions of linear shallow water wave equations for a moving pressure with $v = 0$ m/s, $v = 10$ m/s and $v = 18$ m/s at $t = 50$ s (left column) and $t = 100$ s (right column).

The same comparisons using the Boussinesq equations with $\beta = 1/5$ instead of the long wave equations are made in Figure 6.2. As seen from the figures numerical simulations in both cases agree well with the analytical solution derived from the linearized long wave equations.

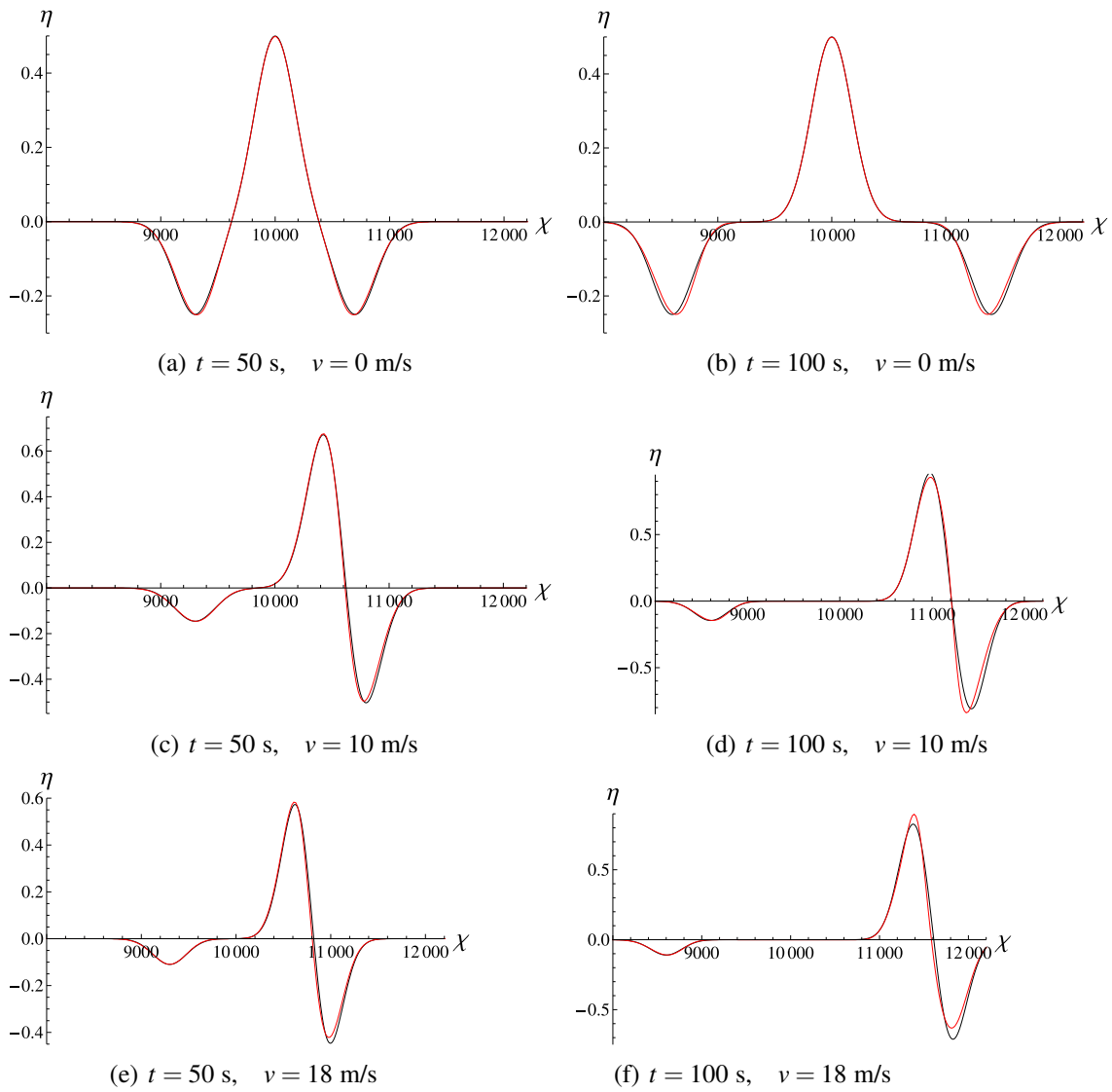


Figure 6.2: Comparison of analytical solution with 1-D Boussinesq solution generated by a moving pressure with $v = 0$ m/s, $v = 10$ m/s and $v = 18$ m/s for $\beta = 1/5$ at $t = 50$ s (left column) and $t = 100$ s (right column).

In Figure 6.3 the average (using 500 points) error percentages between analytical and computational surface elevations are shown for five different pressure field speeds $V = 5, 10, 15, 20$ and 25 m/s which corresponds to depth Froude numbers, $0.4, 0.7, 1.1, 1.4$ and 1.8 at $t = 50$ s when $\beta = 1/5$.

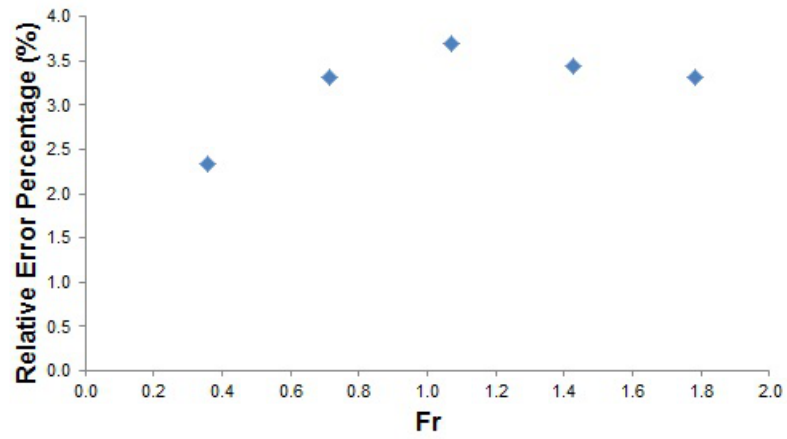


Figure 6.3: Average relative error of the calculated and analytical surface elevation versus Froude number.

Results show that around Froude number 1, the relative error percentage takes its maximum value and as Froude number differs from 1, the error percentage decreases. Having thus established a certain degree of confidence in the numerical scheme regarding the simulation of surface-forced waves the scheme may be used for 2-D simulations.

7. SHIP GENERATED WAVES

As a body moves on the water surface, pressure varies and produces a series of waves within the interface of water and air. The moving point source in deep water generates two sets of waves that move forward and out from the disturbance, which is called divergent waves and the other set of waves moving in the direction of the disturbance is called transverse waves [75].

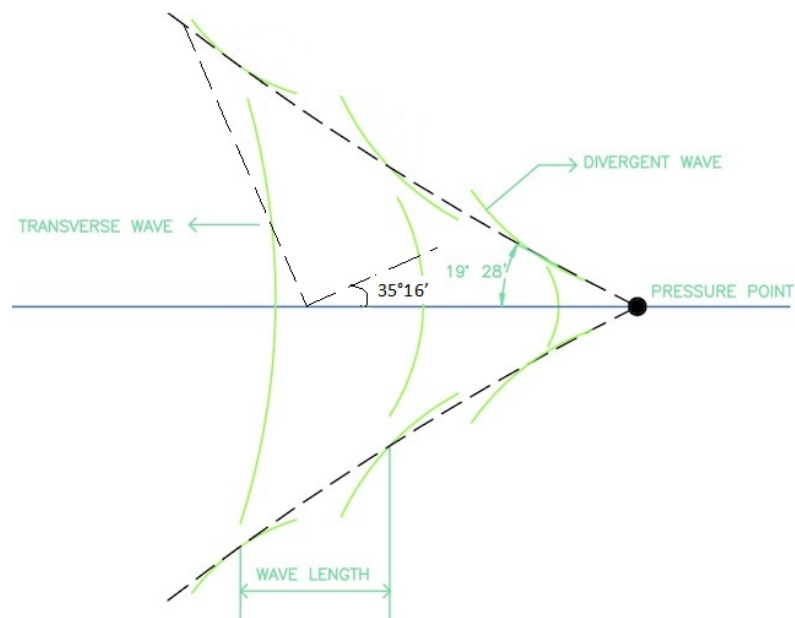


Figure 7.1: Kelvin wave pattern and Kelvin wedge.

7.1 Kelvin Waves for Infinite Depth

In 1887, Lord Kelvin [76] described the wave system produced by a moving vessel in deep water. This wave pattern is confined to a wedge shape known as the Kelvin wedge as seen in Figure 7.1. The envelope of these waves stands at a fixed angle of $19^{\circ}28'$. Diverging waves propagate at an angle of $\theta = 90^{\circ}$ to 35° from the vessel's track but transverse waves propagate at an angle of $\theta = 35^{\circ}$ to 0° from the vessel's track. Under steady conditions, the transverse waves along the vessel's track travel at the same speed as the vessel [77]. Let's assume a single small disturbance that generates waves with

amplitude a . Considering that the coordinate system is moving with the disturbance, the free surface profile will be,

$$\eta = a \cos(kx + \alpha) \quad (7.1)$$

where $k = g/v^2$ and v denotes the velocity of the body and phase angle α considered to be not important. As in kelvin ship waves, surface wave systems of general forms consist of combinations of plane progressive waves which have different frequencies and directions. The most general wave distributions of wave at all possible oblique angles θ can be written as [4],

$$\eta(x, z, t) = Re \int_0^\infty d\omega \int_0^{2\pi} d\theta A(\omega, \theta) \exp[-ik(\omega)(x \cos \theta + z \sin \theta) + i\omega t] \quad (7.2)$$

Equation 7.2 is a two dimensional Fourier integral so the formulas from Fourier theory can be used to find appropriate amplitude functions $A(\omega, t)$ required to generate surface elevation θ . If Equation 7.2 translated into a reference frame moving with the ship in the positive $+x$ direction with velocity v replacing x by $x + vt$ gives,

$$\eta(x, z, t) = Re \int_0^\infty d\omega \int_0^{2\pi} d\theta A(\omega, \theta) \exp[-ik(x \cos \theta + z \sin \theta) + i(\omega - kv \cos \theta)t] \quad (7.3)$$

Here $k(\omega)$ is the wave number corresponding to a given frequency ω in accordance with the dispersion relation $k = \omega^2/g$ for infinite depth or $k \tanh = \omega^2/g$ for finite depth. If we consider the ship as it is moving with the reference frame, the equation (7.3) will be independent of time which means there will be a restriction on the phase velocity of the waves and thus on the wave numbers. In the present situation, equation (7.3) will be independent of time provided that

$$\omega = kv \cos \theta \quad (7.4)$$

This expression is in accordance with stipulating that the phase velocity of each allowable wave component is given by,

$$c = \frac{\omega}{k} = v \cos \theta \quad (7.5)$$

In this manner, as it can be seen in figure (7.2) if a system of plane progressive wave is moving at an angle θ with respect to the x axis, the wave pattern will appear steady state to the observer moving along the x axis with velocity $c \sec \theta$. Note that the phase velocity of the waves, c in the kelvin wake propagating in direction θ must be equal to $v \cos \theta$ otherwise they cannot be stationary relative to the ship. The

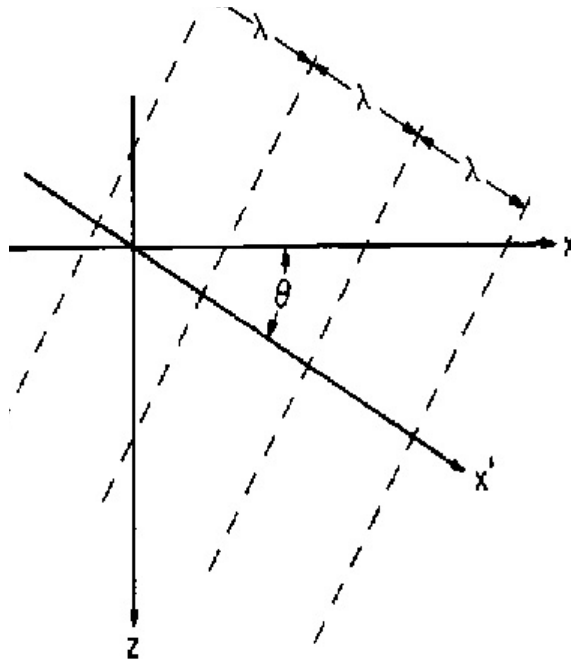


Figure 7.2: View from above of a plane progressive wave system, moving parallel to the x' -axis at an angle θ relative to x . The wave crests are shown by dashed lines, adapted from Newman [4].

restriction given in equation (7.4) can be used to eliminate one of the variables given in equation (7.3). Retaining the wave angle θ , and noting that equations (7.4) and (7.5) require the condition $\cos \theta > 0$, equation (7.3) can be replaced by the single integral,

$$\eta(x, z) = \text{Re} \int_{-\pi/2}^{\pi/2} d\theta A(\theta) \exp[-ik(\theta)(x \cos \theta + z \sin \theta)] \quad (7.6)$$

For deep water, $k = \omega^2/g$ and combining this with the expression (7.4) one gets,

$$k(\theta) = g/v^2 \cos^2 \theta \quad (7.7)$$

The free wave distribution of a given ship considered in equation (7.6) can be simplified if the distance downstream from the position of the ship is very large so one get the classical ship wave pattern derived by Lord Kelvin in 1887. Noting that in two dimensions, wave groups travel with the group velocity $U = \frac{d\omega}{dk}$. Equation (7.6) is a slowly varying two dimensional wave system so the same result should be valid here. Defining x' with respect to a fixed reference frame, then it can be said that x' is the local coordinate normal to the wave crests as seen in figure (7.2). The waves travelling in groups, $U = x'/t$ are determined as [5],

$$\frac{x'}{t} = U = \frac{d\omega}{dk} \quad (7.8)$$

Focusing on the speed of the energy density rather than the speed of wave crests, relative to the earth fixed inclined coordinate system (X', Z') ,

$$x' = \frac{d\omega}{dk}t \Rightarrow \frac{d}{dk}(kx' - \omega t) = 0 \quad (7.9)$$

$$x' = X \cos \theta + Z \sin \theta$$

$$x' = x \cos \theta + z \sin \theta + vt \cos \theta$$

then,

$$kx' - \omega t = k(x \cos \theta + z \sin \theta) + (kv \cos \theta - \omega)t$$

Recalling equation (7.4) and substituting this expression into the above equation yields,

$$kx' - \omega t = k(x \cos \theta + z \sin \theta) \quad (7.10)$$

If expression (7.9) is transformed into the frame of reference of equation (7.6), the waves will satisfy,

$$\frac{d}{dk}[k(\theta)(x \cos \theta + z \sin \theta)] = 0 \quad (7.11)$$

It follows from the chain rule of differentiation $\frac{d}{dk} = \frac{d}{d\theta} \frac{d\theta}{dk}$, since k and θ are related by the equation (7.7), equation (7.11) takes the form,

$$\frac{d}{d\theta} \left(\frac{x \cos \theta + z \sin \theta}{\cos^2 \theta} \right) = 0 \quad (7.12)$$

The equation above is not valid for the points $\theta = 0$ and $\theta = \pm\pi/2$ where $d\theta/dk$ is infinite or zero respectively. Evaluating the above derivative yields,

$$x \sec^2 \theta \sin \theta + z \sec^3 \theta (1 + \sin^2 \theta) = 0 \quad (7.13)$$

Simple algebra results in,

$$\frac{z}{x} = -\frac{\cos \theta \sin \theta}{1 + \sin^2 \theta} \quad (7.14)$$

The solution gives us a relation between z/x and θ which shows that local waves in a Kelvin wake can only propagate in a certain direction θ for a given z/x . The plot of this equation is as follows, As it can be seen in figure (7.3) the maximum value of the ratio, $\tan 19^\circ 28'$, occurs when the wave angle is $\pm 35^\circ 16'$. z/x is antisymmetric about $\theta = 0$ which represents the Kelvin wakes in the port and starboard sides of the vessel. If $\theta = 0$, waves propagate in the same direction as the ship but they only exist at $z = 0$. If $\theta = \pi/2$ this means that waves are propagating at an angle 90° relative to the ship direction of forward translation. Waves propagating $\theta = 35^\circ 16'$ relative to the ship axis are seen at the caustic of the Kelvin wake.

Lighthill [5] showed that during t_g seconds the energy generated in waves with wave speed c does not travel a distance ct_g . Regarding group velocity, the waves travel a distance of vt_g where group velocity is $U = c/2$ for deep water. Therefore all the wave

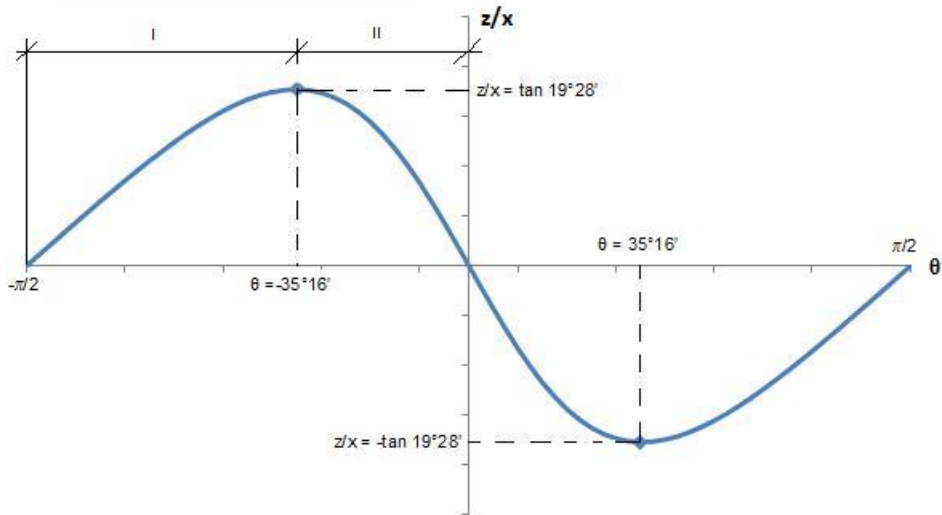


Figure 7.3: Waves situated along the radial line moving in the direction θ , adapted from Lighthill [5].

energy generated t_g seconds earlier has travelled exactly half as far as indicated in Figure 7.4.

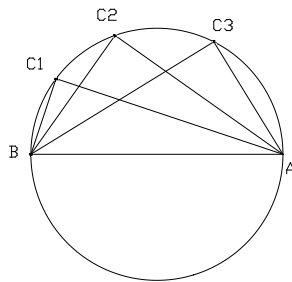


Figure 7.4: Positions C_1, C_2, C_3 of any waves generated t_g seconds ago (when the ship was at A) if their energy had travelled a distance ct_g , adapted from Lighthill [5].

Figure 7.5 shows the real locus of all the wave energy obtained. Here, the locus previously obtained is indicated with a circle of diameter $|AD|$ since D is the halfway from A to B . E_1, E_2 or E_3 indicate the positions of the waves while C_1, C_2 and C_3 are the positions the waves would reach if the energy had travelled at the speed of the crests.

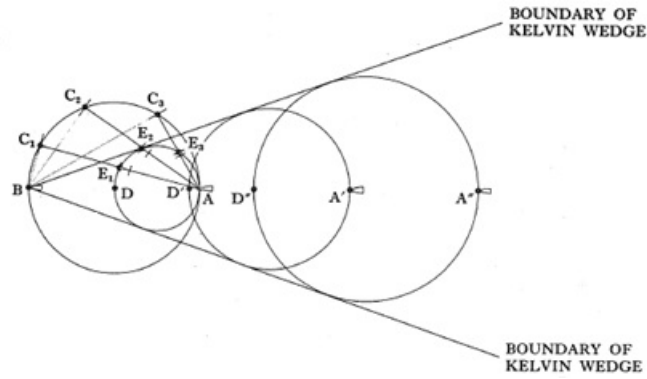


Figure 7.5: Waves generated in deep water by a ship B, adapted from Lighthill [5].

At position E_1 , the waves propagate at a relatively small angle θ to the direction of the ship's motion. On the other hand, at this position waves have higher speeds $c = v \cos \theta$ so these waves are the longer waves in the pattern. The waves at E_3 have smaller wave speed c and much smaller wave length $\lambda = 2\pi c^2/g$. The rest of the ship wave pattern is generated when the ship was at particular points such as A , A' and A'' where the points D , D' and D'' are exactly halfway to B , the present position of the ship. The tangent from B to the circle with diameter $|AD|$ makes an angle $\sin^{-1} 1/3 = 19^\circ 28'$ to the ship's path. The reason is, since $|BD| = |DA|$, the circle's center is at a distance from B of three times its radius $|1/2AD|$. Therefore, all the circles generating the wave pattern lies within a wedge of $19^\circ 28'$ meaning that the wave energy generated at different times carried by these circles are tangent to this wedge. The waves on the boundary of the wedge such as, E_1 , E_2 or E_3 propagate at the angle $1/2(1/2\pi - \sin^{-1} 1/3) = 35^\circ$ to the ship's path.

Let's calculate the crest shapes in the Kelvin ship wave pattern. Supposing that the ship is traveling in the $-x$ direction, the waves generated when it was at $x = vt_g = X$ which refers to a distance of $|AB|$ are now let's say at point E_1 . As seen in Figure 7.6

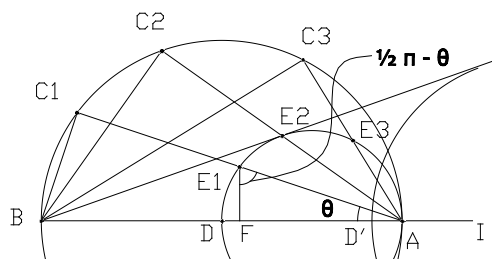


Figure 7.6: Detailed view of Kelvin Wedge, adapted from Lighthill [5].

more detailed, geometrically this point is at $x = |FB|$ and $z = |FE_1|$. Remembering once again that during t_g seconds, the energy generated in waves with speed c does not travel a distance ct_g but travels a distance $c/2t_g$, it can be denoted that $|AB| = vt_g$, $|AC_1| = vt_g \cos \theta$ and $|AE_1| = (vt_g \cos \theta)/2$ respectively.

Substituting $|AE_1|$ into the expression $|FA| = |AE_1| \cos \theta$, one gets $|FA| = (vt_g \cos \theta)/2 \cos \theta$. Considering that $|FB| = |AB| - |FA|$ and by substituting $|AB|$ and $|FA|$ into this expression, $|FB| = vt_g - (vt_g \cos \theta)/2 \cos \theta$. Similarly, $|FE_1| = |AE_1| \sin \theta = (vt_g \cos \theta)/2 \sin \theta$. Substituting vt_g by X and rearranging in expressions $|FB|$ and $|FE_1|$ gives the new position of the wave crest on the x and z axis which are,

$$x = X \left(1 - \frac{1}{2} \cos^2 \theta \right), \quad z = \frac{1}{2} X \cos \theta \sin \theta \quad (7.15)$$

The crest at the above mentioned points (7.15), x and z , make an angle $\frac{1}{2}\pi - \theta$ with the x axis so the slope is,

$$dz/dx = \cot \theta \quad (7.16)$$

Satisfying this crest slope at each point, one should observe that these portions of crest should be varying with positions of generation $(X, 0)$ and directions of propagation θ . Substituting x and z in equation (7.16) and solving for X we obtain,

$$X = X_1 \cos \theta \quad (7.17)$$

where X_1 is a constant. Using equation (7.15), the crest shape can be obtained parametrically as,

$$x = X_1 \cos \theta \left(1 - \frac{1}{2} \cos^2 \theta \right), \quad z = \frac{1}{2} X_1 \cos^2 \theta \sin \theta \quad (7.18)$$

By using equation 7.18, indication of the crest shapes in the Kelvin ship-wave pattern can be plotted for several values of X_1 as seen in Figure 7.7 . On the boundaries of the wedge all the crest shapes have cusps. In addition, the longer waves propagating at

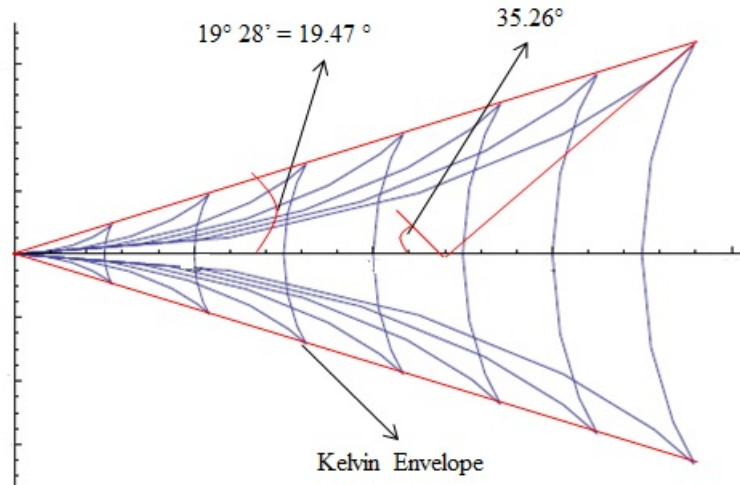


Figure 7.7: Kelvin ship-wave pattern.

small angles θ and the much shorter waves propagating at large angles θ are often superimposed for intermediate Froude numbers [5]. At low Froude numbers, the longer waves with crests nearly perpendicular to the ship's path predominate while at higher Froude numbers much shorter waves predominate as observed for typical high speed boats. On the other hand, for intermediate Froude numbers, the entire Kelvin ship-wave pattern may be apparent. Here the Froude number mentioned is denoted by v^2/gL where L is the ship's length and v is the speed of the ship.

7.2 Havelock's Analytical Solution for Finite Depth

In 1908, Havelock [78] investigated the wave pattern generated by a single point source in shallow water. He introduced the depth Froude number, stating that the characteristics of the wave pattern in depth-limited water are a function of vessel speed and water depth. Later on, Lighthill [5] and Whitham [46] studied the kinematics of ship wave interaction. These researches showed that all steady surface perturbations are inside a wedge which has an angle about 39° . This angle is determined only by the dispersion properties of surface waves. In other words, it does not depend on the ship velocity.

Havelock [78] investigated point impulse moving on water of finite depth. Considering a point impulse moving with a uniform velocity v over the surface of a dispersive medium for which U is the group velocity and c is the wave velocity for a value of wave number, k of $2\pi/\lambda$, he investigated wave patterns for various depth Froude

numbers. This must be emphasized strongly that the Froude numbers defined and used by Havelock is not the same as that of Kelvin. Here the depth-based Froude number is $Fr = v/\sqrt{gh}$ where v is the speed of the disturbance and h is the water depth. Including all wave lengths and water depths, the phase velocity, c and group velocity U are expressed as,

$$c = \left(\frac{g}{k} \tanh kh\right)^{1/2}, \quad U = \frac{1}{2} \left(\frac{g}{k} \tanh kh\right)^{1/2} \left(1 + \frac{2kh}{\sinh 2kh}\right) \quad (7.19)$$

Havelock expressed the group velocity as $U = \frac{1}{2}(n+1)c$ where n varies between 0 and 1 depending on the value of wave number k which is denoted by $n = 2kh/\sinh 2kh$. Besides the defining the parameter n , he defined two other parameters which are $p = gh/v^2 = c^2/v^2 = 1/Fr^2$ and $m = \tanh kh/kh$. The parameters m and n are the function of the wave number k and their limiting values are as $k = 0$; $m = 1$ and $n = 1$. In addition, as $k \rightarrow \infty$; $m = 0$ and $n = 0$. Havelock [78] considered two cases as $p > 1$ where $c < \sqrt{gh}$ and $p < 1$ where $c > \sqrt{gh}$.

For subcritical Froude numbers when $c < \sqrt{gh}$ ($p > 1$) the lines of cusps within which the wave pattern lies are given by such values of k ,

$$\cos^2 \theta = \frac{8(1-n)}{(3-n)^2} \quad (7.20)$$

As it can be seen in Table 7.1 for any value of k , n only lies between 1 and 0. Therefore θ can only take the values between $\cos^{-1}(2\sqrt{2/3})$ and $\pi/2$ which corresponds the values between $19^\circ 28'$ and 90° . For a given Froude number or p in the subcritical range, first kh is solved by iteration from the relationship $m(3-n) = 2/p$. Afterwards, using the computed kh the numerical value of n is obtained to compute θ . Here, the greatest value that the expression $m(3-n) = 2/p$ can take is 2 since $p > 1$. As p approaches 1 the speed of the moving impulse v approaches the critical value \sqrt{gh} . Correspondingly, at the line of cusps m and n both approach to their limiting value 1 while the cusp angle widens out approaching to 90° . On the other hand, if n is 1, the group velocity U is equal to the wave speed c and in such a case the medium is non-dispersive shallow water. Therefore, at \sqrt{gh} which is the critical velocity v , there is a source emitting disturbances and it propagates at the rate of propagation

of disturbances. The pattern seen is a line through the source at right angles to the direction of motion.

Table 7.1: Havelock's analytical results for subcritical Froude numbers ($Fr < 1$) computed from the iterative solution of $m(3 - n) = 2/p$.

$Fr (v/\sqrt{gh})$	n	kh	p	$2/p$	$m(3 - n)$	θ
0.39	0.00	10.00	6.67	0.30	0.30	19.47
0.38	0.00	10.39	6.93	0.29	0.29	19.47
0.38	0.00	10.50	7.00	0.29	0.29	19.47
0.43	0.00	8.00	5.33	0.37	0.37	19.47
0.43	0.00	8.10	5.40	0.37	0.37	19.47
0.42	0.00	8.50	5.67	0.35	0.35	19.47
0.50	0.00	6.00	4.00	0.50	0.50	19.48
0.50	0.00	6.00	4.00	0.50	0.50	19.48
0.55	0.00	4.96	3.31	0.61	0.60	19.50
0.55	0.00	5.00	3.33	0.60	0.60	19.50
0.55	0.00	4.95	3.30	0.61	0.61	19.50
0.60	0.00	4.16	2.78	0.72	0.72	19.58
0.61	0.00	4.04	2.70	0.74	0.74	19.61
0.61	0.01	4.00	2.67	0.75	0.75	19.62
0.63	0.01	3.77	2.52	0.79	0.79	19.69
0.70	0.03	3.02	2.04	0.98	0.98	20.26
0.70	0.03	3.00	2.03	0.99	0.99	20.28
0.71	0.03	2.95	2.00	1.00	1.00	20.35
0.75	0.06	2.58	1.78	1.13	1.12	21.10
0.82	0.13	2.06	1.49	1.34	1.34	23.28
0.83	0.15	2.00	1.45	1.38	1.38	23.69
0.82	0.13	2.09	1.50	1.33	1.33	23.13
0.86	0.20	1.79	1.35	1.48	1.48	25.36
0.90	0.29	1.52	1.23	1.62	1.62	28.50
0.92	0.35	1.37	1.18	1.69	1.69	30.78
0.92	0.35	1.38	1.18	1.69	1.69	30.71
0.93	0.39	1.30	1.16	1.73	1.73	32.06
0.96	0.52	1.05	1.09	1.84	1.84	37.78
0.96	0.53	1.03	1.08	1.85	1.85	38.37
0.97	0.55	1.00	1.07	1.86	1.86	39.32
0.97	0.58	0.95	1.06	1.88	1.88	40.69
0.98	0.65	0.84	1.04	1.92	1.92	44.66
0.99	0.75	0.68	1.02	1.96	1.96	51.01
1.00	0.82	0.55	1.01	1.98	1.98	56.75
1.00	0.84	0.52	1.01	1.98	1.98	58.37
1.00	0.86	0.48	1.01	1.99	1.99	60.43
1.00	0.90	0.40	1.00	1.99	1.99	64.91
1.00	1.00	0.00	1.00	2.00	2.00	89.99

For supercritical Froude numbers when $c > \sqrt{gh}$ ($p < 1$) the outer limit is defined by,

$$\cos^2 \theta = 1 - p \quad \sin^2 \theta = p = gh/v^2 \quad (7.21)$$

where $m = n = 1$. In this zone, the wave pattern is generated by waves travelling at an angle of θ with respect to x axis and as v increases, this angle diminishes. In this situation, the regular waves are contained within a narrower angle radiating from the center of disturbance. As v exceeds \sqrt{gh} the transverse waves disappear. On the other

Table 7.2: Havelock's analytical results for supercritical Froude numbers ($Fr > 1$) computed from the relationship $\cos^2 \theta = 1 - p$.

$Fr (v/\sqrt{gh})$	n	kh	p	$2/p$	$m(3-n)$	θ
1.00	0.26	1.61	1.00	1.00	1.00	90.00
1.01	0.27	1.57	0.99	1.01	1.01	84.28
1.01	0.29	1.53	0.98	1.02	1.02	81.93
1.05	0.54	1.02	0.91	1.10	1.10	72.25
1.10	0.60	0.92	0.83	1.21	1.10	65.38
1.15	0.52	1.05	0.76	1.32	1.10	60.41
1.20	0.54	1.02	0.69	1.44	1.10	56.44
1.25	0.54	1.02	0.64	1.56	1.10	53.13
1.30	0.54	1.02	0.59	1.69	1.10	50.28
1.35	0.54	1.02	0.55	1.82	1.10	47.79
1.40	0.54	1.02	0.51	1.96	1.10	45.58
1.41	0.54	1.02	0.50	1.99	1.10	45.17
1.45	0.54	1.02	0.48	2.10	1.10	43.60
1.50	0.54	1.02	0.44	2.25	1.10	41.81
1.55	0.54	1.02	0.42	2.40	1.10	40.18
1.60	0.54	1.02	0.39	2.56	1.10	38.68
1.65	0.54	1.02	0.37	2.72	1.10	37.31
1.70	0.54	1.02	0.35	2.89	1.10	36.03
1.73	0.54	1.02	0.33	2.99	1.10	35.31
1.75	0.54	1.02	0.33	3.06	1.10	34.85
1.80	0.54	1.02	0.31	3.24	1.10	33.75
1.85	0.54	1.02	0.29	3.42	1.10	32.72
1.90	0.54	1.02	0.28	3.61	1.10	31.76
1.95	0.54	1.02	0.26	3.80	1.10	30.85
2.00	0.54	1.02	0.25	4.00	1.10	30.00
3.00	0.60	0.92	0.11	9.00	1.10	19.47

hand, the transverse wave system can only exist if p is greater than unity. Unlike the previous case where $p > 1$ ($c < \sqrt{gh}$) the wave fronts (lines of equal phase) are concave

to the axis. The values obtained by Havelock's analytical formulas for supercritical Froude numbers are given in Table 7.2.

The detailed plots given in Chapter 8 for various Froude numbers verify the wave patterns described by Havelock [78]. The wave propagation angle θ varies for different Froude numbers which results in generation of different wave patterns as it is obtained from Havelock's analytical formulas. Particularly, the change in propagation angle θ can be observed in two different zones which are subcritical Froude numbers ($Fr < 1$) and supercritical Froude numbers ($Fr > 1$) as it can be seen in Figure 7.8.

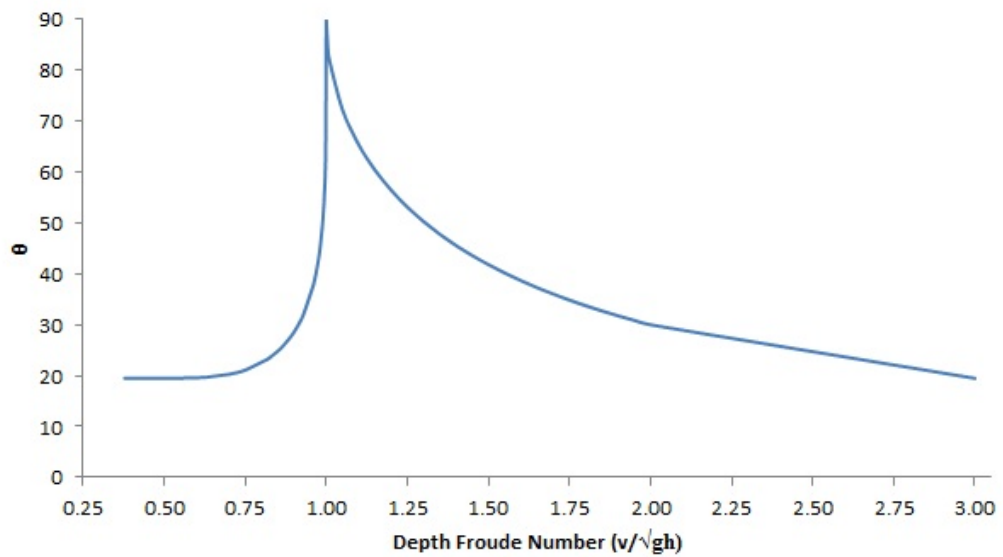


Figure 7.8: Havelock's analytical results for a range of Froude numbers.

8. 2-D NUMERICAL SIMULATIONS OF SURFACE GENERATED WAVES

Ship waves and their effects have been the subject of a large number of studies since they may cause significant environmental damage as well as put a risk on safety and maintenance of moored yachts and boats. Huang et al. [79] studied waves travelling in channels of finite depth and width at near-critical speeds. Theoretical evidence for the excitation of solitons near critical conditions was first studied by the numerical calculations of Wu and Wu [80]. Using as excitation a pressure distribution localized in the streamwise direction but entirely uniform in the spanwise direction, they solved numerically the Boussinesq equations and found a series of solitons propagating ahead of the source. Akylas [81] studied the wave disturbance generated by a localized steady pressure distribution travelling at a speed close to the long-water-wave phase speed on water of finite depth. He developed a nonlinear theory which shows that the generated waves are actually of bounded amplitude, and are governed by a forced Korteweg-de Vries equation subject to appropriate asymptotic initial conditions and a numerical study of the forced Korteweg-de Vries equation revealed a series of solitons which are generated in front of the pressure distribution.

Besides Akylas [81], Ertekin et. al. [82], Chen and Sharma [83] and Lowery and Liapis [84] studied runaway solitons generated by a 3D surface pressure or bottom disturbance limited in a confined fluid domain. Meanwhile, Cole [85] and Grimshaw and Smyth [86] who pointed out, respectively, that the same KdV equation is valid for two-dimensional transcritical flow past a bump and stratified flow over topography. Also, Miles (1986) showed analytically that no nonlinear steady state exists for a certain range of transcritical speeds which are in agreement with the continuous radiation of solitons revealed by the numerical calculations.

Later on, Katsis and Akylas [87] studied the three-dimensional wave pattern generated by a moving pressure distribution of finite extent acting on the surface of water of depth h and they showed that when the pressure distribution travels at a speed near the linear-long-wave speed, the response is governed by a forced

nonlinear Kadomtsev-Petviashvili (KP) equation, which describes a balance between linear dispersive, nonlinear and three-dimensional effects. This equation is the two-dimensional counterpart of the forced KdV equation [81].

A fundamental work on the forced KdV equation was carried out later by Wu [88] to examine the mechanism of the so called runaway solitons. In addition to early studies of Wu and Wu [80] and Wu [88], Lee et al. [89] carried out a series of experimental measurements on the generation of solitary waves by a submerged moving object. This problem was also examined by Zhang and Chwang [90] with solutions from 2D momentum equations. Katsis and Akylas [87], Pedersen [91], Lee and Grimshaw [92] and Li and Sclavounos [93] extended the wave generation related researches using depth-averaged models to an unbounded fluid region. Sung and Grilli [94] modeled fully nonlinear free surface waves caused by a translating disturbance made by a pressure patch and/or a surface-piercing body (ship) by using potential flow theory.

Peters [95] and Peregrine [96] have also studied waves propagating in channels with arbitrary cross-section. Liu and Wu [17] modified fully nonlinear and weakly dispersive depth-integrated wave equations to include the effects of moving free surface pressure and investigated waves generated by a moving free surface pressure distribution in rectangular and trapezoidal channels. For the rectangular channels, Liu and Wu [17] compared their numerical results with those obtained by the forced KdV equations, Green-Naghdi (GN) equations and the Boundary Integral Equation (BIEM) formulation based on the potential flow theory. Results have been checked with Cao et al.'s [97] BIEM results and Ertekin et al.'s [82] 2D GN results. Cao [97] solved the problem in time domain using a time-stepping procedure combined with a two-dimensional version of the desingularized boundary integral method and compared the results with Wu's [88] fKdV model. Liu and Wu, Henn et al. [98] and Torsvik [99] studied the generation of upstream propagating waves in nonrectangular channels.

The common point of these studies are channels with trapezoidal cross-section profiles, but Jiang et al. [100] also include results for a channel with a deep trench along the center line, which is similar to Torsvik's studies [99]. Many of these studies considered the moving pressure distribution as a sinusoidal shape moving on the free surface. The pressure acts inside a rectangle symmetric about the x - and y -axes with length L

and width B and vanishes outside the rectangle while Sung and Grilli [94] used a theoretical Gaussian shape for the moving pressure. Apart from these moving pressure disturbance, in this thesis 2-D simulations of waves generated by moving pressure fields are performed for two different surface pressure functions; a hemispherical pressure field and a slender-body type pressure field.

8.1 Hemispherical Pressure Forcing

A hemispherical pressure field of the form

$$p(x,y) = p_0 \sqrt{R^2 - x^2 - y^2} \quad (8.1)$$

is used for the first simulation. Here p_0 is the peak value of the pressure distribution and R is the radius of the hemisphere. Figure 8.1 shows the hemispherical field. In the

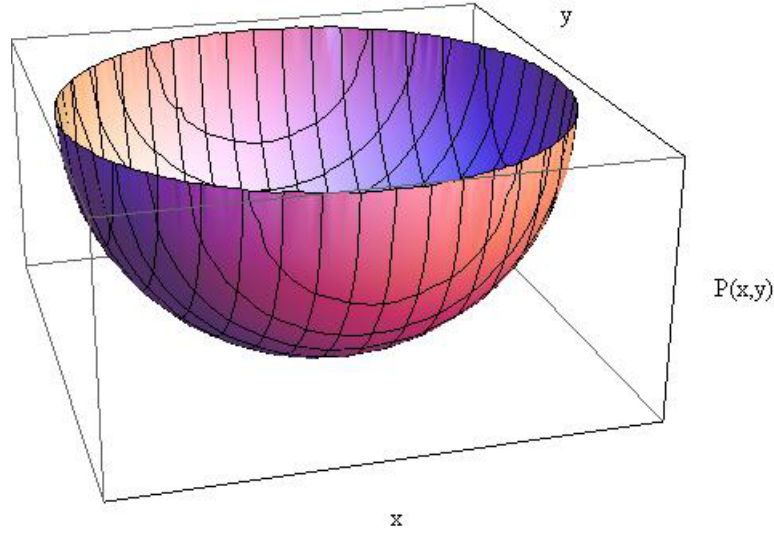


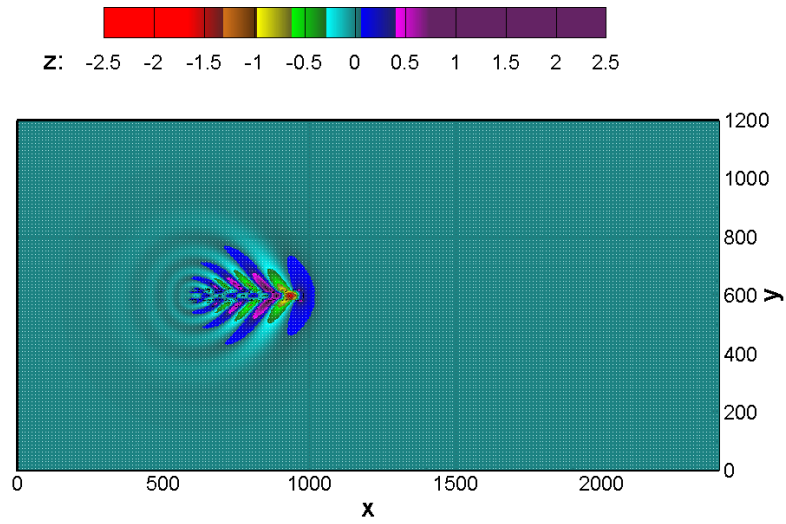
Figure 8.1: Definition of the pressure distribution $p(x,y) = p_0 \sqrt{R^2 - x^2 - y^2}$.

simulation R is taken as 40 m, $p_0 = 300$ Pa and the water depth $h = 10$ m which gives $c = \sqrt{gh} = 10$ m/s. The simulation region is 2400 m \times 1200 m with $\Delta x = \Delta y = 4$ m. Time step is taken as $\Delta t = 0.2$ s. In the x -momentum equation $p_x = -xp_0/(R^2 - x^2 - y^2)^{1/2}$ and in the y -momentum $p_y = -yp_0/(R^2 - x^2 - y^2)^{1/2}$. Figure 8.2 shows the contour plots of the simulated wave field at $t = 28$ s, 60 s and 92 s for the depth-based Froude number $Fr = v/c = v/\sqrt{gh} = 0.99$ and 1.3 which corresponds the pressure field speed $v = 0.99\sqrt{gh} = 0.99c = 9.9$ m/s and $v = 1.3\sqrt{gh} = 1.3c = 13$ m/s. It is to be noted that for $Fr = 0.99$ and $Fr = 1.3$ the wedge angles 48° and 47° measured

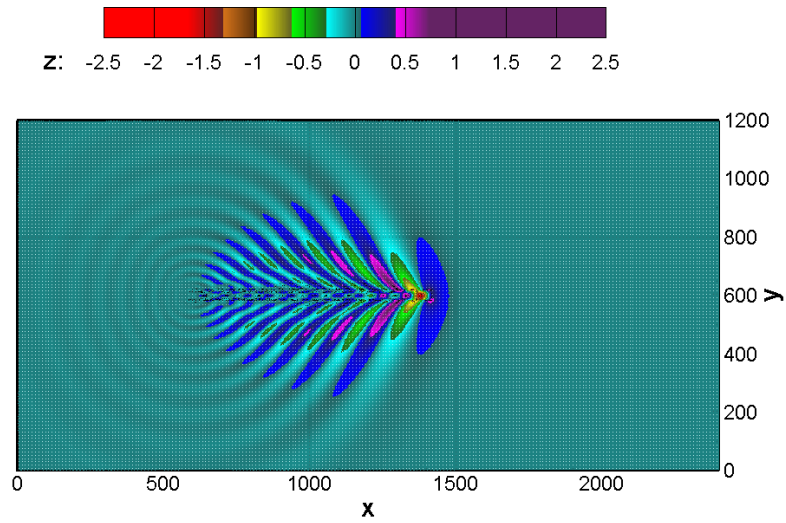
from the simulated wave fields at $t = 92$ s respectively are acceptable approximations to the theoretical values 51° and 50° of Havelock [78] as can be seen in Table 8.1 and Figure 8.7.

Table 8.1: Comparisons of numerically obtained wedge angles (a hemispherical moving pressure field) from with Havelock’s analytical results for a range of depth-based Froude numbers.

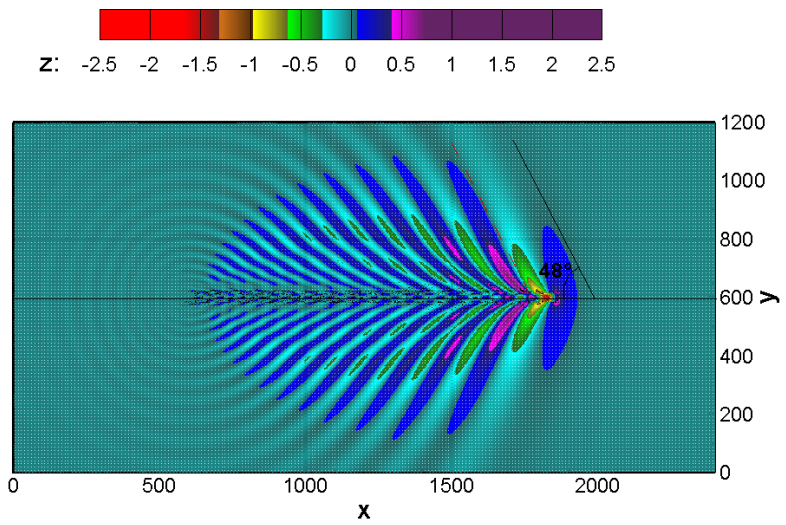
Fr	Wedge Angle		
	Boussinesq (Numerical)	Havelock (Analytical)	Relative error percentage (%)
0.63	18	19.69	8.58
0.70	20	20.26	1.29
0.75	21	21.10	0.47
0.86	25	25.36	1.43
0.90	25	28.50	12.28
0.96	40	37.78	5.86
0.97	40	40.69	1.69
0.98	39	44.66	12.68
0.99	48	51.01	5.90
1.01	82	81.93	0.08
1.05	72	72.25	0.34
1.10	65	65.38	0.58
1.20	54	56.44	4.33
1.30	47	50.28	6.53
1.40	43	45.58	5.67
1.50	42	41.81	0.45
1.60	36	36.03	0.09
1.80	33	33.75	2.22
2.00	30	30.00	0.00



(a) $t = 28$ s, $Fr=0.99$

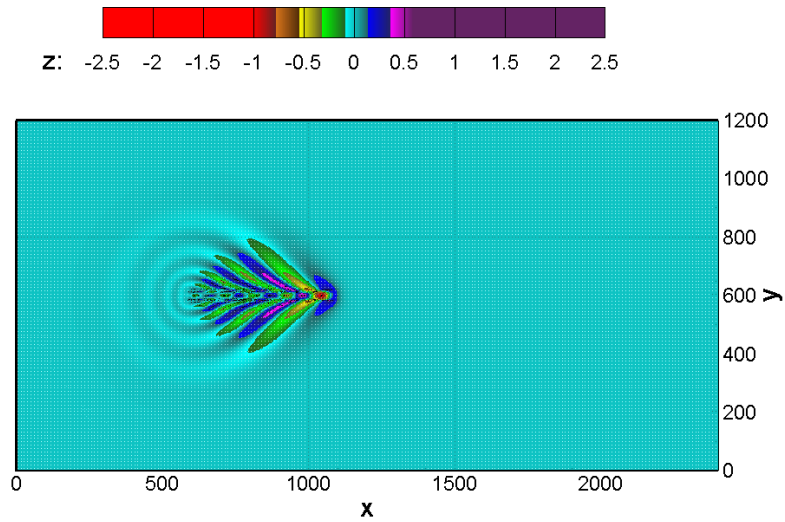


(b) $t = 60$ s, $Fr=0.99$

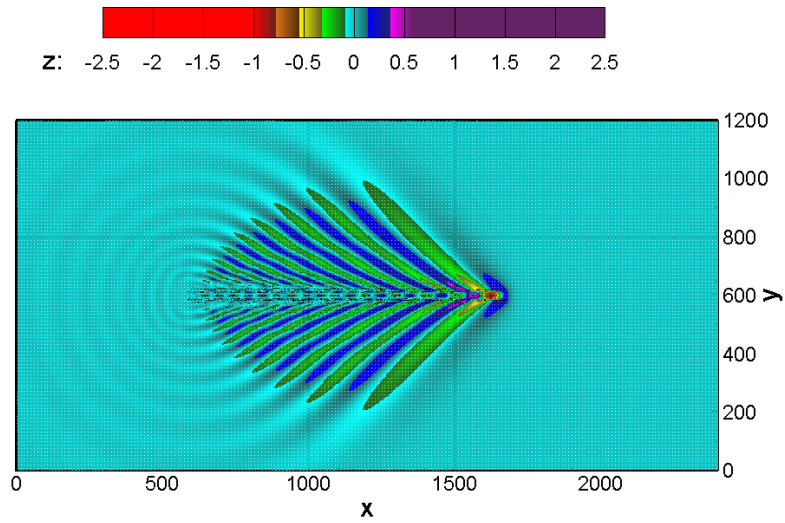


(c) $t = 92$ s, $Fr=0.99$

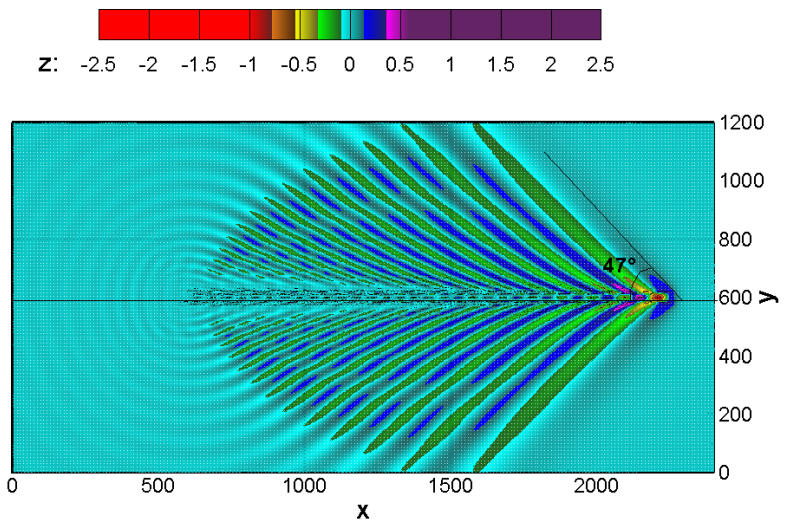
Figure 8.2: Wave contours of a moving hemisphere at different time steps using Boussinesq model with $\beta = 1/5$ for $Fr = 0.99$.



(a) $t = 28$ s, $Fr = 1.3$



(b) $t = 60$ s, $Fr = 1.3$



(c) $t = 92$ s, $Fr = 1.3$

Figure 8.3: Wave contours of a moving hemisphere at different time steps using Boussinesq model with $\beta = 1/5$ for $Fr = 1.3$.

8.2 Slender-Body Type Pressure Forcing

For a more ship-like form a slender body shaped pressure field of the form

$$p(x,y) = p_0 [1 - 16(x/L)^4] [1 - 2(y/B)^2] \exp[-16(y/B)^2] \quad (8.2)$$

is used. Here p_0 is the peak pressure value which is set to 3000 Pa, L is the length-wise and B is the breadth-wise parameter. The pressure field $p(x,y)$ is defined only within the intervals $-L/2 \leq x \leq L/2$ and $-B/2 \leq y \leq B/2$ and set to zero outside these regions. Figure 8.4 shows the slender parabolic type pressure field.

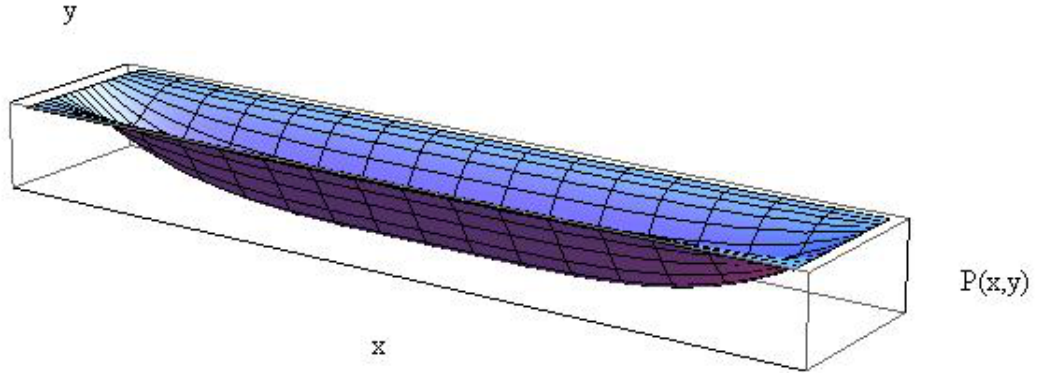
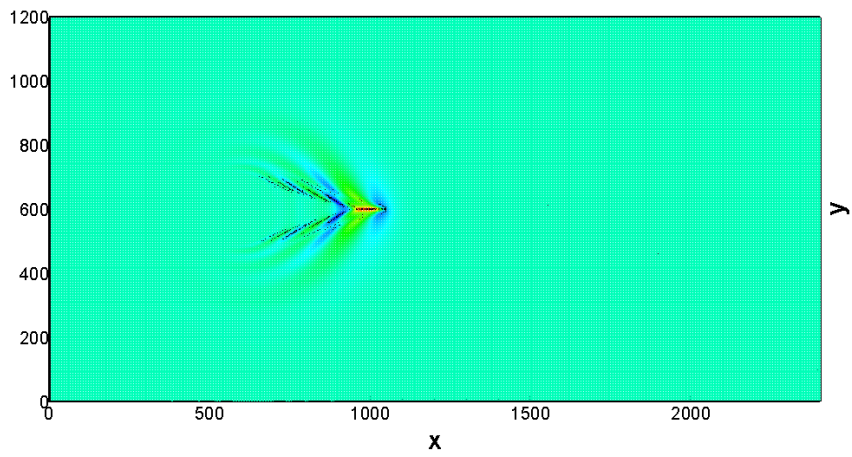
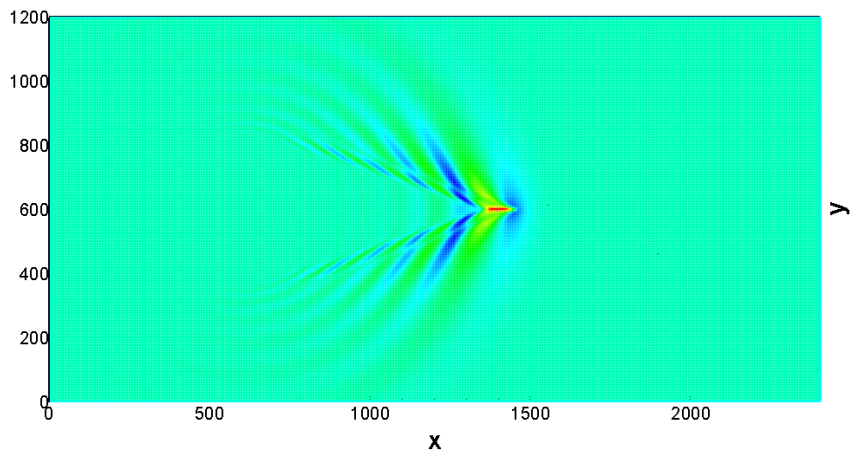


Figure 8.4: Perspective view of the slender-body type pressure distribution.

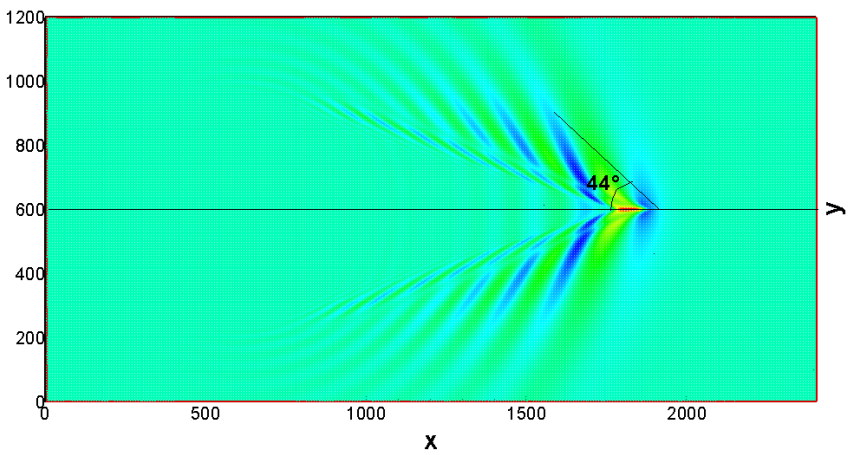
The simulation area is $2400 \text{ m} \times 1200 \text{ m}$ with grid sizes of $\Delta x = \Delta y = 1 \text{ m}$ and the time step $\Delta t = 0.06 \text{ s}$. In the simulations the length to beam ratio L/B is set to 5 with $L = 100 \text{ m}$ and $B = 20 \text{ m}$ and the water depth is $h = 20 \text{ m}$, resulting in $c = \sqrt{gh} = 14 \text{ m/s}$. Note that in the x -momentum equation $p_x = -64x^3 e^{-16(y/B)^2} (1 - 2(y/B)^2) / L^4$ and in the y -momentum equation $p_y = 4y e^{-16(y/B)^2} (L^4 - 16x^4) (16y^2 - 9B^2) / (LB)^4$. Unlike the previous test case, a range of depth-based Froude numbers is covered. Out of 19 test cases the contour plots of only three cases, corresponding to $Fr = 0.98$ and 1.30 are shown in Figures 8.5 and 8.6.



(a) $t = 30$ s, $Fr = 0.98$

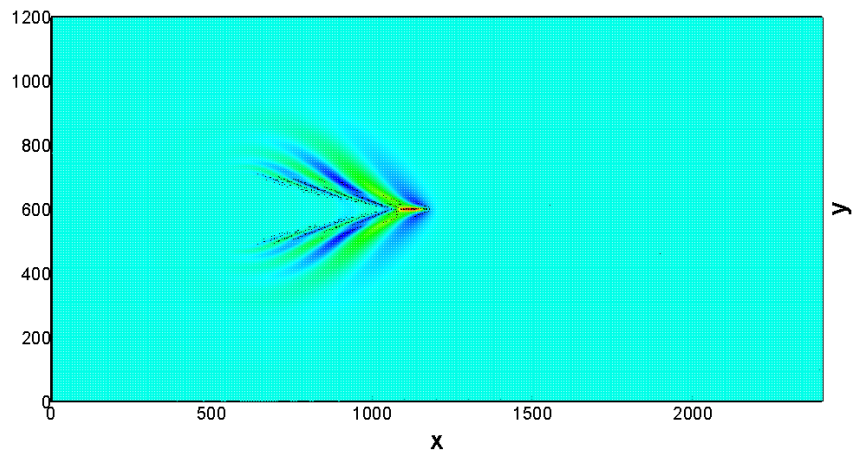


(b) $t = 60$ s, $Fr = 0.98$

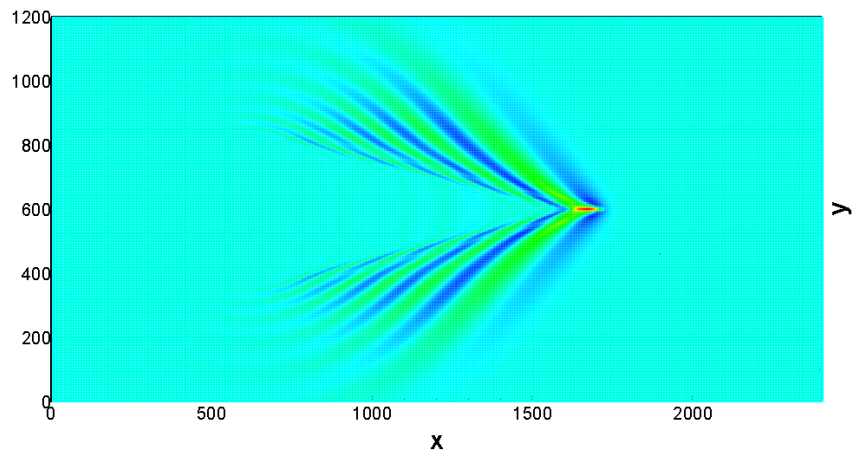


(c) $t = 90$ s, $Fr = 0.98$

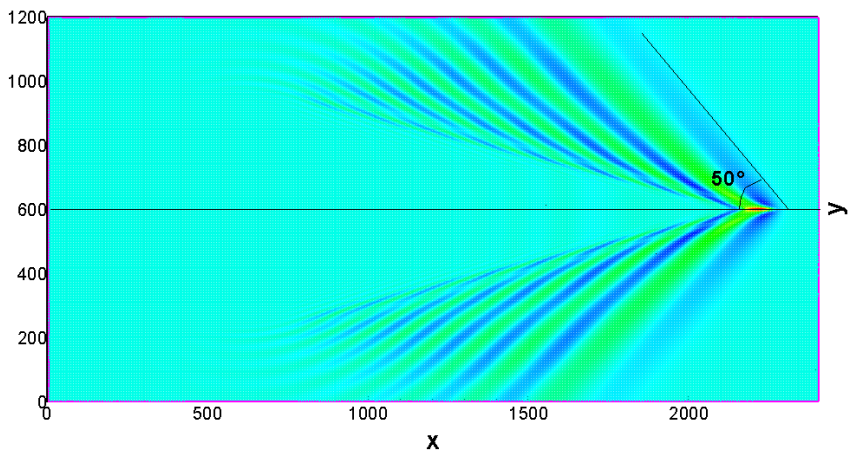
Figure 8.5: Wave contours generated by a slender-body type moving pressure field using Boussinesq model with $\beta = 1/5$ for $Fr = 0.98$.



(a) $t = 30$ s, $Fr = 1.3$



(b) $t = 60$ s, $Fr = 1.3$



(c) $t = 90$ s, $Fr = 1.3$

Figure 8.6: Wave contours generated by a slender-body type moving pressure field using Boussinesq model with $\beta = 1/5$ for $Fr = 1.3$.

The tabular form of the numerically and analytically computed wedge angles for the Froude numbers considered are given below in Table 8.2. Havelock [78] investigated

Table 8.2: Comparisons of numerically obtained wedge angles (a slender-body type moving pressure field) from with Havelock's analytical results for a range of depth-based Froude numbers.

Fr	Wedge Angle		
	Boussinesq (Numerical)	Havelock (Analytical)	Relative error percentage (%)
0.63	18	19.69	8.58
0.70	20	20.26	1.29
0.75	20	21.10	5.21
0.86	24	25.36	5.37
0.90	28	28.50	1.75
0.96	40	37.78	5.86
0.97	39	40.69	4.15
0.98	44	44.66	1.49
0.99	49	51.01	3.94
1.01	80	81.93	2.36
1.05	72	72.25	0.34
1.10	66	65.38	0.95
1.20	58	56.44	2.76
1.30	50	50.28	0.57
1.40	44	45.58	3.48
1.50	42	41.81	0.45
1.70	37	36.03	2.69
1.80	33	33.75	2.22
2.00	30	30.00	0.00

the wave patterns due to a moving surface pressure and showed the main differences between subcritical and supercritical Froude numbers. The results for the wedge and propagation angles show that as the Froude number decreases the divergent waves become more dominant while transverse wave's position, whether being crest or trough, changes with respect to ship velocity. For the wedge angle of a point impulse moving on water of finite depth Havelock gives

$$\alpha = \arccos \sqrt{8(1-n)/(3-n)} \quad \text{if } Fr \leq 1$$

$$\alpha = \arcsin \sqrt{p} \quad \text{if } Fr > 1$$

where $p = gh/v^2 = c^2/v^2 = 1/Fr^2$.

For a given Froude number or p in the subcritical range, first kh is solved by iteration from the relationship $m(3 - n) = 2/p$ where $m = \tanh kh/kh$ and $n = 2kh/\sinh 2kh$. Afterwards, using the computed kh the numerical value of n is obtained to compute α .

For the supercritical range α is a function of p alone therefore no additional computation is needed. It is to be noted that in the subcritical range as Froude number approaches zero the relative depth kh becomes larger. On the other hand, in the entire supercritical range kh assumes the limiting case of zero and disappears from the wedge angle computations. Thus, in a sense, low Froude numbers represent relatively deep waters while high Froude numbers correspond to very shallow waters.

For $Fr = 0$ Kelvin's well-known result of a deep-water wedge angle $\alpha = 19^\circ 28'$ is obtained as may be seen in Figure 8.7 where the wedge angles computed from Havelock's analytical formulas and measured from the graphs of the numerical solutions of the present Boussinesq model are shown.

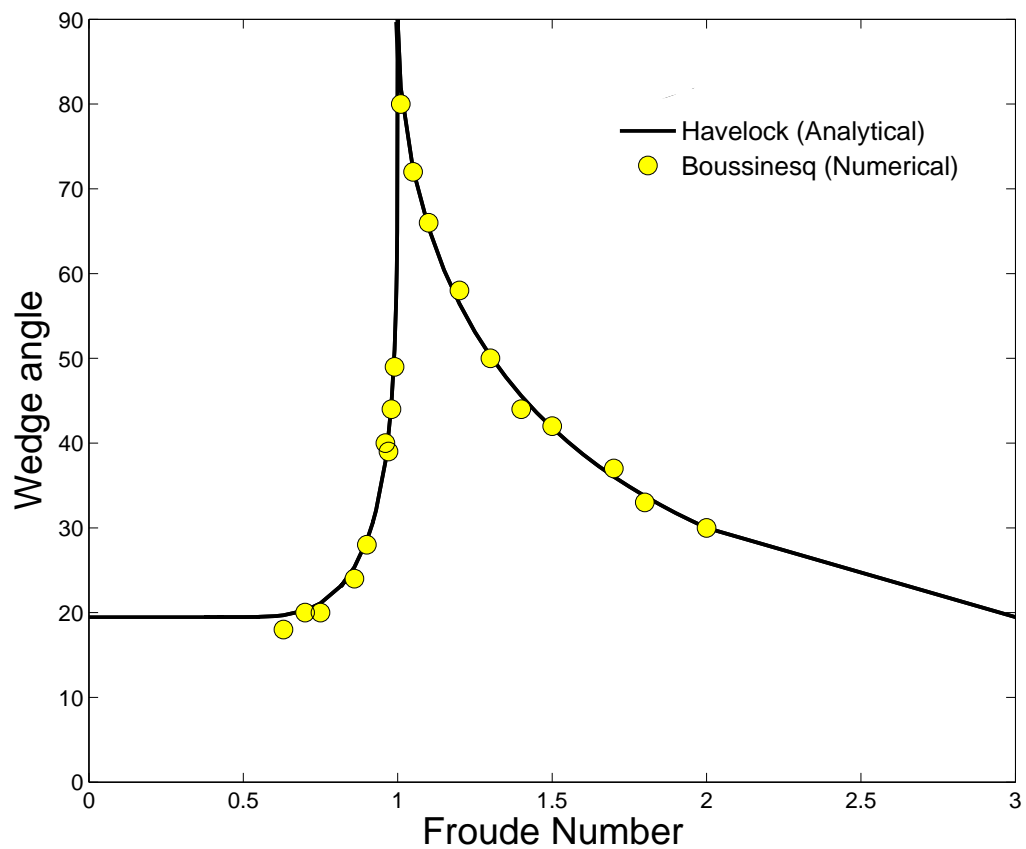
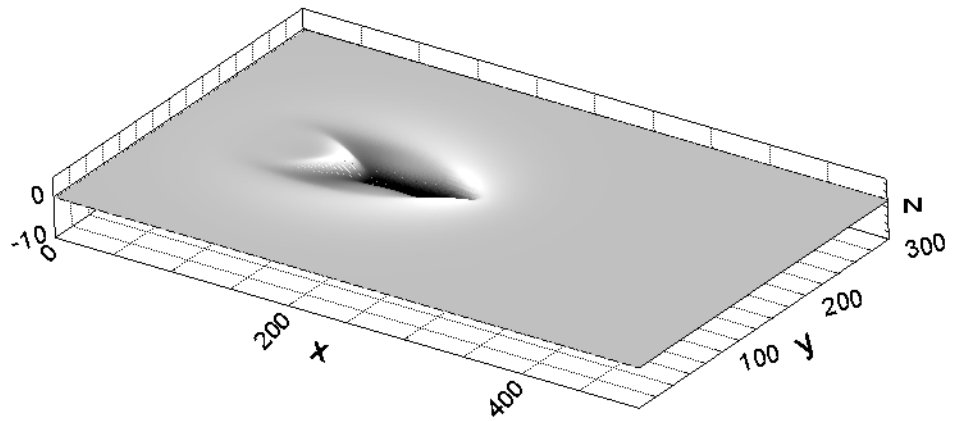
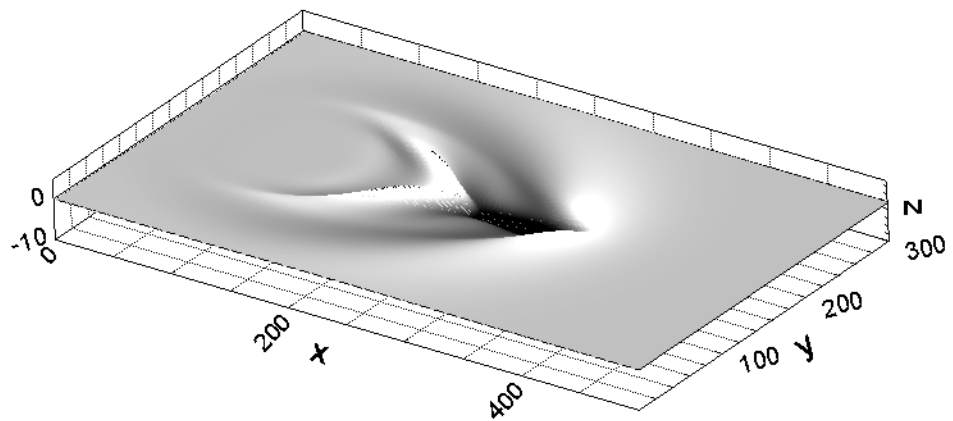


Figure 8.7: Comparison of numerically obtained wedge angles with Havelock's theoretical formulas.

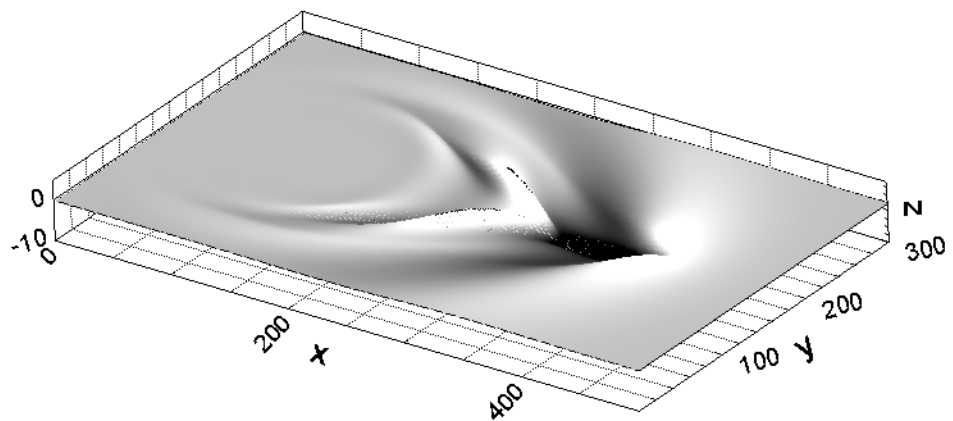
Finally, two perspective views of a nonlinear simulation with slender-body shaped pressure field for $Fr = 0.9$ are shown in Figure 8.8. The nonlinearity is ascertained by considerably increased pressure amplitude p_0 (twice the previous simulations). Nevertheless, no appreciable differences are observed in the wedge angles for the simulation shown here and for the other simulations not shown. The nonlinearity appears to affect the vertical symmetry of the wave profile only. Otherwise, the essential characteristics of the wave pattern remain nearly the same.



(a) $t = 9$ s for $Fr = 0.9$



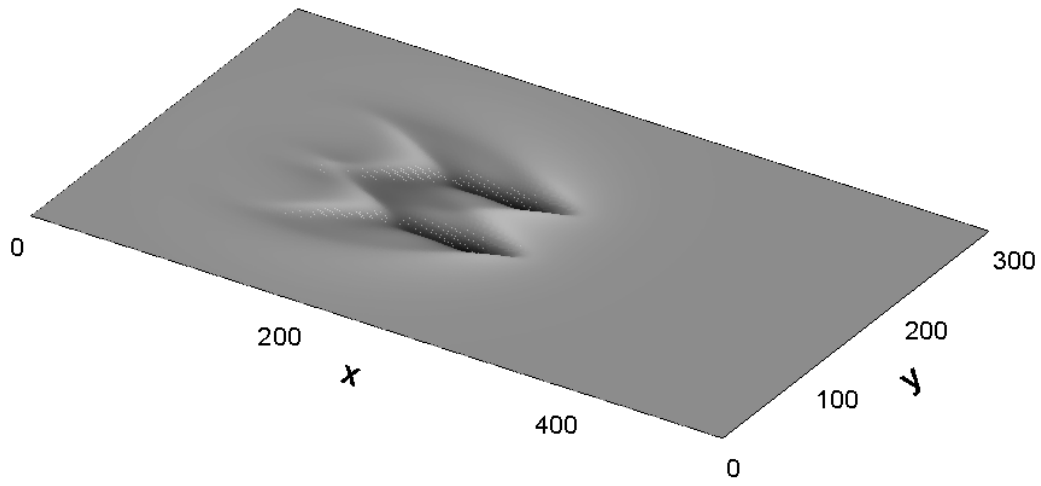
(b) $t = 18$ s for $Fr = 0.9$



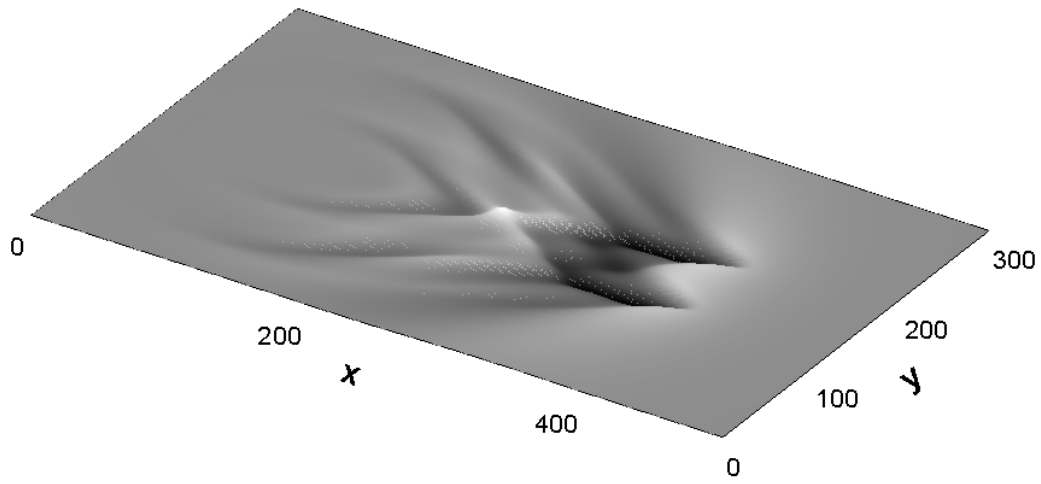
(c) $t = 24$ s for $Fr = 0.9$

Figure 8.8: Perspective views of nonlinear waves generated by slender-body type moving pressure for $Fr = 0.9$ at $t = 9$ s, $t = 18$ s and $t = 24$ s.

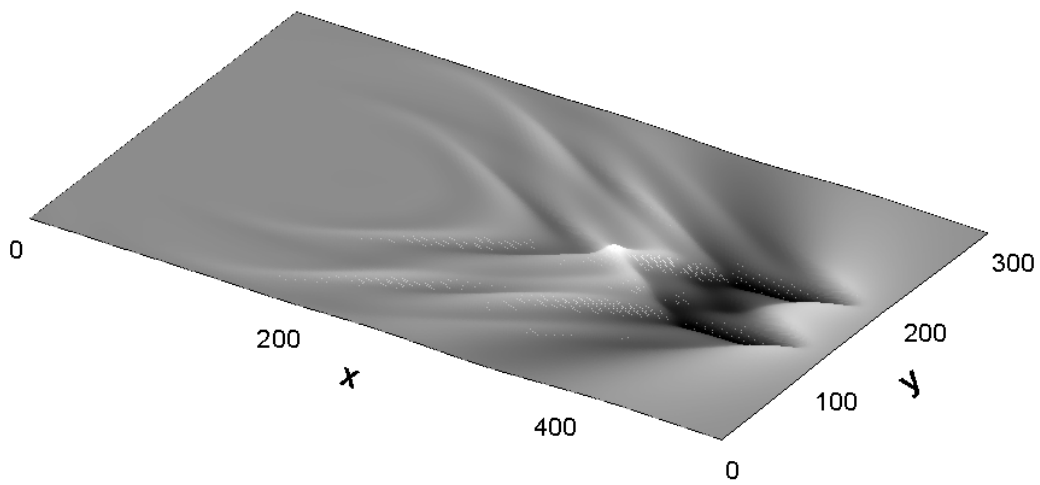
Besides using one slender-body shaped pressure field for representing the ship itself, a catamaran-like vessel may also be represented by using two slender bodies. The waves generated and their interaction are shown visually in Figure 8.9 for $Fr = 0.97$ at $t = 9$ s, $t = 18$ s and $t = 24$ s respectively.



(a) $t = 9$ s for $Fr = 0.97$



(b) $t = 18$ s for $Fr = 0.97$



(c) $t = 24$ s for $Fr = 0.97$

Figure 8.9: Perspective views of nonlinear waves generated by two slender-body type moving pressures for $Fr = 0.9$ at $t = 9$ s, $t = 18$ s and $t = 24$ s.

9. RESULTS AND CONCLUSION

Several types of Boussinesq equations are in use for modeling nearshore waves or waves in intermediate water depths. Besides these rather common applications, the Boussinesq equations may also be employed to model wave generation and propagation by moving surface disturbances. The surface disturbance may come from a moving free surface object which is associated with a moving surface vessel. By adding a moving surface pressure into Boussinesq equations, the wave patterns for different depth based Froude numbers are investigated. In this work an improved Boussinesq model [12] with a surface pressure term is discretized by a new approach. With this new discretization the program can be run either in the long wave mode without dispersion terms or in the Boussinesq mode by specifying a single parameter. In any one of these modes it is possible to specify a fixed or a moving surface pressure for simulating a moving object on the surface. Although in several studies in literature, the moving object has been represented by a cosine function, in this study, a hemispherical pressure function and a slender-body type pressure function are used for numerical simulation of waves generated. Moreover, visualization of waves due to a catamaran-like vessel is also obtained by using two slender-body shaped pressure fields.

Before simulating the 3-D moving objects, the numerical scheme is tested for its discretization and absorbing boundaries. The discretization of 1-D Boussinesq model has been tested by Green's theoretical formula. Two different bathymetries which are sinusoidal and parabolic are used for testing the linearized original Boussinesq equations ($\beta = 0$) and the linearized improved Boussinesq equations ($\beta = 1/5$). Comparisons show that computational wave amplitudes are almost perfectly matching with Green's formula. Secondly, the numerically 2-D but actually 3-D model is tested for the performance of its non-reflective boundaries. These boundaries are checked by a ring test which reveals the symmetrical accuracy of the model. The ring tests for all the modes (long wave, classical Boussinesq and Boussinesq with Padé (2,2)) of the

numerical scheme are performed. Only the test for the improved Boussinesq model is shown. The contour plots show nearly perfect symmetry hence confirms that the radiation boundaries perform well.

The numerical model is also tested for its nonlinear properties by comparing the numerically simulated solitary waves with their analytical counterparts. These simulations serve to a twofold purpose; namely, testing of the nonlinear and the dispersive performance of the numerical model. The analytical and computational results agree fairly well for both $\beta = 0$ and $\beta = 1/5$, although from analytical point of view, the solitary waves corresponding to the improved Boussinesq equations should be slightly different. Differences in height between analytical and computational results are given as the relative error percentage for different ε values. It is observed that as nonlinearity parameter, ε , increases, the relative error percentage increases linearly. However, in general the relative error percentages are reasonably low hence establish the reliability of the numerical approach adopted.

For testing the accuracy of numerically simulated waves due to a moving pressure field, a 1-D case with known analytical solution is considered. The analytical solution for the 1-D linearized long wave equations is recapitulated first and then comparisons with the numerical solutions are given. For the test case the pressure function is selected in the form of a Gaussian distribution function. The analytical solution is compared with the numerical solution of long wave equations for different depth based Froude numbers. The comparisons using the Boussinesq equations with $\beta = 1/5$ instead of the long wave equations are also made. The results show that numerical simulations in both cases agree well with the analytical solution derived from the linearized long wave equations. Besides, from the average relative error of the calculated and analytical surface elevation versus Froude number plots, it is observed that around critical Froude number, the error increases but for Froude numbers different than unity, the error percentage decreases again.

Finally, 2-D simulations of waves generated by moving pressure fields are performed for two different surface pressure functions; a hemispherical pressure field and a slender-body type pressure field. The waves generated by these pressure fields are simulated for various depth based Froude numbers. For the verification of the numerical simulation, the wedge angles are compared with Havelock's theoretical

formulations. With surface pressure terms in the momentum equations the numerical scheme is run for a moving 3-D hemispherical pressure field and a slender-body type pressure field for a range of depth based Froude numbers. The wedge angles obtained from both simulations are compared with the values calculated from the analytical formulas of Havelock [78]. For hemispherical pressure field, in the subcritical range, $Fr \leq 1$, the average error percentage between the computed and the theoretical values in the subcritical range is around 5.58%, considerably greater than those of the supercritical range, which is on the average 2.03%. In addition, for a slender-body type pressure field, the average error percentage between the computed and the theoretical values in the subcritical range is around 4.18%, which is again greater than those of the supercritical range, being on the average 1.58%.

In both cases, the average error percentage for super critical Froude numbers is relatively small and the reason for this is probably due to the depth limited character of the Boussinesq equations. Note that the subcritical range indicates relatively greater depths with completely deep water for zero Froude number. Therefore, the relatively poor performance of the numerical model in the subcritical range may be attributed to the deep water characteristics of the waves generated. Moreover, it is observed that the average error percentage of the slender-body type pressure is less than the hemispherical pressure field. The reason, might be the form of the slender-body shape, creating better defined waves.

Although, the calculated wedge angles can vary according to the specified speed of moving pressure field, the nonlinearity which is determined by increasing the pressure amplitude, p_0 , appears to play only a relatively minor role by affecting the wave symmetry without altering the overall wave patterns such as the wedge angles as observed from the comparisons of the linear and nonlinear simulations. Since there are no appreciable differences between the calculated wedge angles, other simulations for different Froude numbers are not given.

In addition, the two slender-body type pressure fields are used for visual demonstration purpose of waves due to a catamaran-like surface object. The interaction of waves generated are clearly visible in the simulations which might be a useful tool for investigating similar vessels sailing in different water depths. In general, the simulation of the waves generated whether by a catamaran or ship-like vessel is an important

matter, especially for the cases where moving object's speed is relatively high. With the wide popularity of high speed vessels in waterways, large amplitude wake wash generated by those vessels cause erosion of the shore, sea bottoms and the biological environment. Besides, these waves have a significant impact on the safety of people and vessels moored along the shore. Considering those effects, in future work, the simulation of waves generated especially at high speeds can be utilized for investigating such effects.

REFERENCES

- [1] **U.S. Army Corps Of Engineers, N.** (2002). *Coastal Engineering Manual*.
- [2] **Dean, R. and Dalrymple, R.** (1991). *Water wave mechanics for engineers and scientists*, Advanced series on ocean engineering, World Scientific.
- [3] **Sarpkaya, T. and Isaacson, M.** (1981). *Mechanics of Wave Forces on Offshore Structures*, Van Nostrand Reinhold Co., New York.
- [4] **Newman, J.** (1971). *Marine Hydrodynamics*, M.I.T. Dept. of Naval Architecture and Marine Engineering.
- [5] **Lighthill, M.J.** (1996). *Waves in fluids*, Cambridge University Press.
- [6] **Boussinesq, J.V.** (1872). Theory of waves and surges which propagate the length of a horizontal rectangular canal, imparting to the fluid contained within the canal velocities that are sensibly the same from the top to the bottom, *Journal de Mathématiques Pures et Appliquées*, **17**, 55–108.
- [7] **Mei, C. and Meháute, L.** (1966). Note on the equations of long waves over an uneven bottom, *Journal of Geophysical Research*, **71**, 393–400.
- [8] **Peregrine, D.H.** (1967). Long waves on a beach, *Journal of Fluid Mechanics*, **27**(04), 815–827.
- [9] **Witting, J.M.** (1984). A unified model for the evolution nonlinear water waves, *Journal of Computational Physics*, **56**(2), 203 – 236.
- [10] **Madsen, P.A., Murray, R. and Sørensen, O.R.** (1991). A new form of the Boussinesq equations with improved linear dispersion characteristics, *Coastal Engineering*, **15**(4), 371 – 388.
- [11] **Madsen, P.A. and Sørensen, O.R.** (1992). A new form of the Boussinesq equations with improved linear dispersion characteristics. Part 2. A slowly-varying bathymetry, *Coastal Engineering*, **18**(3-4), 183 – 204.
- [12] **Beji, S. and Nadaoka, K.** (1996). A formal derivation and numerical modelling of the improved Boussinesq equations for varying depth, *Ocean Engineering*, **23**(8), 691–704.
- [13] **Nwogu, O.** (1993). Alternative form of Boussinesq Equations for nearshore wave propagation, *Journal of Waterway, Port, Coastal and Ocean Engineering*, **119**, 618.

- [14] **T., K.J., G., W., Q., C., B., K.A. and A., D.R.** (1998). FUNWAVE 1.0. Fully Nonlinear Boussinesq Wave Model, Documentation and users manual, **Technical Report**, Center for Applied Coastal Research, Department of Civil and Environmental Engineering, University of Delaware.
- [15] **Chen, Y. and Liu, P.L.F.** (1995). Modified Boussinesq Equations and associated parabolic models for water wave propagation, *Journal of Fluid Mechanics*, **288**, 351.
- [16] **P.L.F.Liu** (1995). Advances in Coastal Engineering, volume 1, chapter Model Equations for Wave Propagation from Deep to Shallow Water, Singapore: World Scientific, pp.125–57.
- [17] **Liu, P.L.F. and Wu, T.R.** (2004). Waves generated by moving pressure disturbances in rectangular and trapezoidal channels, *Journal of Hydraulic Research*, **42**(2), 163–171.
- [18] **Torsvik, T., Pedersen, G. and Dysthe, K.** (2009). Waves generated by a pressure disturbance moving in a channel with a variable cross-sectional topography, *Journal of Waterway Port Coastal and Ocean Engineering*, **135**(3), 120–123.
- [19] **Lynett, P.J., Wu, T.R. and Liu, P.L.F.** (2002). Modeling wave runup with depth-integrated equations, *Coastal Engineering*, **46**(2), 89–107.
- [20] **Nascimento, M.F., Neves, C.F. and Maciel, G.F.** (2009). Propagation of ship waves on a sloping bottom, pp.696–708, 31st International Conference on Coastal Engineering, Hamburg, Germany, Aug. 31-Sep. 05, 2008.
- [21] **Wei, G. and Kirby, J.T.** (1995). Time-dependent numerical code for extended Boussinesq equations, *Journal of Waterway Port Coastal and Ocean Engineering*, **121**(5), 251–261.
- [22] **Airy, G.B.** (1841). Tides and waves, **E. Al**, editor, Encyclopedia metropolitana (1817-1845, London.
- [23] **Stokes, G.** (1847). On the theory of oscillatory waves, *Transactions of the Cambridge Philosophical Society*, **8**, 441–455.
- [24] **Mei, C.** (1989). *The applied dynamics of ocean surface waves*, Advanced series on ocean engineering, World Scientific.
- [25] **Stokes, G.** (1846). Report on Recent Research in Hydrodynamics, *Mathematical and Physical Paper*, **1**, 167–187.
- [26] **De, S.C.** (1955). Contribution to the Theory of Stokes Waves, *Proc. Phil. Soc.*, **51**, 713–736.
- [27] **Bretschneider, C.L.** (1960). A Theory for Waves of Finite Height, volume 1, Proc. 7th Coastal Engr. Conf., pp.146–183.
- [28] **Skjelbreia, L. and Hendrickson, J.** (1961). Fifth Order Gravity Wave Theory, volume 1, Proc. 7th Coastal Engr. Conf., pp.184–196.

- [29] **Laitone, E.V.** (1960). The Second Approximation to Cnoidal and Solitary Waves, *Jour. Fluid Mech.*, **9**, 430–444.
- [30] **Laitone, E.V.** (1962). Limiting Conditions for Cnoidal and Stokes Waves, *Journal of Geophysical Research*, **67**, 1555–1564.
- [31] **Laitone, E.V.** (1962). Series Solutions for Shallow Water Waves, *Journal of Geophysical Research*, **70**, 995–998.
- [32] **Chappelear, J.E.** (1962). Shallow Water Waves, *Journal of Geophysical Research*, **67**, 4693–4704.
- [33] **Fenton, J.** (1985). A Fifth-Order Stokes Theory for Steady Waves, *ASCE Jour. Waterw., Port, Coastal and Ocean Engr*, **111**, 216–234.
- [34] **Schwartz, L.W.** (1974). Computer Extension and Analytic Continuation of Stokes' Expansion for Gravity Waves, *Jour. Fluid Mech.*, **62**, 553–578.
- [35] **Cokelet, E.D.** (1977). Steep Gravity Waves in Water of Arbitrary Uniform Depth, *Philosophical Transactions of the Royal Society*, **286**, 183–230.
- [36] **Williams, J.** (1981). *Limiting gravity waves in water of finite depth*, Philosophical transactions of the Royal Society of London, Royal Soc.
- [37] **Williams, J.** (1986). *Tables of Progressive Gravity Waves*, John Wiley & Sons, Incorporated.
- [38] **Phillips, O.** (1966). *The dynamics of the upper ocean*, Cambridge monographs on mechanics and applied mathematics, Cambridge U.P.
- [39] **Chakrabarti, S.** (1987). *Hydrodynamics of offshore structures*, Computational Mechanics.
- [40] **Dean, R.G.** (1965). Stream function representation of nonlinear ocean waves, *Journal of Geophysical Research*, **70**, 4561–4572.
- [41] **Dean, R. and (U.S.), C.E.R.C.** (1974). *Evaluation and Development of Water Wave Theories for Engineering Application: Tabulation of dimensionless stream function theory variables*, Special report, U.S. Coastal Engineering Research Center.
- [42] **Dalrymple, R.A.** (1974). A finite amplitude wave on a linear shear current, *Journal of Geophysical Research*, **79**, 4498–4504.
- [43] **Chaplin, J.R.** (1980). Developments of stream-function wave theory, *Coastal Engineering*, **3**(3), 179–205.
- [44] **Rienecker, M.M. and Fenton, J.D.** (1981). A Fourier approximation method for steady water waves, *Journal of Fluid Mechanics*, **104**, 119–137.
- [45] **Peregrine, D.H.** (1976). Interaction of water waves and currents, *Advances in Applied Mechanics*, **16**, 9–117.
- [46] **Whitham, G.B.** (1974). *Linear and Nonlinear Waves*, Pure and Applied Mathematics, Wiley-Interscience, New York, NY.

- [47] **Miles, J.W.** (1981). The Korteweg-de Vries equation: a historical essay, *Journal of Fluid Mechanics*, **106**, 131–147.
- [48] **Peregrine, D.H.** (1972). Waves on Beaches and Resulting Sediment Transport, chapter Equations for water waves and the approximation behind them, Academic Press, New York, pp.95–121.
- [49] **Eckart, C.** (1952). The Propagation of Gravity Waves From Deep to Shallow Water, **Technical Report Circular 521**, Natl. Bur. Standards, Washington, DC.
- [50] **Ippen, A.T.** (1966). *Estuary and Coastline Hydrodynamics*, McGraw-Hill Book Company, New York.
- [51] **Lamb, H.** (1932). *Hydrodynamics*, The University press, Cambridge Eng.
- [52] **Sukardi, Y.** Boussinesq Equation, <http://boussinesq-equation.blogspot.com>, date cited: 26.03.2012.
- [53] **Korteweg D. J., d.V.G.** (1895). On the change of form of long waves advancing in a rectangular canal, and on a new type of long stationary waves, *Philos Mag*, **5**(39), 422–443.
- [54] **Ursell, F.** (1953). The long-wave paradox in the theory of gravity waves, *Proceedings of the Cambridge philosophical society*, **49**, 685–694.
- [55] **Benney, D.J.** (1966). Long nonlinear waves in fluid flows, *J. Math. Phys.*, **45**, 52–63.
- [56] **Murray, R.J.** (1989). Short Wave Modelling Using New Equations of Boussinesq Type, *Ninth Australasian Conference on Coastal and Ocean Engineering*, Institution of Engineers, Australia.
- [57] **Beji, S. and Nadaoka, K.** (2004). Fully dispersive nonlinear water wave model in curvilinear coordinates, *Journal of Computational Physics*, **198**(2), 645–658.
- [58] **Wei, G., Kirby, J.T., Grilli, S.T. and Subramanya, R.** (1995). A fully nonlinear Boussinesq model for surface waves. Part 1. Highly nonlinear unsteady waves, *Journal Fluid Mechanics*, **294**, 71–92.
- [59] **Russell, J.** (1844). Report on waves, **Technical Report**, 14th meeting of the British Association for the Advancement of Science, John Murray, London.
- [60] **Fenton, J.** (1972). A ninth-order solution for the solitary wave, *Journal of Fluid Mechanics*, **53**(02), 257–271.
- [61] **Miles, J.W.** (1980). Solitary Waves, *Annual Review of Fluid Mechanics*, **12**, 11–43.
- [62] **Rayleigh, L.** (1876). On Waves, *Philosophical Magazine*, **1**, 257–279.
- [63] **Keller, J.** (1948). The Solitary Wave and Periodic Waves in Shallow Water, *Communications on Pure and Applied Mathematics*, **1**, 323–339.

- [64] **Munk, W.** (1949). The Solitary Wave Theory and Its Application to Surf Problems, *Annals of the New York Academy of Sciences*, **51**, 376–423.
- [65] **Longuet-Higgins, M. and J.D., F.** (1974). On the mass, momentum, energy and calculation of a solitary wave, *Proceedings of the Royal Society A*, **340**, 471–493.
- [66] **Byatt-Smith, J.G.B. and Longuet-Higgins, M.** (1976). On the Speed and Profile of Steep Solitary Waves, *Proceedings of the Royal Society A*, **350**, 175–189.
- [67] **Zabusky, N.J. and Kruskal, M.D.** (1965). Interaction of "Solitons" in a Collisionless Plasma and the Recurrence of Initial States, *Phys. Rev. Lett.*, **15**, 240–243.
- [68] **Zabusky, N.J.** (2005). Fermi-Pasta-Ulam, solitons and the fabric of nonlinear and computational science: History, synergetics, and visiometrics, *Chaos: An Interdisciplinary Journal of Nonlinear Science*, **15**(1).
- [69] **Longuet-Higgins, M.S.** (1974). On the mass, momentum, energy and circulation of a solitary wave, *Proceedings of the Royal Society A*, **337**, 1–13.
- [70] **Wiegel, R.L.** (1964). *Oceanographical Engineering*, Prentice-Hall, Englewood Cliffs, NJ.
- [71] **Keulegan, G. and Patterson, G.** (1940). *Mathematical theory of irrotational translation waves*, National Bureau of Standards.
- [72] **Wiegel, R.L.** (1959). A presentation of cnoidal wave theory for practical applications, *Journal of Fluid Mechanics*, **7**, 273–286.
- [73] **Fenton, J.D.** (1979). A high-order cnoidal wave theory, *Journal of Fluid Mechanics*, **94**(01), 129–161.
- [74] **Fenton, J.D. and McKee, W.D.** (1990). On calculating the lengths of water waves, *Coastal Eng.*, **14**, 499–513.
- [75] **Quak, E. and Soomere, T.** (2009). *Applied Wave Mathematics: Selected Topics in Solids, Fluids, and Mathematical Methods*, Springer.
- [76] **Thomson, W.** (1887). *On ship waves*.
- [77] **Commission, M.N.** (2003). Guidelines For Managing Wake Wash From High-Speed Vessels, **Technical Report**, International Navigation Association.
- [78] **Havelock, T.** (1908). The propagation of groups of waves in dispersive media, with application to waves on water produced by a travelling disturbance, *Proceedings of the Royal Society of London*, **81**(549), 398–430.
- [79] **Huang, D.B., Sibul, O., Webster, C., Wehausen, V., Wu, D.M. and Wu, T.** (1982). Ships moving in the transcritical range, *Proc. Conf. on Behaviour of Ships in Restricted Waters*, volume 2, Varna, Bulgaria, pp.26–1–26–10.

- [80] **Wu, D.M. and Wu, T.** (1982). Three dimensional nonlinear long waves due to moving surface pressure, number 1 in Fourteenth Symposium on Naval Hydrodynamics, National Academy Press, Washington DC, USA.
- [81] **Akylas, T.** (1984). On the excitation of long nonlinear water waves by a moving pressure distribution, *Journal of Fluid Mechanics*, **141**, 455–466.
- [82] **Ertekin, R.C., Webster, W.C. and Wehausen, J.V.** (1986). Waves caused by a moving disturbance in a shallow channel of finite width, *J Fluid Mechanics*, **169**, 275–292.
- [83] **Chen, X.N. and Sharma, S.D.** (1995). A slender ship moving at a near-critical speed in a shallow channel, *Journal of Fluid Mechanics*, **291**, 263–285.
- [84] **Lowery, K. and Liapis, S.** (1999). Free-surface flow over a semi-circular obstruction, *International Journal for Numerical Methods in Fluids*, **30**, 43–63.
- [85] **Cole, S.** (1985). Transient waves produced by flow past a bump, *Wave Motion*, **7**, 579–587.
- [86] **Grimshaw, R.H.J. and Smyth, N.** (1985). Resonant flow of a stratified fluid over topography, **Technical Report14-1985**, University of Melbourne, Dept Maths Res.
- [87] **Katsis, C. and Akylas, T.** (1987). On the excitation of long nonlinear water waves by a moving pressure distribution. Part 2. Three-dimensional effects, *Journal of Fluid Mechanics*, **177**, 49–65.
- [88] **Wu, T.Y.** (1987). Generation of upstream advancing solitons by moving disturbances, *J. Fluid Mech.*, **184**, 75–99.
- [89] **Lee, S.J., Yates, G.T. and Wu, T.Y.** (1989). Experiments and analyses of upstream-advancing solitary waves generated by moving disturbances, *Journal of Fluid Mechanics*, **199**, 569–593.
- [90] **Zhang, D.H. and Chwang, A.T.** (1996). Numerical study of nonlinear shallow water waves produced by a submerged moving disturbance in viscous flow, *Phys. Fluids*, **8**(1), 147–155.
- [91] **Pedersen, G.** (1988). Three-dimensional wave patterns generated by moving disturbances at transcritical speeds, *Journal of Fluid Mechanics*, **196**, 39–63.
- [92] **Lee, S.J. and Grimshaw, R.** (1990). Upstream-advancing waves generated by three-dimensional moving disturbances, *Phys. Fluids A*, **2**, 194–201.
- [93] **Li, Y. and Sclavounos, P.** (2002). Three-dimensional nonlinear solitary waves in shallow water generated by an advancing disturbance, *Journal of Fluid Mechanics*, **470**.

- [94] **Sung, H.G. and Grilli, S.T.** (2005). Numerical modeling of nonlinear surface waves caused by surface effect ships dynamics and kinematics, volume 3, Proceedings of the Fifteenth International Offshore and Polar Engineering Conference, Seoul, South Korea, pp.124–131.
- [95] **Peters, S.A.** (1966). Rotational and irrotational solitary waves in a channel with arbitrary cross-section, *Communications on Pure and Applied Mathematics*, **19**(4), 445–471.
- [96] **Peregrine, D.H.** (1968). Long waves in a uniform channel of arbitrary cross-section, *Journal of Fluid Mechanics*, **32**(2), 353–365.
- [97] **Cao, Y., Beck, R. and Schultz, W.W.** (1993). Numerical computations of two-dimensional solitary waves generated by moving disturbances, *International Journal for Numerical Methods in Fluids*, **17**(10), 905–920.
- [98] **Henn, R., Sharma, S. and Jiang, T.** (2001). Influence of canal topography on ship waves in shallow water, *Proc., 16th Int. Workshop on Water Waves and Floating Bodies*, Hiroshima, Japan, pp.22–25.
- [99] **Torsvik, T., Pedersen, G. and Dysthe, K.** (2008). Influence of cross channel depth variation on ship wave patterns, *The Quarterly Journal of Mechanics and Applied Mathematics*, **2**, 1–23.
- [100] **Jiang, T., Henn, R. and Sharma, S.D.** (2002). Wash waves generated by ships moving on fairways of varying topography, *Proceedings for the 24th Symposium on Naval Hydrodynamics*, Fukuoka.

CURRICULUM VITAE

Name Surname: Deniz Bayraktar Ersan

Place and Date of Birth: Istanbul, 08.09.1983

Address: Istanbul Teknik Universitesi, Gemi Insaati ve Deniz Bilimleri Fakultesi
34469 Maslak/Istanbul

E-Mail: bayraktard@itu.edu.tr

B.Sc.: Istanbul Technical University, Faculty of Naval Architecture and Ocean Engineering Department of Shipbuilding and Ocean Engineering (2005)

M.Sc.: Istanbul Technical University, Faculty of Naval Architecture and Ocean Engineering Department of Shipbuilding and Ocean Engineering (2007)

PUBLICATIONS/PRESENTATIONS ON THE THESIS

- **Bayraktar Ersan D.** and Beji S., 2011: A New Numerical Scheme For Improved Boussinesq Equations with Surface Pressure. *IMAM 2011 XIV Congress of the International Maritime Association of the Mediterranean*, September 12-16, 2011 Genova, Italy.
- **Bayraktar Ersan D.** and Beji S., 2012: Water Waves Generated by Moving Pressure Fields. *ISOPE-2012 Rhodes Conference The 22nd International Ocean and Polar Engineering Conference*, June 17-22, 2012 Rhodes, Greece.
- **Bayraktar Ersan D.** and Beji S., 2012: Numerical Simulation of Waves Generated By A Moving Pressure Field. *Ocean Engineering*, (In Press).